MICROARRAY FOR SINGLE-PARTICLE TRAP WITH ADDRESSABLE CONTROL BASED ON NEGATIVE DIELECTROPHORESIS

LI HUAXIANG

(B.Sc. Fudan University)

A THESIS SUBMITTED

FOR THE DEGREE OF DOCTOR OF PHILOSOPHY

DEPARTMENT OF MECHANICAL ENGINEERING

NATIONAL UNIVERSITY OF SINGAPORE

2010

Acknowledgements

I would like to thank my respectful supervisors, Professor Lim Siak Piang and Professor Khoo Boo Cheong, for giving me this great research opportunity to work in the Bio-MEMS field, and I sincerely thank them for all the academic guidance and advices,as well as the non-academic ones during my stay at National University of Singapore.

I would also like to express my gratitude to Professor Lim Kian Meng and Professor Lee Heow Pueh for all the precious advices they gave me.

This work could not be done without the help of our SIMTech colleages, Dr. Wang Zhenfeng on the fabrication process.

In addition, I would like to acknowledge the members of my lab, Dr Cui Haihang, Dr He Xuefei, Dr Zhuang Han, Dr Liu Yang, who have always listened and never failed to provide valuable insights. Their friendship will be treasured for a long time.

This doctoral program certainly would not have been possible without the encouragement and support by my wife Zhou Min and my parents.

Contents

Summary

Biological sample analysis is a costly and time-consuming process. In the world of rising health-care cost, the drive towards a more cost-effective solution calls for a point-of-care device that performs accurate analyses of small samples. To achieve this goal, today's bulky laboratory instruments need to be scaled down and integrated on a single microchip of only a few square centimeters or millimeters in size. However, it is the challenge to trap single particles and to sort them. Several novel micro-devices for particle sorting and trapping are presented based on dielectrophoresis (DEP). The devices use the phenomenon of dielectrophoresis-the force on polarizable bodies in a non-uniform electric field-to generate potential energy wells. In previous works, researchers have presented lots of micro-devices based on dielectrophoresis. However, most of them are 2D structure. This report investigates a 3D structure. The sorting device is presented first. By using the Comsol software to design an improved grid electrode structure, this 3D electrode structure is arranged in a trapezoidal fashion to enhance the electric field and sorting efficiency. Fabrication process for the electrodes uses photolithography to achieve the required geometries. The trapping device is introduced next. The trap consists of three layers, well layer, two electrode layers. Besides photolithography for the formation of ITO electrode and the well array, the fabrication for middle electrodes of these traps involved lift-off process. At last, a multifunctional microarray is presented. This design has the advantage of

simple fabrication, single particle trapping and sorting with addressable control.Top-bottom electrodes structure is used in this design. Due to the small jags on the electrodes, a virtual electrical cage can be formed to trap particles. Experiments were performed with beads and cells to verify the design of these micro-devices. This multi-functional and simple design has the potential to be commercialized. All of the knowledge can be very useful in designing and operating a dielectrophoretic barrier or filter to sort and select particles entering the microfluidic devices for further analysis.

List of Tables

List of Figures

Chapter 1

Introduction

It is not that difficult to pick up an object with our fingers if the object has a size of around one centimeter, but it is much harder to pick up smaller objects like a strand of hair. Micro-sized devices and systems provide us a platform for manipulating objects in the micro-world. The Micro-electro-mechanical system (MEMS) is a technology of the very small, and merges at the nano-scale into nano-electro-mechanical systems (NEMS) and nanotechnology. MEMS are made up of components typically between 1 to 100 micrometers in size (i.e. 0.001 to $0.1mm$) and MEMS devices generally range in size from $20\mu m$ to $1mm$.

1.1 Micro-electro-mechanical system

MEMS has great potential advantages over traditional macrosystems for certain applications due to their unique characteristics, such as the small size, multifunctional, low cost and ease of disposal. Small size is the most obvious advantage. Many different components can be integrated on one chip to make it multifunctional. The incorporation of optical, electrical, or chemical sensing components into MEMS devices endears MEMS to different researchers from

different backgrounds. MEMS has become prevalent in many research areas. For example, in chemistry, micro-pumps, micro-mixers and micro-reactors are used to conduct research experiments. In environmental science, microarrays are used to monitor the number and type of bacteria in the environment. In medicine, several research groups have also shown the possibility of using micro-cantilevers for the diagnosis of prostate cancer [1], myocardial infarction [2] and glucose monitoring [3]. Such MEMS chips could lower the production cost and reduce production waste due to its small size. In addition, besides research, MEMS has also been widely used in daily life, such as accelerometer in cars and micro-speaker in cellphones. MEMS is a major breakthrough in technology and many new MEMS applications will continue to emerge, expanding beyond what is currently identified or known. MEMS is an extremely diverse technology that potentially could significantly impact every aspect of our life, such as traffics, military, diagnostics, and medicine. To design a multifunctional MEMS, researchers must have a wide knowledge of multidisciplinary in physics, chemistry and biology.

With the development of micro-fabrication, MEMS is now routinely manufactured. The manufacturing techniques used in the microelectronics industry lead to greater uniformity and reproducibility of such devices. MEMS technology can be implemented using a number of different materials such as silicon, glass, polymer and metal. Silicon or glass is commonly used in MEMS just as it is a common material used in consumer electronics in the modern world. The basic techniques for producing silicon or glass based MEMS devices are deposition of material layers, patterning of these layers through photo-lithography and followed by etching (wet etching and dry etching) to produce the required structures. Polymers are also commonly used in MEMS, because they have the advantage of being easily produced in large volume. MEMS devices can be made from polymers through conventional processes such as injection molding and embossing, and are especially well suited to micro-fluidic applications such as disposable

blood testing cartridges. Metal is another important material in MEMS technology. Metals can be deposited through the process of electroplating, evaporation, and sputtering processes. Commonly used metals include gold, nickel, aluminum, chromium, titanium, tungsten and platinum.

1.2 MEMS in Bio-science

In the past 20 years there has been an increased interest in research on the so-called Bio-MEMS and Lab-on-Chip(LOC). The application of micro-fabrication techniques has entered the life science field and started to serve as a driving force for discovery in cell biology, neurobiology, pharmacology and tissue engineering. Today, several methods for manipulating large numbers of cells simultaneously can be used in micro-fluidic systems. Micro-mechanical devices are capable of manipulating single objects with cellular dimensions since the size of cells fits very well with that of the commonly used micro-fluidic devices(10-100μm). The integration of all kinds of analytical standard operations into a micro-fluidic system become possible. This paves the way for the design of experimental platform in micro-world.

Mini-biosystem (BioMEMS) enables us to work with minute sample volumes in the nano-liter or micro-liter range. By combining micro-sensors with fluidic components into systems [4, 5], it is possible to do some further studies of proteins, DNA or RNA. For example, in genomics, DNA analysis can be achieved with miniaturization of analytical chemical methods[6, 7]. As genetic analysis has now become a more or less routine method, the new focus has been and still is polymerase chain reaction (PCR) [8]in bioengineering. In the past few years, the interest in analysis of even more complex biological systems such as living cells with the use of microfabricated structures has attracted increased attention, e.g. cell lysis[9–14], electropora-

tion [15–17], cell fusion [18, 19], cell cultivation [20–24] and ion channel studies [25–28]. In the future, the biomedical applications will likely dominate the progress of MEMS. The applications of MEMS for medical diagnosis, drug synthesis, PCR, and cell analysis will all be interesting developments.

1.3 Manipulation of micro-sized particles

Manipulation of micro-particles is fundamental to many different scientific areas, especially for biology and bio-medicine. For example, studying how cells interact with the medium and detecting the cancer cells in human body requires manipulating the cells [29]. However, not only for cells, manipulating the proteins, nucleic acids [30, 31], and other sub-cellular entities are also required. Owning to the small size and the large number of micro-particles, we need a 'mini-robot' which can work in the mini-world to help us access those micro-particles physically.

Manipulating micro-particles is quite akin to organizing cells in vito and for sorting cells. As such, the quest to manipulate micro-particles on length scales which commensurate with their size has led to the development of a host of technologies for investigating the optical, chemical, mechanical, electrical, and other properties or characteristics of the MEMS devices and cells. In the realm of the manipulation of micro-particles, there has been significant progress in miniaturized flow-based optical devices, mechanical devices, and electrical devices.

Up to now, many techniques exist to physically manipulate micro-particles. Micro-fabricated mechanical filters have been described for trapping different cell types from blood [32, 33]. Acoustic forces [34], optical tweezers [35],magnetic tweezers [36] and optoelectronic tweezers(OET) [37, 38] have been employed to manipulate micro or submicro particles. Also, there are some technique which combine the optical tweezers and hydro-gel to immobilize single cell

[39, 40]. Electrical technique is an increasingly common approach for enacting these manipulations. The electric field-based approach is well suited for miniaturization because of relative ease of micro-scale generation and structuring an electric field on microchips. Furthermore, electrically driven microchips provide the advantages of speed, flexibility, controllability, and ease of application to automation. Depending on the nature of bioparticles to be manipulated, different types of electric fields can be applied: (1) a DC field for electrophoresis (EP) of charged particles, (2) a non-uniform AC field for dielectrophoresis (DEP) of polarizable (charged or neutral) particles, (3) the combined AC and DC fields for manipulating charged and neutral particles. Compared with EP, DEP has the advantage of manipulating neutral particles, which is consistent with most of biological particles. DEP has thus become more prevalent. DEP has been successfully applied on microchip scales to manipulate and separate a variety of biological cells including bacteria, yeast and mammalian cells [41–48]. Depending on the electric field distribution, micro-particles can be moved, sorted, trapped, oriented, or rotated. In most instances inhomogeneous fields are applied, which lead to the attraction of polarizable material towards the regions of highest field strength(positive DEP), but also to apparent repulsion (negative DEP), depending on the frequency and electric properties of both the object and the surrounding solution. Thus far, many configurations of electrode geometries have been used to generate non-uniform electric field,such as ring-dot [49], points-lid [39, 50], quadrupole electrodes [51], octopole electrodes [52–54], grid electrodes [55], transistor-based structure [56] and so on. The next chapter will review the manipulation of micro particles briefly in order to evaluate the advantages and disadvantages of previous designs and the demands of commercial use.

The drawbacks of devices that require complicated fabrication or have unreliable performance may prevent or limit routine employment. To overcome these problems, a smart multi-

functional microarray, which can sort and trap single particles, is needed. Besides, addressable control is another big issue that needs to be dealt with.

1.4 Purpose and scope

Due to the shortcomings of previous designs, which will be analyzed in detail in Chapter 2, a new design is required to overcome these drawbacks. The objectives of this study are

1. to develop a smart microarray for both particle sorting and single particle trapping with addressable control.

   To integrate more functions into one structure is a challenge. In this microarray, one feature is that this microarray can be used for sorting particles with different sizes as well as different electrical properties, all with a single-particle resolution. Secondly, the number of traps can be scaled up, which is very important in microarray technique. Thirdly, the density of the traps is uniform and very large so as to ensure sensitivity of detected signals for ease of analysis by computers. Fourthly, multiplexing technique was used in this design in order to meet the requirement of control of large number of traps. By using this technique, a device with n by n traps can be controlled separately by 2n control points. Finally, the fabrication must be simple, thus is attractive to commercialization.

2. to model the device theoretically.

   In a coupled electric field and fluidic field, the model should cover every major parameter. In previous works, rotation was neglected. In this work, the rotation of the idealised particle is included in the modeling. This allows for a more comprehensive understanding of a particle's motion under the Stokes flow force and dielectrophoretic force. Electrostatic

interaction between particles is studied since it is an important problem in single-particle trap. The results provide a viable means to reduce the electrostatic interaction force.

3. to evaluate this device, such as the resolution and the efficiency.

   A new method is developed and its efficiency is evaluated. Due to the limitation of experiment, traditional methods cannot be used to test the efficiency. A large trap, which can trap a number of particles, is set up before and after the microarray. By comparing the different number of particles trapped between the two traps, efficiency can be determined.

4. to test this device with cells.

   Most of previous work only showed test results of polystyrene particle. In this work, several types of cells are used to test the device. The results indicate that cells can work well with this device.

The expected advantage of this microarray is that it could be used for cell patterning to observe the bio imaging effect in bio-science. It also can be used for toxin ascertain to inspect the quality of the liquid in environmental science. Further improvement in the design should allow analysis of single cells in tissue engineering. This device could serve as a better platform for pathologists to classify the different subtypes of more heterogeneous complex disease. It could reduce the noise of the output detection signal due to its addressable control and large number of traps.

The primary focus of this study is to develop methods for designing a microdevice based on DEP, and implementation of these methods in a proof-of-concept of a small array as a demonstration of the micro-device. Other associated problems involved in developing the device, such as imaging, scaling up the number of traps, designing the electrical control systems to operate

the traps, glass quality, temperature non-uniformity, or bubbles that occur during experimentation, are not considered. To avoid the brown effect and due to the limitation of fabrication, only $3\mu m-, 5\mu m-, 8\mu m-, 10\mu m-, 20\mu m-$ beads are used to mimic cells in the experiment. To test this device whether it is feasible in bioscience, K562 cells are used to verify the design due to the fact that K562 cells are easy to control and culture.

In the next Chapter 2, a detailed review of particle manipulation will be conducted. Then basic theories about DEP are described, such as the dipole theory and the Maxwell Stress Tensor, either of which can serve as the foundation for the quantitative design of the microdevices. The modeling and design of the device will be followed. Finally, contributions and limitations of this work will be discussed.

Chapter 2

Review

The current methods commonly used in biological-based laboratories for manipulation, concentration, and separation of bio-particles include optical tweezers, fluorescence or magnetic activated cell sorting, centrifuging, filtration and electric field-based manipulations and separations. In the following, several concepts for the trapping and sorting of cells will be described.

2.1 Sorting System

Sorting biological particles mechanically on a microchip poses challenges because of the complex physical properties and variation of biological particles. Micro-fabricated mechanical filters have been described for trapping different cell types from blood. These filters were made of arrays of rectangular, parallel channels on chip of a width and height that would not allow particles larger than the channels to enter the channel network along the axis parallel to the chip surface. A cell filter fabricated in quartz consisting of a network of intersecting $1.5\mu m \times 10\mu m$ channels is shown in He et al. [57]. This filter is shown to be efficient in trapping animal cells and E.coli. However, the cell properties must be studied and determined before using all these mechanical

filters. The deformity of cells will affect such filters' performance. As such, these filters cannot be used universally or there is no prescribed changes to be made for the trapping of other types of cells.

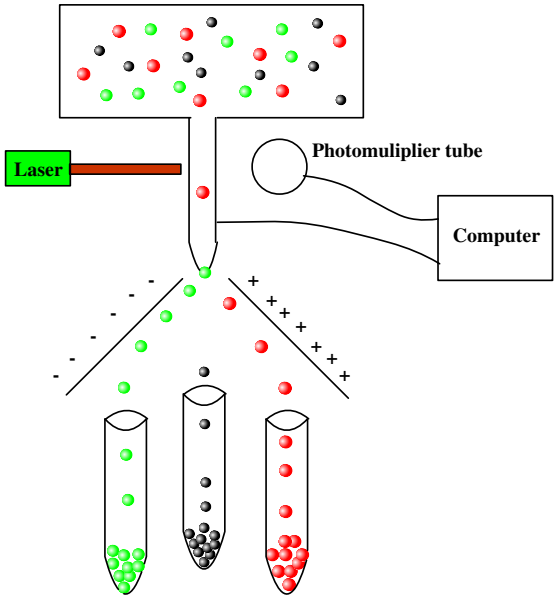

Figure 2.1: Fluorescence Activated Cell Sorter

Another common approach for sorting cells is based on some phenotypic marker. A micro-fabricated Fluorescence Activated Cell Sorting (FACS) has been constructed to sort microbeads and bacterial cells using electrokinetic flow[58]. The disposable sorting device is fabricated using lithography, which enables the design of inexpensive and flexible miniaturized fluidic devices.

The basic mechanism of FACS is shown in Figure 2.1. It is widely used in bio-research. Different groups of cells are labeled first by different colors of fluorescence materials. Then these cells are charged differently according to their color when passing through the detector. At last these differently charged cells will be deflected in an electric field. Because of the different deflection distance, the different cells can be sorted. This method is very efficient and reliable. A throughput of the order of 10^4 cells/s is common with available machines. High throughput and high resolution have contributed to its employment in the research field. However, this

device suffers from other drawbacks, such as frequent change of voltage settings due to ion depletion and pressure imbalance. Another similar method is magnetophoresis [36, 59] as shown in Figure 2.2. The difference is the use of different magnetic materials to label different cells, followed by passing through a magnetic field. The magnetic particles were separated from non-magnetic particles by deflection in a magnetic field gradient. Both of these phenotypic methods need the labeling of the cells first. Therefore, suitable label material becomes very important. There should be no harmful effect on live cells and must be accepted by all the cells under consideration prior to sorting.

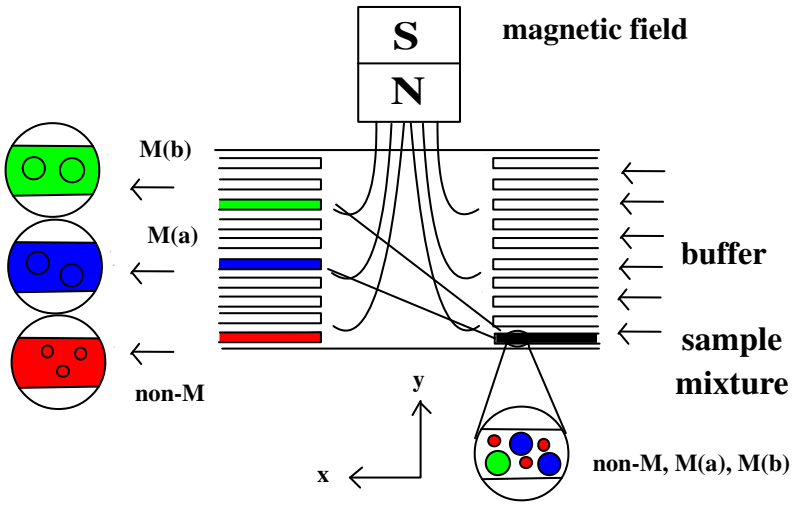

Figure 2.2: Magnetophoresis sorter[36]

To obviate labeling, sorting methods based on the internal properties of particles have been proposed. Impedance Spectroscopy(Figure 2.3) [60, 61]is a method for sorting different particles based on different resistance. In bio-science, different cells usually have different resistance. A detector can detect the difference so that they can be sorted. Gawad et al.[60] used impedance at two different frequencies to effectively distinguish erythrocytes from cells with a typical transit time in the order of 1ms. However, even the same cell type sometimes can have different

resistance due to their different shape or different physiological status. The resolution cannot be very high. Acoustic sorter [62, 63], as shown in Figure 2.4, is fast developing as a viable alternative due to its high resolution and low cost. When applying a standing acoustic wave within the cavity of a micro-device, the cells of different density will stay either on the nodes or between them. The standing wave is very sensitive to the distance between the source and the reflector. However, this separation is based on the differences of the density and compressibility. Before conducting the sorting experiment based on acoustic standing wave, these two properties must be predetermined. Sometimes, it is not that easy to decide the density of unknown particles. On the other hand, optical method may overcome such shortcoming. Recently, researchers use the optical grid generated by interference or diffraction to sort two groups of particles with different sizes [64]. This method is based on the different index of different cells. But the requirement of sophisticated and expensive optical equipment is a huge impediment. A much simpler and cheaper method-Field Flow Fractionation (FFF) as shown in Figure 2.5, is proposed to sort different sized particles [65–67]. In a parabolic flow field, different particles at different layers have different speed. Given a sufficiently long time, they can be sorted. Usually, a perpendicular force, in the form of a gravitational, thermal or electric field is included to improve the separation. Researchers have combined different techniques to make improvement, such as DEP/G-FFF(shown in Figure 2.6) [48]. Still, FFF is a batch-to-batch sorting method. This will lower the efficiency.

Dielectrophoresis (DEP) has seen much development in the past 20 years due to the rapid development of micro-fabrication. Due to the low cost and easy operation on neutral particles, DEP has attracted much attention and research.

DEP has been increasingly used to sort micro-particles. In a micro-device, the high electric fields/gradients do not require high voltage due to its small size. As a result, it can produce

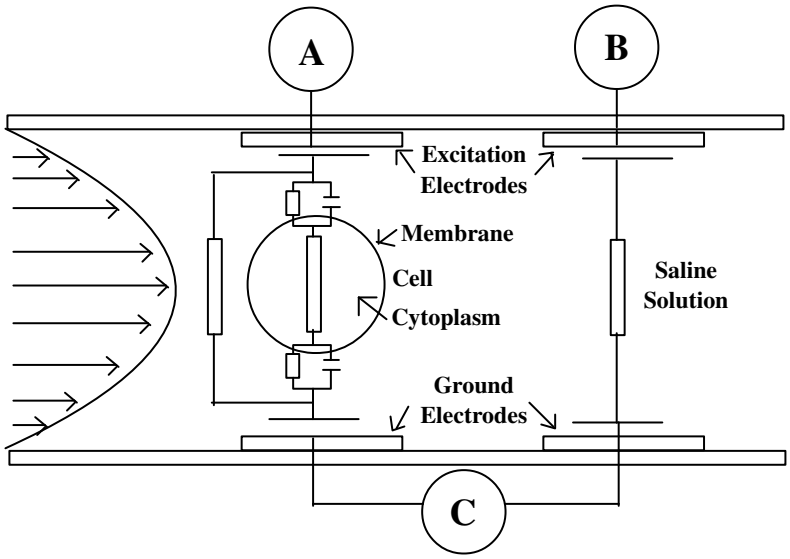

Figure 2.3: Impedance Spectroscopy[61]

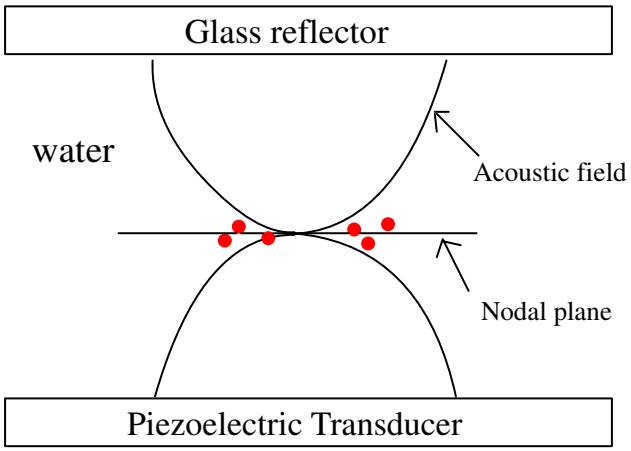

Figure 2.4: Acoustic sorter[62]

strong forces in a range well suited for particle manipulation. Sorting of particles has been carried out based on the differences of their electrical properties, such as different signs of CM(Clausius-Mossotti) factors, which is a common way used in the sorter due to the reliability of these signs. According to sign of CM-factors, some group will experience positive-DEP (pDEP) and the other negative-DEP (nDEP) [68, 69]. In such a situation, the pDEP subpopulation will be attracted to the electrodes whereas the nDEP sub-population will be repelled. By using this method, many types of cells have been sorted, including HeLa cells from blood cells [70], human breast cancer cells from blood cells [71], yeast based upon viability [72–74], CD34+ stem cells from bone marrow and peripheral blood cells [75], and bacteria from blood cells [42, 74]. The array of metallic circles is an early design in particle separation [42, 70]. The function of the array is to utilize nDEP and pDEP to separate two types of particles. The electric field is strongest near the edge of the electrodes while the minimum exist in between the electrodes. In one application, E. Coli bacteria are separated from the blood cells. After washing the blood cells off the surface of the electrodes, bacterial DNA strands are released by high voltage via the electro-poration of E. Coli. In a separate experiment, human cervical cancer cells are separated from human blood cells using the same procedure. However, the need for a wash-off procedure means the accuracy of the particle separation is compromised.

Castellated electrodes are useful in generating multiple zones of electric field maximum and minimum (Figure 2.7) [74]. The four separated electrodes with castellated shape are activated with opposing voltages to generate strong non-uniform electric fields in between the electrodes. In one experiment, viable cells are separated from nonviable cells using this method [76]. It has also been demonstrated that live cells can be trapped by nDEP in the electric field minima for live cell imaging and assay. The locations of the trapped cells are known and can be held there for an indefinite period. Another advantage is that since pDEP are used, the cells are not in

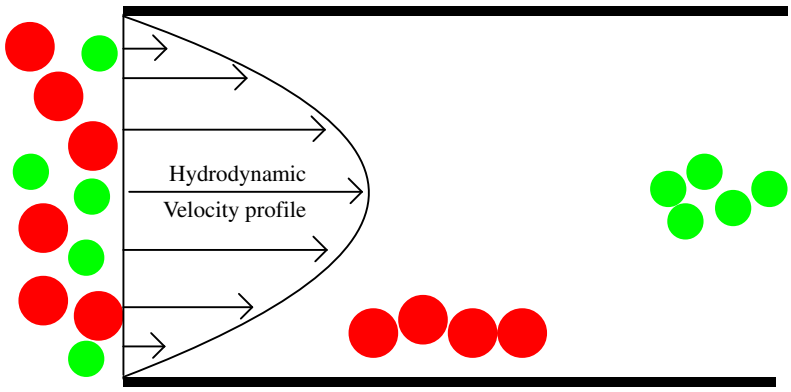

Figure 2.5: Field Flow Fractionation[65]

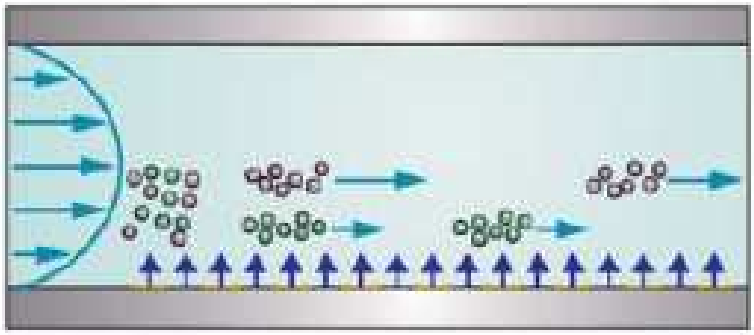

Figure 2.6: Field Flow Fractionation combined with Dielectrophoresis[48]

contact with electrodes and their survival rate increases.

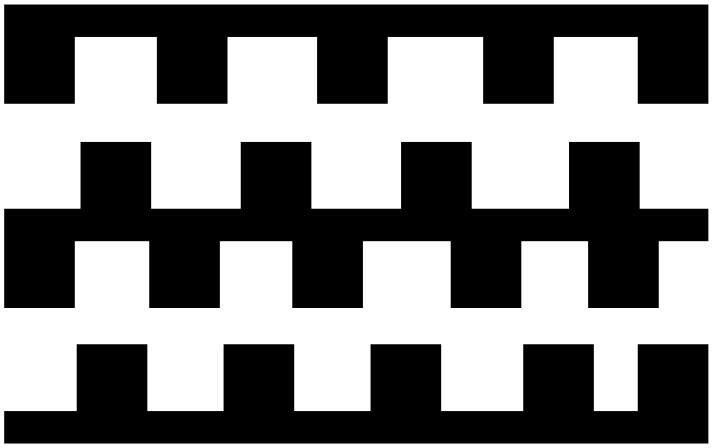

Figure 2.7: Castellated electrodes structure[74]

However, the method based on different signs of CM factor is not a feasible approach for sorting two types of live cells. To conduct such sorting, most of live cells must be placed into the low conductive buffer, which would affect the physiological properties of live cells, or sometimes killing the live cells. Therefore, sorting of live cells should be conducted in the nutritional medium, in which, most live cells will experience nDEP. Based on nDEP, the micro-particles can be also sorted based on different nDEP force magnitudes due to either the difference between CM factors or difference in particle size. In this case, the forces are of the same sign, but of different strength, which provides the basis for sorting live cells.

Isomotive sorting structure, as shown in Figure 2.8, is based on the different magnitude of CM factors, which can cause differences in the magnitude of nDEP force [77]. Particles with different CM factors will be deflected to different distance in a non-uniform electric field due to the different nDEP forces acting on them. But for the particles with close electrical properties, the difference between CM factors cannot be very large. This means that the travel time in the device must be long enough in order to increase the difference,which is perpendicular to the

flow direction, between the deflection distances of different particles so that different particles can be sorted completely. An improvement of this method is to engender a PH-value gradient in the fluid by adding some solution(PBS) [78]. This method increased the change in CM factor so that the resolution and efficiency are improved. To conduct sorting based on the different CM factors, the electrical properties of particle and that of the medium around particles should be measured.

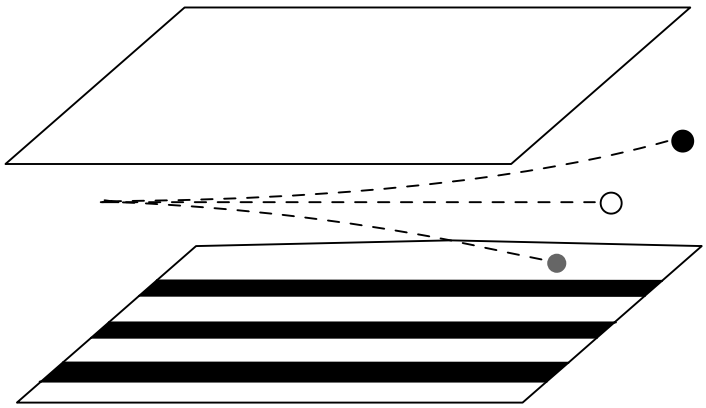

Figure 2.8: Isomotive sorter[77]

Different sizes of particles also can cause different nDEP force. This method based on different sizes of particles is usually coupled with the hydrodynamic force. By using this method, many different geometries of the electrodes have been fabricated. Parallel(Figure 2.9) [79] and trapezoid(Figure 2.10) [80] electrodes are two popular structures due to simpler fabrication. The particles with different sizes will be deflected from their original direction over a different distance as a result of different DEP force acting on them during their flow though the electrodes.

Besides 2D structures, 3D structures [43, 81–83] are also used to sort particles. The electric field in a 3D structure is stronger than that in 2D structure for the same voltage. However,

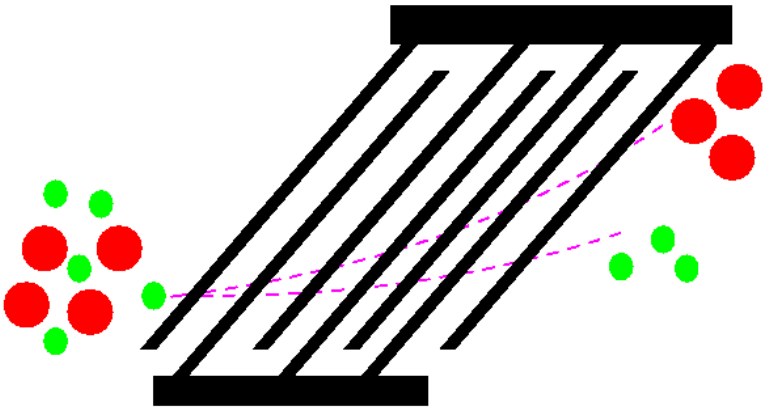

Figure 2.9: Parallel electrodes[79]

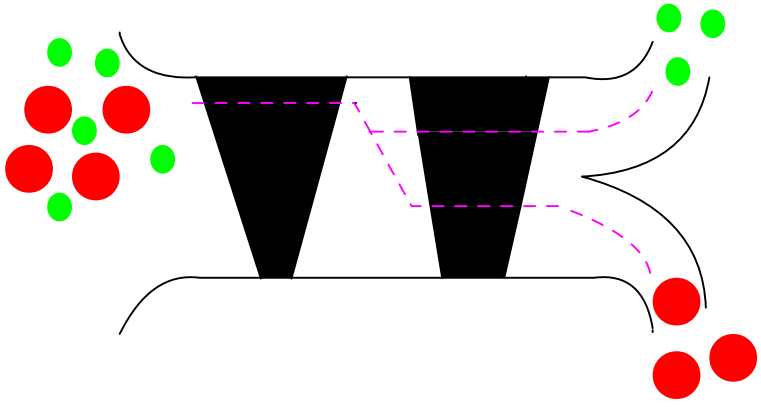

Figure 2.10: Trapezoid electrodes[80]

the challenge is to to fabricate such 3D electrodes due to the limitation in technique of micro-fabrication.

A compromised method is to fabricate a 3D structure with 2D electrodes, such that both high electric field and simple fabrication can be achieved. Paired electrodes structure is one of such structures. Schnelle et al.[84] developed the parallel electrodes by putting the electrodes opposed from one another, with one on the substrate and one on the sorting chamber ceiling. The electrodes are at angle with the fluid flow direction. These have been used to create nDEP "barriers". These structures have even been used for magnitude-based particle sorting by controlling the nDEP barrier such that it deflects particles with large radius but allowing passage for those with small radius. The fabrication process of this is much simpler, which is similar with the parallel electrodes. But one intractable part of the fabrication is that alignment is needed during packaging.

Traveling Wave Dielectrophoresis (twDEP) is also used to separate particles of different sizes [85, 86], as shown in Figure 2.11 and Figure 2.12. Spiral electrode design for TWD is one of the more popular alternatives to the parallel track design. The reason for its popularity is its simplicity. It is relatively easy to draw and inexpensive to manufacture. Spiral designs involve four parallel lines running in a growing concentric geometric shape such as a square or a circle. As the four lines spiral outward, more and more parallel tracks are created for TWD. Furthermore, extending the spirals will not increase the number of required metal contacts. This is a crucial advantage for spiral electrodes over the conventional parallel track design. Research literature has shown that the spiral design is able to transport particles from the outer rings to the inner rings efficiently. However, there are several drawbacks. First, the outside track has to circle a far bigger area then the inner tracks. In a structure as small as a MEMS device, area is scarce and a large spiral design has too much wasted area to be

practical. Second, the spiral design spreads outward in a radial direction implying that instead of transporting targeted particle from a fixed point to another, particles move into the inner circle from all angles regardless of their initial position. Furthermore, once the particles are gathered inside the concentric circle, it is difficult to move them elsewhere.

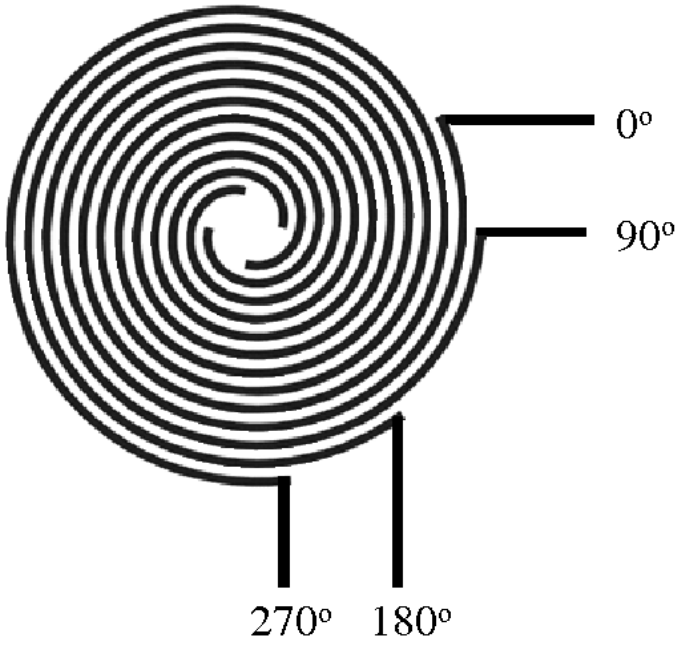

Figure 2.11: Traveling Wave Dielectrophoresis[86]

2.2 Trapping System

Particle traps is another thrust of today's research. A direct approach to trap cells may be obtained by using micro-pipettes. These devices have been successfully used by Rusu et al.[87] to aspire beads and draw them out of an optical trap, and may be interesting tools to manipulate individual cells. Chip-based patch clamping has the objective to replace traditional patch electrodes with a planar array of recording interfaces miniaturized on the surface of either a silicon polymer or glass substrate. Three dimensional silicon oxide micro-nozzles integrated

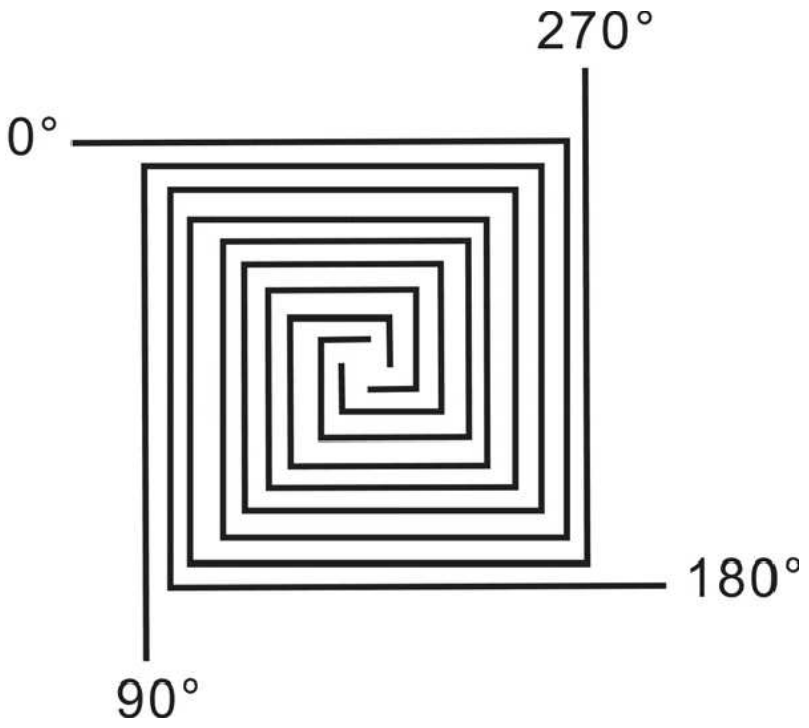

Figure 2.12: Traveling Wave Dielectrophoresis[85]

into a fluidic device for patch clamping has been developed by Gijs and co-workers [25]. A cell can be positioned on the nozzle by suction through the hollow nozzle that extends to the back opening of the chip.

Another direct approach is simply to use physical barriers to contain particles. This can take the form of arrays of micro-fabricated wells into which particles can be deposited and shielded from destabilizing fluid flows, thus effecting trapping [88, 89]. Besides physical method, biochemical method can be used for particle traps. Some researchers trapped particles by modifying the surface[90]. This method has the advantage of high resolution. But the drawback is that each modification can only trap one specific type of particles. Optical methods can solve this problem. There are two types of devices that researchers use: highly divergent lasers that form tweezers to trap particles in three dimensions, and less divergent laser that push particles along the path of the laser. The former has the advantage of creating a stable trap for

cell manipulation, whereas the latter uses simpler optics. Both have the attractive quality of partitioning the system complexity off the micro-fabricated device, resulting in a simpler (and thus less expensive) device. Acoustic tweezers with focused high-frequency ultrasound (3.5 MHz) have been shown to create gradient forces around 10 nN (i.e. three orders of magnitude greater than optical forces), which are able-by counter two propagating beams-to trap large ($270\mu m$ diameter) polystyrene spheres and clusters of frog eggs without damaging them [34]. However, the acoustic tweezers are difficult to manipulate to form an array like the optical tweezers [91]. Both optical tweezers and acoustic tweezers suffers from problems of sufficient localization to trap single particles.

The DEP chip has the advantage of free labelling, low cost, and easy control. Many micro-devices based on DEP have been developed. In a DEP chip, how to generate non-uniform electric field is a big issue. So far, numerous geometries of electrodes have been used to generate non-uniform electric field. As with particle sorting, pDEP was the first choice in these designs because of its strong force and easy fabrication. One geometry is the points-lid structure(Figure 2.13) developed by two research groups [39, 50] for trapping micro-particles. In this structure, a uniform top "lid" conductor and a bottom conductor patterned into "points" using some type of insulator. Particles experiencing pDEP can be attracted by the points on one plate. Researchers used this geometry to pattern cells to study cell-cell interactions [50]. This is one of the few DEP geometries where researchers have positioned cells and then had them attached. Most of other geometries have been only used for positioning. However, the challenge in creating such a system is electrically addressing the 100 to 1000 cell traps, which would be needed in practical system. A system where each of those traps requires even one electrical connection to the outside world would result in the need to make an impractical number of connections to the device.

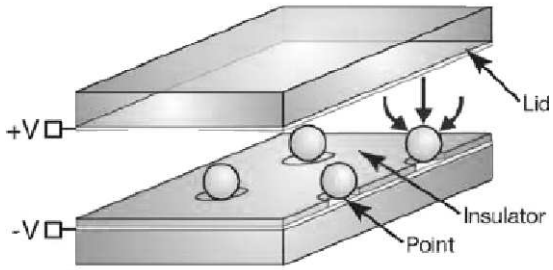

Figure 2.13: Points-Lid Structure [39]

The ring-dot structure [49] can solve this addressing problem. In this structure as shown in Figure 2.14, there are two layers of electrodes forming the "ring" and "dot". Particles are attracted via pDEP to the field maximum at the dot. Within this structure many single particles can be observed and then desired particles can be sorted out. The distinct advantages of this geometry are that this two-layer structure allows the use of multiplexing technique, which can control the particle at each site separately. However, both of these structures cannot be used for trapping live cell as mentioned above. Therefore, it is better to keep the live cells in the culture medium, in which, most of the cells always experience nDEP force.

Based on this concept, many nDEP chips have come into being. Quadrupole(Figure 2.15) [53] electrodes structure is a reliable structure used for trapping particles based on nDEP. Quadrupole electrodes are four electrodes with alternating voltage polarities applied to every other electrode. Planar quadrupole electrodes were used for nDEP cell trapping by Fuhr et al. [92, 93]. It is possible to create single-cell traps by making the electrodes' space only one-cell width. Additionally, one can make large arrays of quadrupole electrodes. However, planar quadrupole electrodes are not commonly used for handling cells because the trapping force is very weak. The traps are in the in-plane directions, and trap out of plane by balancing the nDEP

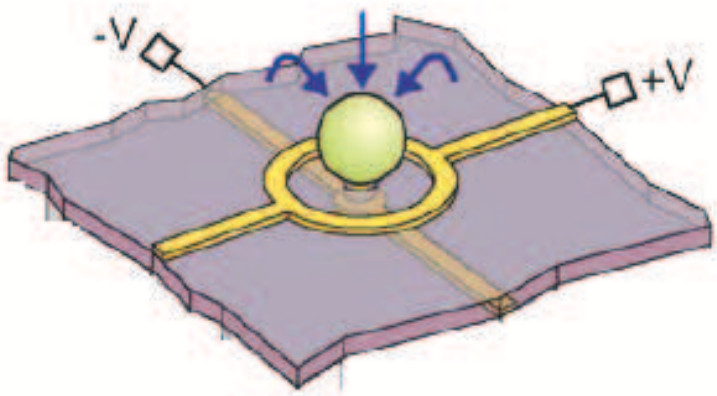

Figure 2.14: Ring Dot Structure [49]

force against gravity. That means these traps suffer from the drawback that increasing the field only pushes the particle farther out of the trap and does not increase the holding strength [94]. One way to increase the strength is to extend the electrodes into the third dimension, creating extruded quadrupole traps(Figure 2.17) [47, 51]. This four pillars can provide a tighter trap for holding single particles. Another three-dimensional design is the elliptic-like electrodes that surround the circular micro-channel [95]. The alternating fields generate nDEP conditions and the resulting force lifts the particle into the center of the channel. But the difficulty of fabricating these 3D electrodes will hinder its routine use. Another way to increase the strength of quadrupole-electrode traps is to put another quadrupole on the top to provide further particle confinement. This octopole electrodes structure(Figure 2.16) is much simpler to fabricate than the extruded quadrupole electrodes structure as well as the eliptic-like electrodes structure. Additionally, this octopole trap is significantly stronger than planar quadrupole electrodes, and are used for single-cell trapping [53, 54]. The German team[52] that developed these traps has also combined them with electro-rotation to study cell properties. Besides, this can be

arrayed just like planar quadrupole electrodes. Their primary challenge is that they require precise alignment of the two opposed quadrupoles. Besides, it is difficult to control such a large microarray because each trap needs eight control points.

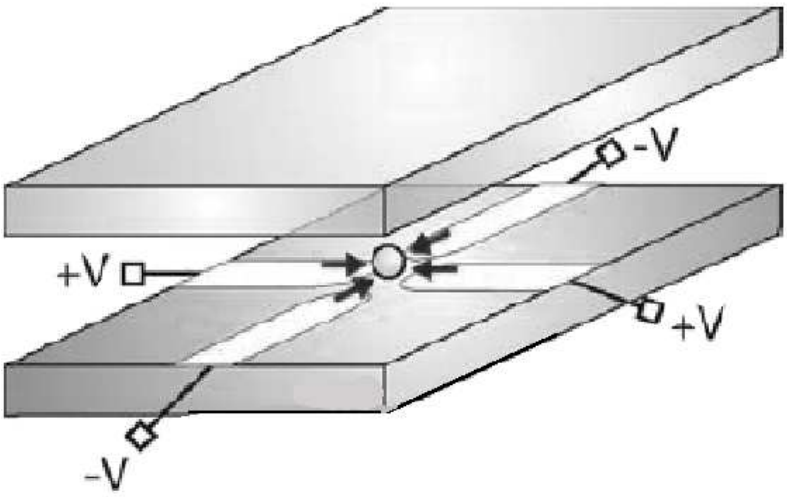

Figure 2.15: Planar Quadrupole Electrodes[53]

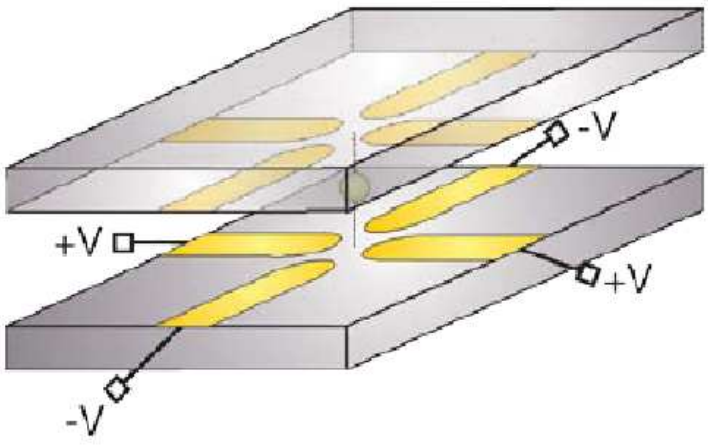

Figure 2.16: Octopole Electrodes[53]

To solve the control problem, an European team has developed an active Transistor-based trapping array [56],as shown in Figure 2.18, consisting of an array of square electrodes on bottom

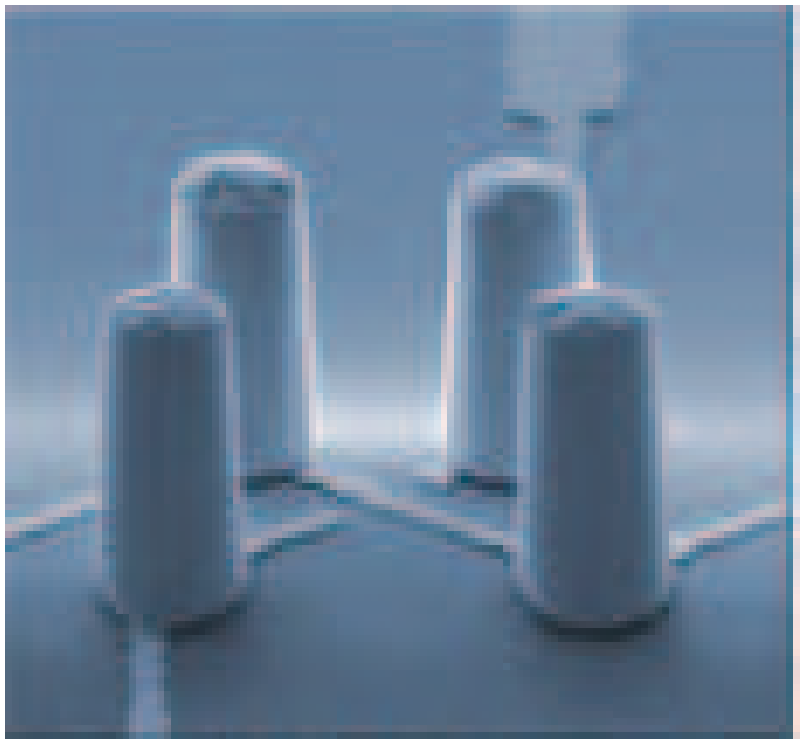

Figure 2.17: Extruded Quadrupole Electrodes [52]

and a conductive lid on top. The structure incorporated the CMOS circuit which allows each square electrode to be connected to an AC power source in a programmable fashion. By putting a center square at +V and the surrounding squares at -V, they can create an in-plane trap. Furthermore, setting the chamber top to +V closes the cage, forming a 3D electrical cage. In this structure, each particle can be controlled by programming. In addition, it can be used for live cells. But the complex circuit behind the device would prevent it from large scale routine usage.

Besides the said different geometries of electrodes, another category is the electrodless dielectrophoretic traps. Such devices are fabricated on an insulation substrate composed of geometrical constrictions [31]. The constriction is used to squeeze the electric field in a conducting solution, thereby creating a high field gradient with a local maximum. One notable example [96] is a concentrator using an insulating cylindrical posts etched into a channel to create the

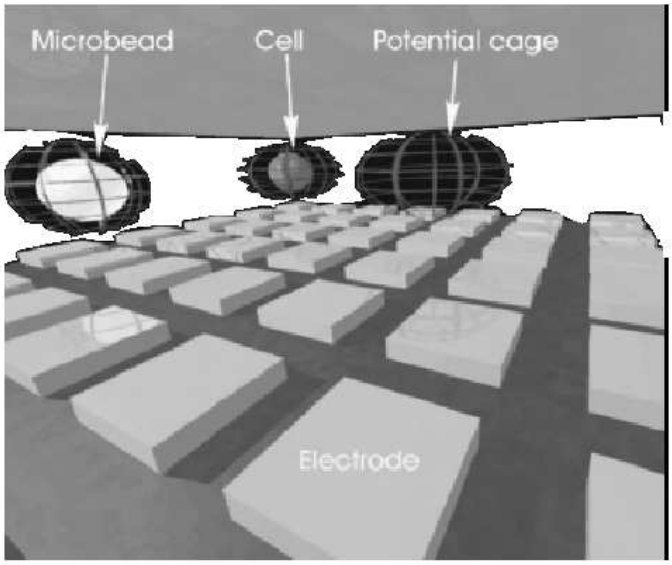

Figure 2.18: CMOS-based trapping array [56]

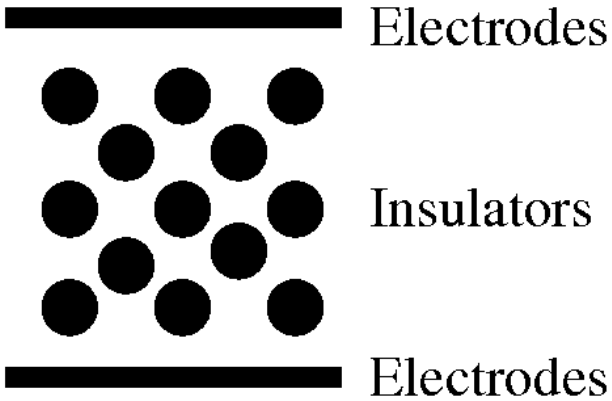

Figure 2.19: Electrodless Dielectrophoretic Trap [96]

field obstructions necessary for DEP as shown in Figure 2.19. By applying a DC voltage to the device, they obtain EP, DEP, and electro-osmotic flows. They apply a large electric field so that DEP will dominate and trap particles. To date, they have shown concentration and live or dead discrimination of bacteria [96]. A distinct advantage of this approach is that the channel is completely passive and can be made out of plastic/polymer.

Another method for trapping single particle is to combine two or more techniques. An optical image-driven dielectrophoresis technique [37] permits high-resolution patterning of electric fields on a photo-conductive surface for manipulating single particles. It requires $100,000$ times less optical intensity than optical tweezers. Using an incoherent light source (a light-emitting diode or a halogen lamp) and a digital micro-mirror spatial light modulator, the author demonstrated parallel manipulation of 15000 particle traps on a $1.3 \times 1.0 mm^2$ area. With direct optical imaging control, multiple manipulation functions are combined to achieve complex, multi-step manipulation protocols.

Thus far, we know that DEP has the advantage of low cost, easy control, and ensuring no harm to live cells. Besides, DEP can manipulate the micro-particles rather easily. DEP has become a prevalent technique nowadays to sort and trap cells. In this study, we will demonstrate several designs based on negative DEP to manipulate micro-particles.

Chapter 3

Simulation

Dielectrophoresis(DEP) is a much-written topic of many review papers, for example see [97, 98]. It was first reported by Dr.Herbert Pohl at the Princeton University in 1958 [99]. DEP effect was demonstrated to be able to suspend tiny droplets of water in mid air. Dr. Pohl showed that the most interesting aspect about DEP is its ability to work with neutral particles that are "larger than molecules" [99]. In the last ten years or so, the DEP effects have garnered much interest from the research and industry communities. DEP is suitable for manipulating biological particles because it is observed that the AC excitation allows the use of high frequency voltage which will not induce electrolysis and the corrosion of the electrodes. The type of particles demonstrated to have dielectrophoretic effects included mammalian cells [28, 41, 85, 100–102], yeast [68, 71, 72, 81, 100], bacteria [9, 42, 44, 96, 103], virus [45, 69, 86, 104], DNA [6, 30, 31, 42, 105, 106], protein [2, 12, 107], and polystyrene beads [38, 79, 80]. It is clear that particles with a wide range of sizes from μm to nm are susceptible to DEP forces.

In this chapter, the physics behind DEP is firstly described. Dipole and Maxwell Stress Tensor theory will be introduced. Secondly, we will carry out an analysis of different types of electric field. A comparison of the electric field between the 3D structure and 2D structure will

be discussed. Thirdly, we study the electrostatic interaction between particles in electric field, and the rotation of particles in fluid field. Finally, the modeling tools will be demonstrated. The simulation results in this chapter will guide and improve the design and provide a good preparation for the following modeling.

3.1 Basic theory of dielectrophoresis

3.1.1 Dipole approximation

Dielectrophoresis is the motion of a neutral object in a non-uniform electric field due to the fact that the object and the surrounding medium have different polarization properties. We can explain DEP easily with reference to Figure 3.1(a). A neutral object is placed into a medium with a different polarization in a uniform electric field. It is not subject to a net force while experiencing an induced dipole moment.

This is because each half of the induced dipole is subjected to opposite and equal forces, which cancel out each other. In Figure 3.1(b), this same object is placed in a non-uniform electric field. Now the two halves of the induced dipole experience different forces and a net force is produced. This is the dielectrophoretic force.

Depending on the relative polarizabilities of object and medium, the object will feel a force that propels it towards the field maximum (termed positive DEP as shown in Figure 3.2(a)) or field minimum (negative DEP as shown in Figure 3.2(b)). The direction of the force is independent of the polarity of the applied voltage. Switching the polarity of the voltage does not change the direction of the force. It is still pointing to the field maximum.

The force in Figure 3.1(b), where an induced dipole is affected by a non-uniform electric

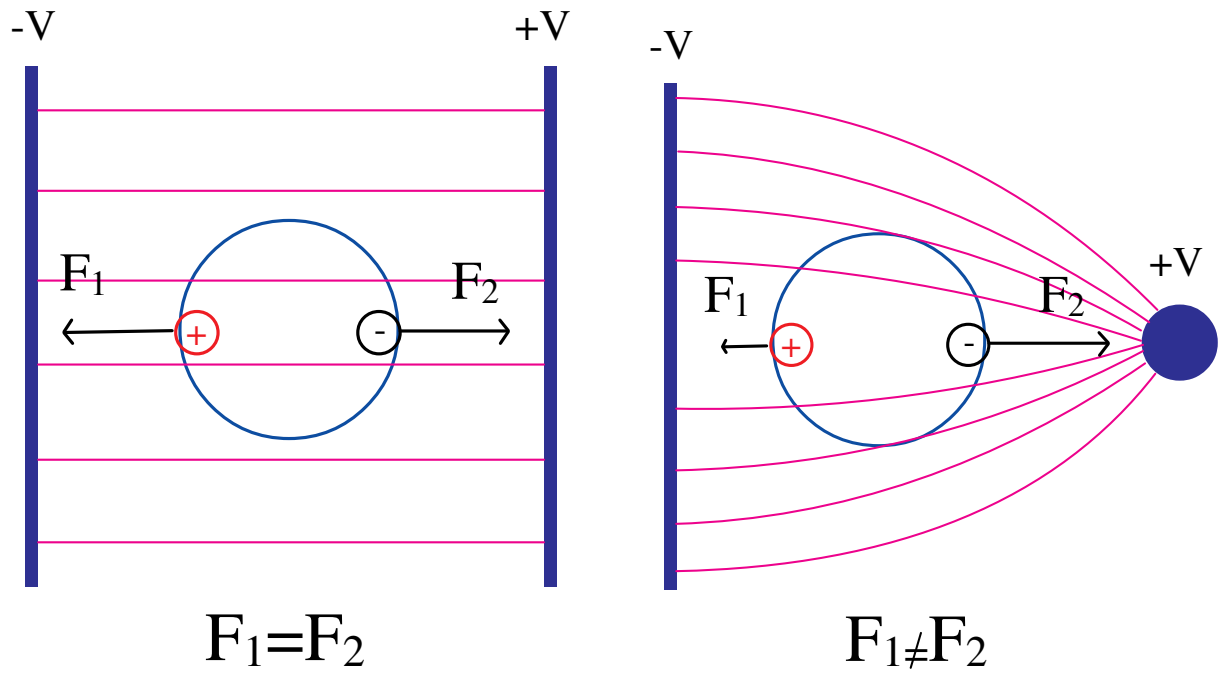

(a) Uniform electric field (b) Non-uniform electric field

Figure 3.1: A neutral body in an electric field

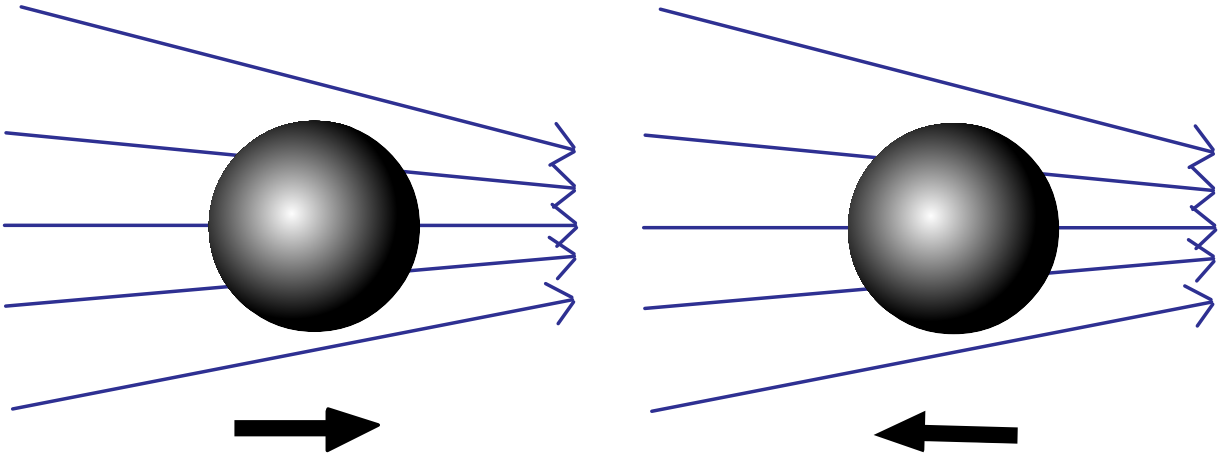

(a) Positive DEP (b) Negative DEP

Figure 3.2: Schematic diagram of the DEP force

field, is given by[99]

$$\boldsymbol{F}_{dep} = 2\pi\varepsilon_m R^3 \mathrm{Re}[\mathrm{CM}(\omega) \cdot \nabla|\boldsymbol{E}|^2] \tag{3.1}$$

where ε_m is the permittivity of the medium surrounding the particle, R is the radius of the particle, ω is the radian frequency of the applied field, and $\boldsymbol{E}$ is the complex applied electric field.

The Clausius-Mossotti (CM) factor gives the frequency (ω) dependence of the force and its sign determines whether the particle experiences positive or negative DEP. The Clausius-Mossotti factor comes from solving the Laplace's equation and matching the boundary conditions for the electric field at the surface of the particle. For a homogeneous spherical particle in an electric field, the CM factor is given by

$$\mathrm{CM} = \frac{\varepsilon_p^* - \varepsilon_m^*}{\varepsilon_p^* + 2\varepsilon_m^*} \tag{3.2}$$

where ε_m^* and ε_p^* are the complex permittivity of the medium and the particle, respectively, and are each given by $\varepsilon^* = \varepsilon + \dfrac{\sigma}{\mathrm{j}\omega}$, where ε is the permittivity of the medium or particle, σ is the conductivity of the medium or particle, and j is $\sqrt{-1}$.

3.1.2 Maxswell Stress tensor

We can calculate DEP force according to Dipole model. However, if the object is placed close to the electrodes or at a high gradient electric field, the dipole model will give incorrect results. Another approach to calculate DEP force is based on Maxwell stress tensor (MST) formulation wherein the stress tensor $\vec{\vec{T}}$ is integrated over the surface of the particle:

$$\boldsymbol{F_{DEP}}(t) = \oint (\vec{\vec{T}} \cdot \boldsymbol{n}) \mathrm{d}A \tag{3.3}$$

where $\boldsymbol{n}$ is the unit vector normal to the surface. This method is regarded as the most accurate approach to derive the field-induced forces. However, due to its mathematical complexity,

application of this approach has been limited until now to the case of a homogeneous spherical particle subjected to an electrical field[53, 108, 109]. Although in many cases the expressions derived from the MST formulation agree with those obtained from the effective moment approach, some discrepancies have been reported even in a loss free medium[110, 111], and these discrepancies have been attributed to intrinsic differences between these methods.

The momentum change of a volume V of dielectric in an electromagnetic field satisfies the following:

$$\frac{\mathrm{d}}{\mathrm{d}t}(\boldsymbol{P_{mass}} + \boldsymbol{P_{field}}) = \oint_A (\vec{\vec{T}} \cdot \boldsymbol{n})\mathrm{d}A \tag{3.4}$$

where $\boldsymbol{P_{mass}}$ is the momentum of the mass inside V, $\boldsymbol{P_{field}}$ is the total electromagnetic momentum of the field, A is the surface enclosing volume V, and $\vec{\vec{T}}$ is the Maxwell stree tensor, given by

$$\vec{\vec{T}} = \varepsilon(\boldsymbol{EE} - \frac{1}{2}E^2\vec{\vec{I}}) + \mu(\boldsymbol{HH} - \frac{1}{2}|\boldsymbol{H}|^2\vec{\vec{I}}). \tag{3.5}$$

Here $\boldsymbol{E}$ and $\boldsymbol{H}$ are the electric and magnetic fields, respectively, $\vec{\vec{I}}$ is the unit tensor, and the product of two vectors without a dot denotes the dyadic product. Eq. 3.4 implies that the total force by the electromagnetic field acting on this volume V can be calculated by

$$\boldsymbol{F} = \oint_A (\vec{\vec{T}} \cdot \boldsymbol{n})\mathrm{d}A = \oint_A \varepsilon(\boldsymbol{EE} - \frac{1}{2}|\boldsymbol{E}|^2\vec{\vec{I}}) \cdot \boldsymbol{n}\mathrm{d}A + \mu(\boldsymbol{HH} - \frac{1}{2}|\boldsymbol{H}|^2\vec{\vec{I}}) \cdot \boldsymbol{n}\mathrm{d}A \tag{3.6}$$

In most DEP studies, the applied electric field is in the low frequency range (< 100MHz) for which the corresponding wavelength is at least a few meters, several orders of magnitude larger than the dimensions of typical DEP electrodes. In this case, the so-called near field approximation can be made and effects due to the fact that magnetic field components can be ignored. Then, for a general, conductive dielectric medium, the Maxwell stress tensor is

$$\vec{\vec{T}}(t) = \frac{1}{2}(\boldsymbol{DE} + \boldsymbol{ED} - \boldsymbol{E} \cdot \boldsymbol{D}\vec{\vec{I}}) = \mathrm{Re}(\varepsilon^*)(\boldsymbol{EE} - \frac{1}{2}|\boldsymbol{E}|^2\vec{\vec{I}}) \tag{3.7}$$

where $\varepsilon^* = \varepsilon + \dfrac{\sigma}{\mathrm{j}\omega}$. Only the real part of the medium permittivity $\mathrm{Re}(\varepsilon^*) = \varepsilon$ apears in the stress tensor.

For an applied harmonic electric field we usually express $\boldsymbol{E}(\boldsymbol{r},t) = \boldsymbol{E_0}(\boldsymbol{r})\mathrm{e}^{\mathrm{j}\omega t}$ and for convenience written as,

$$\boldsymbol{E}(\boldsymbol{r},t) = \mathrm{Re}(\boldsymbol{E}(\boldsymbol{r})\mathrm{e}^{\mathrm{j}\omega t}) = \frac{1}{2}(\boldsymbol{E}(\boldsymbol{r},t) + \boldsymbol{E}^*(\boldsymbol{r},t)). \tag{3.8}$$

In this notation the Maxwell stress tensor given by Eq. 3.7 is

$$\vec{\vec{T}} = \frac{1}{2}\mathrm{Re}(\varepsilon^*)[(\boldsymbol{E}+\boldsymbol{E}^*)(\boldsymbol{E}+\boldsymbol{E}^*) - \frac{1}{2}((\boldsymbol{E}+\boldsymbol{E}^*)\cdot(\boldsymbol{E}+\boldsymbol{E}^*))\vec{\vec{I}}] = \vec{\vec{T}}_1 + \vec{\vec{T}}_2 \tag{3.9}$$

where

$$\vec{\vec{T}}_1 = \frac{1}{4}\mathrm{Re}(\varepsilon^*)((\boldsymbol{E}\boldsymbol{E}^* + \boldsymbol{E}^*\boldsymbol{E}) - |\boldsymbol{E}|^2\vec{\vec{I}}) \tag{3.10}$$

is the time-averaged stress tensor, and

$$\vec{\vec{T}}_2 = \frac{1}{4}\mathrm{Re}(\varepsilon^*)((\boldsymbol{E}\boldsymbol{E}^* + \boldsymbol{E}^*\boldsymbol{E}) - \frac{1}{2}(\boldsymbol{E}\cdot\boldsymbol{E} + \boldsymbol{E}^*\cdot\boldsymbol{E}^*)\vec{\vec{I}}) \tag{3.11}$$

is an instantaneous term that vanishes under time averaging. We can readily obtain the time-averaged DEP force $< \boldsymbol{F_{DEP}} >$ on a particle from the expression

$$< \boldsymbol{F_{DEP}} >= \oint \vec{\vec{T}} \cdot \boldsymbol{n}\mathrm{d}A. \tag{3.12}$$

Consider a homogeneous dielectric medium with a complex permittivity $\varepsilon_m^* = \varepsilon_m + \sigma_m/\mathrm{j}\omega$ (permittivity ε_m, conductivity σ_m) in a harmonic field $\boldsymbol{E_0}$ of frequency ω, into which we place a spherical dielectric particle of radius r having complex permittivity $\varepsilon_p = \varepsilon_p + (\sigma_p/\mathrm{j}\omega)$ (permittivity ε_p, conductivity σ_p). Because of polarization, fields both inside and outside the particle will differ from $\boldsymbol{E_0}$, and we shall assume that they have distributions $\boldsymbol{E_2}$ and $\boldsymbol{E_1}$, respectively. The time-averaged net DEP force on the particle according to Eq. 3.12 can then be written as

$$< \boldsymbol{F_{DEP}} >= \frac{1}{4}\mathrm{Re}(\varepsilon_m)\oint((\boldsymbol{E_1}\boldsymbol{E_1^*} + \boldsymbol{E_1^*}\boldsymbol{E_1}) - |\boldsymbol{E_1}|^2\vec{\vec{I}})\cdot\boldsymbol{n}\mathrm{d}A. \tag{3.13}$$

This is the MST expression of DEP force.

3.2 Formation of non-uniform electric field

Conventionally, there are three basic types of electrodes structures as shown in Figure 3.3. By using Comsol(Femlab) software, we can calculate the electric gradients of different structures. Since the upstream and downstream electrodes geometry (Figure 3.3(a)) and the top and bottom electrodes (Figure 3.3(b)) geometry have the same result for the electric field, only a comparison between the top-bottom and planar electrodes is made. We can see that stronger E-field gradients are generated as shown in Figure 3.4(b) compared with Figure 3.5(b), therefore the top-and-bottom electrode structure performs superior to the planar array for negative DEP. Besides, the resistance of the 3D electrodes geometry is smaller than that of the planar electrodes geometry [112].

(a) Up-and downstream electrodes (b) Top and bottom electrodes (c) planar electrodes

Figure 3.3: Different electrode geometries

So far, most of DEP microchips for trapping cells are designed with planar electrodes structure. However, they still have some drawbacks since particles tend to overlap and aggregate. The electric field is smaller than that of others for the same applied voltage. Single-particle resolution only happens sporadically. Some researchers tried to fabricate the up-down stream electrodes to generate a high electric field. But it is proved that such structure is difficult to fabricate. Hence, we select the 3D structure which is based on the top and bottom configuration to overcome these drawbacks.

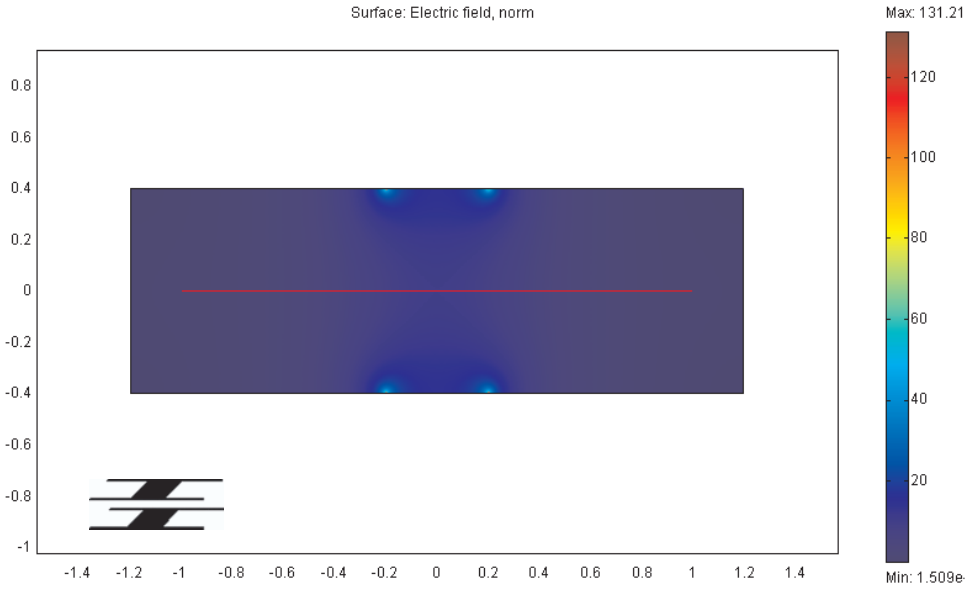

(a) Distribution of the electric field of top-bottom electrodes geometry

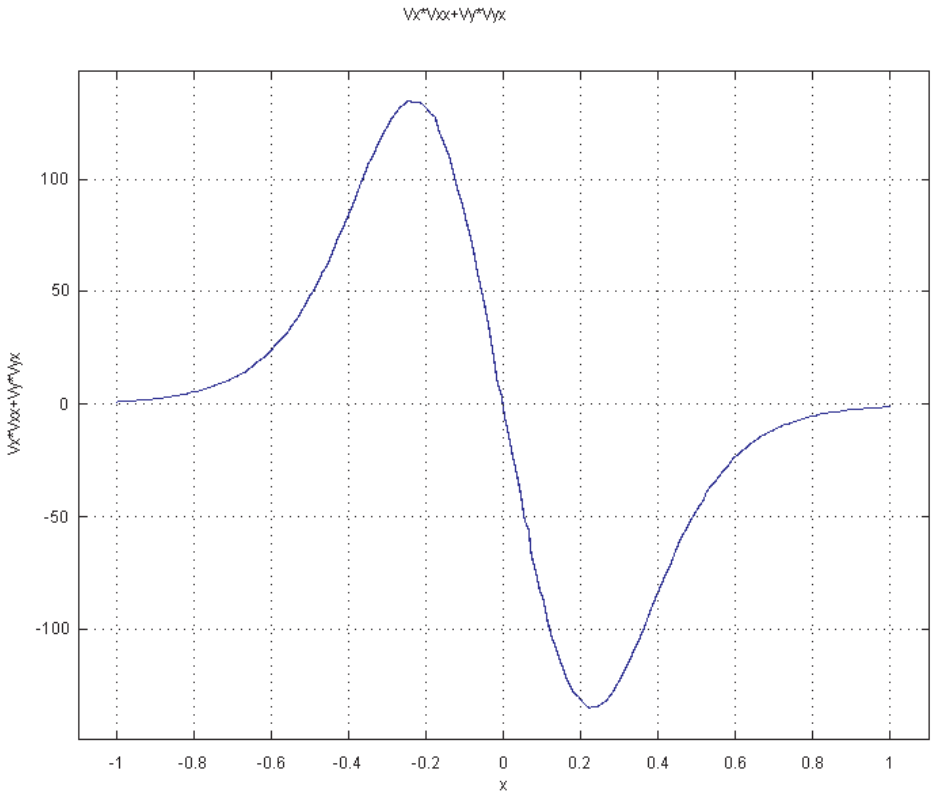

(b) Gradient of the electric field square along the line($\nabla|E^2|$)

Figure 3.4: Simulation of the top-bottom electrodes

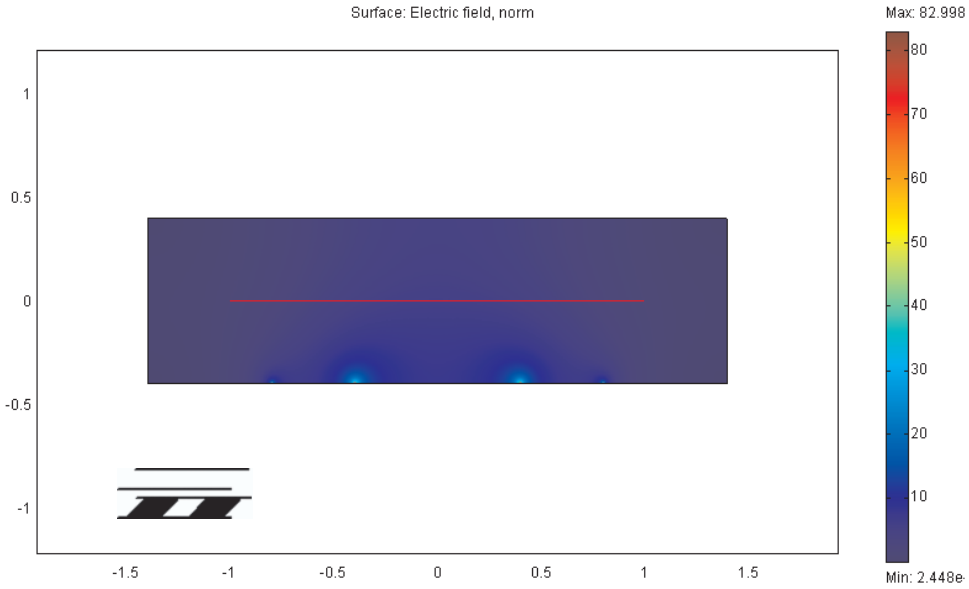

(a) Distribution of the electric field of planar electrodes geometry

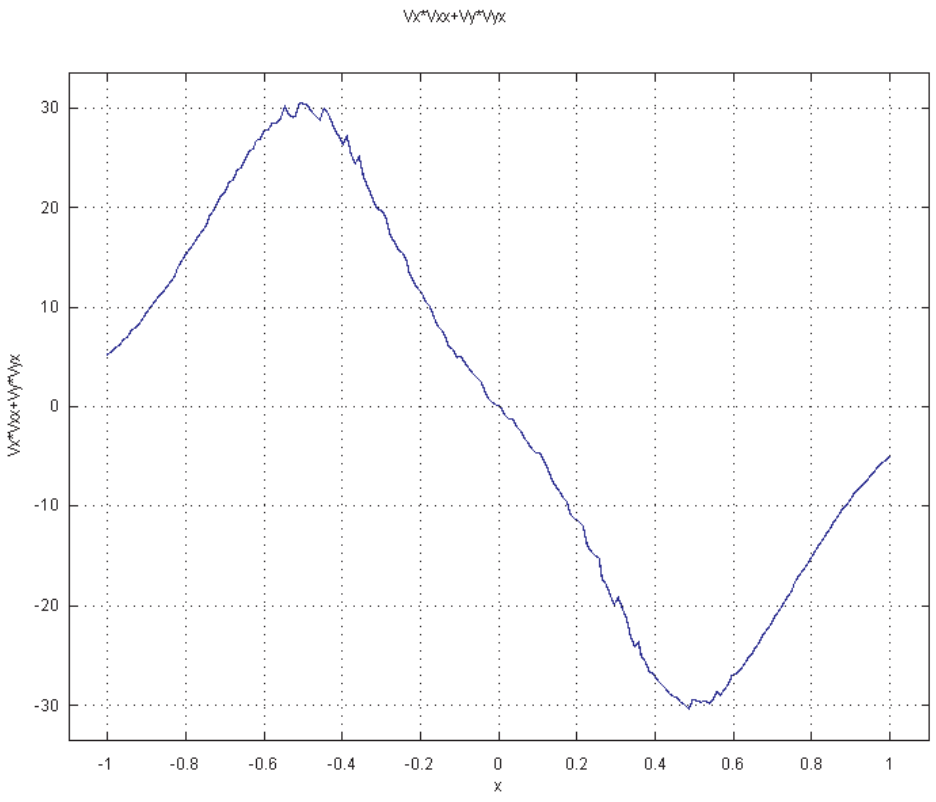

(b) Gradient of the electric field square along the line($\nabla|E^2|$)

Figure 3.5: Simulation of the planar electrodes

3.3 Electrostatic interaction

3.3.1 Motivation

So far, we have assumed that the particles are isolated entities or at least are sufficiently separated so that they do not interact with each other. However, in real situations, the interaction cannot be neglected. To design a trap for single-particle resolution, the interaction between particles should be studied. In this section, we will study the electrostatic force between two particles. The results will be used to optimize our design of dielectrophoretic microdevice.

It is shown that the DEP forces created by a pulsed electric field can be used to separate DNA molecules based on their sizes, provided the particle-particle interactions can be assumed negligible[105]. In this section, we would investigate other parameters which can affect the interaction.

3.3.2 Character of the interaction force

From basic electrostatics, we know that dielectric particle will be polarized when placed in an electric field. The field produced by the particle's induced charge rapidly decays with distance into the suspending medium, so that any long-range electrostatic interaction with other particles does not occur. The electrostatic interaction occurs only when the particles are very close.

Firstly, we will carry out the qualitative analysis of the electrostatic force with the relative change of the direction of two particles' alignment and electric field. In this part, we used MST to calculate the DEP force and the electrostatic interaction force. To simplify the analysis, 2D model is used.

As a qualitative example, we consider two particles suspended in a uniform electric field. We will calculate the interaction force between the two particles as the angle between the

two particles' alignment and the direction of electric field varies from 0° to 90°, as shown schematically in Figure 3.6. Since our design is based on the nDEP force, we only consider the case that the two particles are much less polarisable than the suspending medium, which means both of them are subject to nDEP force. In the simulation, we use Comsol 3.3 software with the following parameter: The distance between particles is $5\mu m$ (edge to edge, which is fixed in the calculation); the relative permittivity of the particle is $\varepsilon_p = 2.5$. The surface conductivity of the particle is $\sigma_p = 2e-5\mathrm{S/m}$. The relative permittivity of the medium is $\varepsilon_m = 78$. The conductivity of the medium is $\sigma_m = 3e-5\mathrm{S/m}$. The frequency of the AC power is $f = 10\mathrm{MHz}$. Under such conditions, the particle will experience nDEP force, because the CM factor is always negative as shown in Figure 3.7,

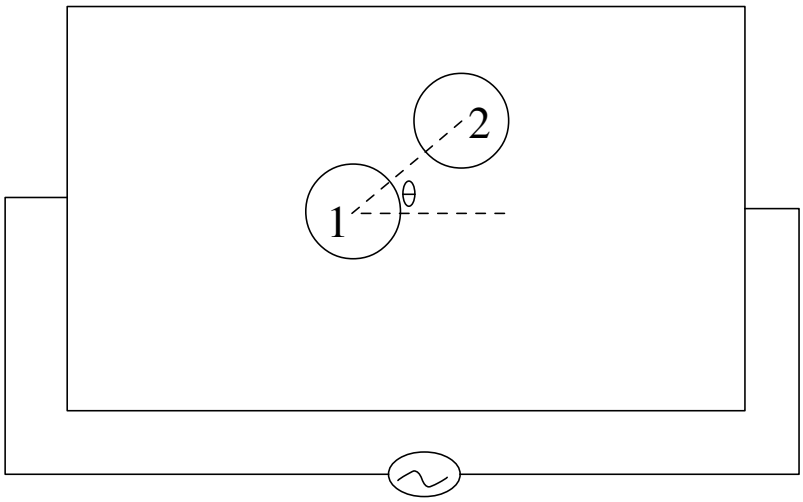

Figure 3.6: Scheme of electrostatic interaction model

We compute the electrostatic force acting on the two particles located near each other. We then perform a second calculation in which the second particle is removed and compute the force acting on the first particle. Let $\boldsymbol{F}$ be the force on the first particle when it is alone in the domain and $\boldsymbol{F}'$ when the second particle is added. Thus, the particle-particle interaction force on the first particle, due to the presence of the second particle, is $\boldsymbol{F}_{inter} = \boldsymbol{F}' - \boldsymbol{F}$. The result

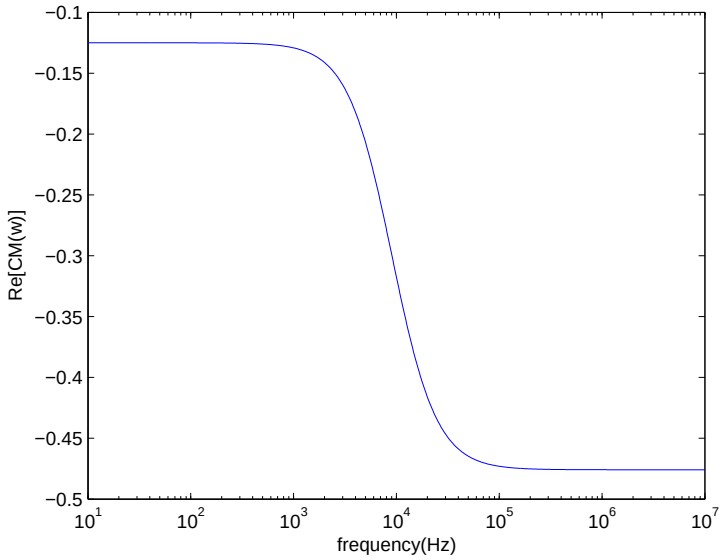

Figure 3.7: CM factor on the change of frequency

is shown in Figure 3.8.

We shall start analysis with the two special cases (0° and 90°) of this result.

We begin by considering two particles aligned along the direction of a uniform electric field. The distribution in the field magnitude around the particles is shown in Figure 3.9(a). We can see the electric field between the two particles is lower than that at the sides of the two particles. Since both particles experience negative dielectrophoresis, they will move towards the low field regions and therefore express the attractive force. In this case the particles will line up along the direction of the electric field. This can be explained easily by using dipole model as shown in Figure 3.9(b). The negative induced charge will attract the positive induced charge. Therefore the two particles tend to line up along the direction of the electric field.

Now, we consider the second case that the two particles are aligned perpendicularly to the applied field. Figure 3.10(a) shows the electric field distribution around the two particles. We find that the stronger electric field is located at the region between the two particles. Since the particles experience negative dielectrophoresis, they will be pushed away from the high field

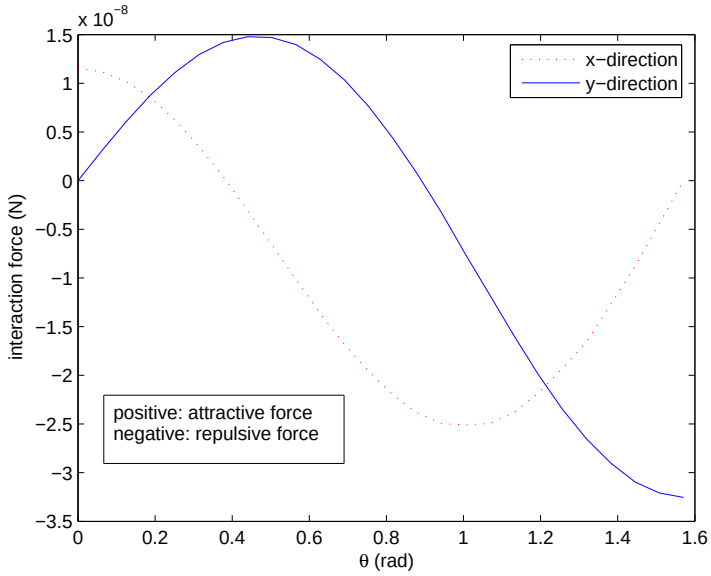

Figure 3.8: Results of electrostatic interaction between two particles

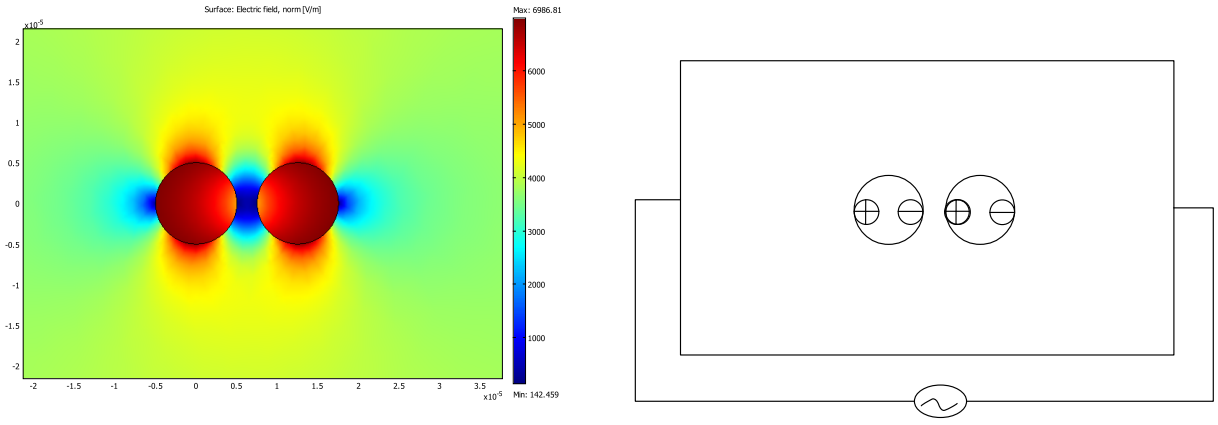

(a) Distribution of the electric field

(b) Dipole approximation

Figure 3.9: Two particles aligned along the electric field

region and therefore they express repulsive force. The same can be said similar to the analysis of the attractive force; we can use dipole model to explain these results (Figure 3.10(b)). The two parallel dipoles will repel each other due to the Coulomb's law that two charges are repulsive if the charges have the same sign.

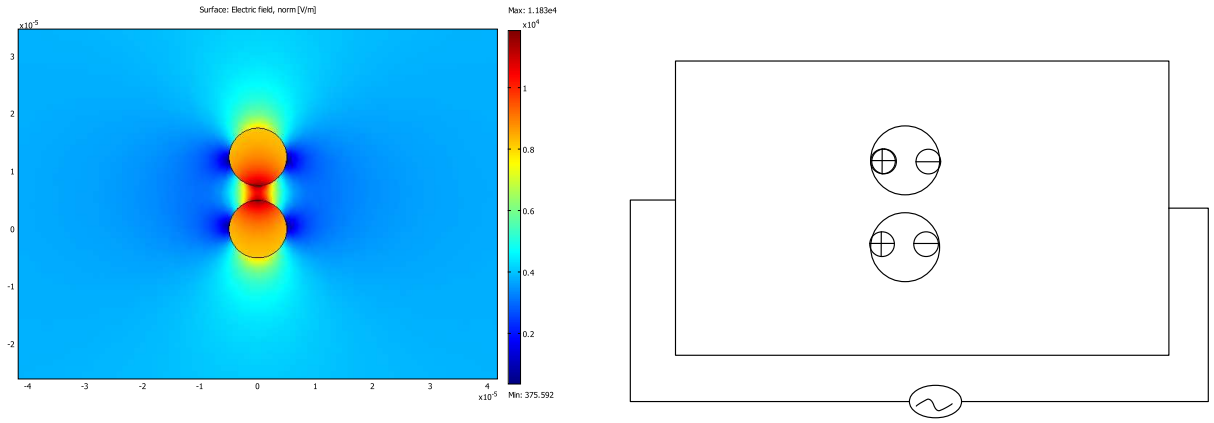

(a) Distribution of the electric field

(b) Dipole approximation

Figure 3.10: Two particles aligned perpendicular to the electric field

Between 0° and 90°, we can see that the resultant force is not only along the two particles aligned direction(Figure 3.8). There is a component force pushing the particle to one of the above two cases. However, only the 0° position is stable. This means, if there are more than two particles in the electric field, the particles tend to form a chain in the field, which is parallel to the electric field. If the particles position is 90° initially as shown above, the particles will form a chain if there are some disturbances from outside. From these calculations, we can determine the characteristic of the feature force in the experiment and improve our design based on these results.

3.3.3 Other factors affecting the interaction force

It is shown that the influence of the particle-particle interactions can be made insignificant by selecting a frequency close to the crossover frequency at which the Clausius-Mossotti factor is zero [113]. It has been studied that the particle-particle interaction depends upon the particle radius, the distance between the particles and CM factors[114]. The numerical results show that the electrostatic interaction force become more significant for the smaller particle against DEP force. Besides, the authors also claim that if the size of the two particles is fixed, the interaction will increase as the distance between the two particles decrease. Another important result is that the ratio between the interaction and the DEP force will vanish when the CM factor approach zero. This was verified using the point-dipole model and MST model[114].

3.3.4 Summary

In this section, we study the problem of electrostatic interaction between two particles. We can conclude that two same particles will be attracted to each other when they align along the electric field, and be repulsive when they align perpendicular to the electric field. Besides, according to previous works[114], we know that the interaction force is more significant against DEP force for smaller particles, and for larger CM factor.

To trap one single particle, we should reduce the attractive force. One easy way is to use larger particles to test our design since large particles' interaction force can be neglected. Another possible way of reducing the particle-particle interactions is to make CM factor small. In AC dielectrophoresis of conducting particles and liquids, it may be possible to achieve the same result by selecting a frequency such that CM factor is small. Increasing the repulsive force is another way to trap one single particle. To achieve this, we should let particles align

perpendicularly to the electric field when the particles are trapped. A third way is to change the PH value of the liquid. The conductivity of the liquid is changed once we change the PH value. This also can affect the crossover frequency. All these should be considered in the design of a particle trap with single-particle resolution.

3.4 Rotation of particles

3.4.1 Motivation

Particles in fluid experience viscous force and pressure force due to the fluid flow. These two forces act differently at different parts on the particle's surface. Therefore, there is net resultant moment on the particle giving rise to rotation until the external torque becomes zero. Particles will always rotate in a non-uniform fluid field (and a non-uniform electric field). Thus far, in DEP calculation, no one has considered the rotation of particles. In this section, we will discuss the particles' rotation in the fluid field to obtain a more complete picture of particles' motion.

3.4.2 Method

We will start with the flow of a viscous fluid in a channel as shown in Figure 3.11. In the simulation, we use Comsol 3.3 software with the following parameter: The particle's diameter is $10\mu m$ and initially placed at the bottom of the channel. (We shall keep a $0.5\mu m$ gap between the wall and particle for the convenience of calculation.) The density of the particle and the medium are both 1g/cm^3. The viscosity of the medium is $1 \times 10^{-3}\text{Pa} \cdot \text{s}$. The channel has a width in the y-direction of $W = 3\text{mm}$, a length in the x-direction of $L = 5\text{mm}$, and a height in the z-direction of $H = 40\mu\text{m}$. The direction of the flow is in the x-direction. For the computation, we shall consider the domain as between two infinite parallel plates. As such, the

problem can be treated as a 2D problem as shown in Figure 3.12.

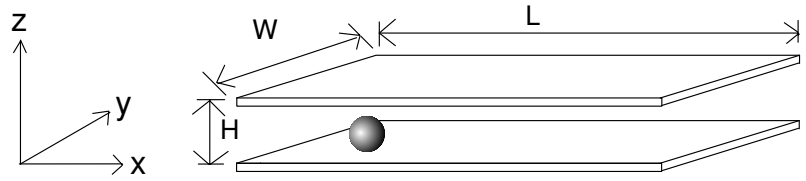

Figure 3.11: Geometry of the microdevice

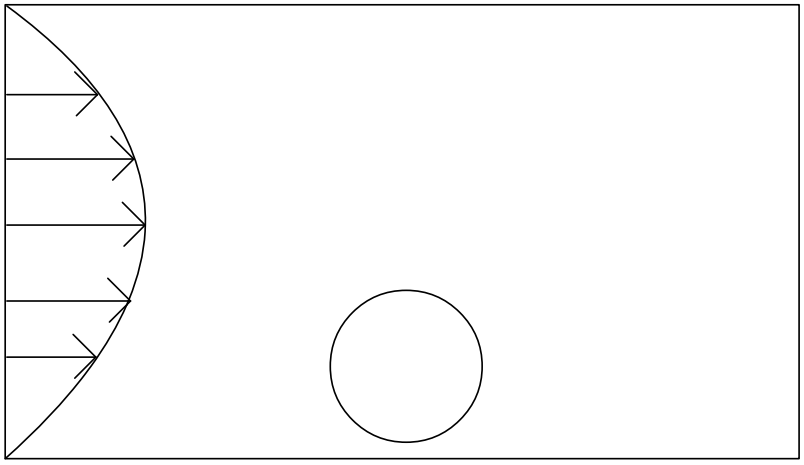

Figure 3.12: Sectional view of the microdevice

We consider a sphere that is allowed to rotate freely in the microchannel. The sphere is initially held fixed until a fully developed steady flow field is established. Then it is allowed to rotate freely due to the imposed stress on its surface. The position of the sphere is held fixed and thus, no translational motion is allowed. The sphere accelerates angularly and eventually reaches the torque-free condition for rotation. We can calculate the instantaneous hydrodynamic force by Comsol software. And acceleration can be calculated from

$$\boldsymbol{T}_{Stokes} = I\frac{\mathrm{d}\omega}{\mathrm{d}t} \tag{3.14}$$

where $I = \frac{1}{2}mr^2$ is the moment of inertia, m is the mass of the sphere and r is the radius of the sphere.(Comsol considers the 2D "sphere" as a cylinder when conducting 2D torque calculation.)

3.4.3 Results and discussions

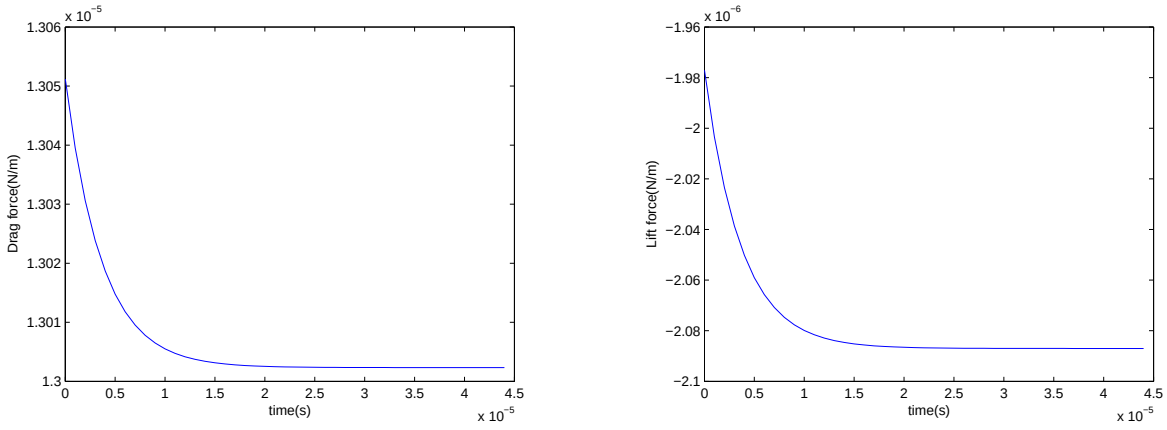

(a) Instantaneous drag force

(b) Instantaneous lift force

Figure 3.13: Hydrodynamic force during acceleration process

Figure 3.13 shows the hydrodynamic force change with time. At the beginning, there is no rotation. Particle will accelerate due to the hydrodynamic torque on its surface. When the rotation speed increases, the hydrodynamic torque will decrease. Until the hydrodynamic torque becomes zero, which means the rotation acceleration becomes zero, the particle achieves terminal rotation speed. This is the torque-free status. At this time, the hydrodynamic force becomes a constant. Figure 3.13(a) shows us the hydrodynamic force in the x-direction(drag force) versus time. We can find that the change of this curve from the beginning to the terminal condition is very small, with only a 0.4% difference in the force calculation between non-rotation and rotation cases. Figure 3.13(b) shows the hydrodynamic force in the y-direction(lift force) with time until it reaches the steady state. We find that there is a larger change to 0.5% from the beginning to the terminal condition. However, when we compare the absolute value between these two curves, we find that the lift force is very much smaller (a few times smaller) than the drag force. As we know, the DEP force is in the same order as the drag force. Therefore, we can neglect the lift force when calculating the resultant force, also neglect the rotation in the

simulation (though the rotation exits).

3.4.4 Summary

In this section, we study the rotation of particles qualitatively. The results show that the hydrodynamic force in the x-direction (drag force) and y-direction (Lift force) are not affected much by the rotation. Because the lift force is much smaller than the drag force used to balance the DEP force, it is possible to neglect the effect of rotation which greatly simplify the calculation of the hydrodynamic behavior.

3.5 Modeling of device

3.5.1 Overview

To analyze our design quantitatively, we developed some modeling tools to optimise the experimental setup and verify experimental measurement. In order to understand the behaviour of particles in DEP based microfluidic system, we developed this modeling approach to predict the trace of particles' motion. The rotating acceleration has been analyzed above. The conclusion is that the rotation can be neglected in our calculation. Here, we will study the translational acceleration. The 3D structure will be used to study this problem as shown in Figure 3.11. Voltage and flow rate are fixed. Then we can track the particle's velocity change by the following equations:

$$m\frac{\mathrm{d}\boldsymbol{v_{i+1}}}{\mathrm{d}t} = \boldsymbol{F^i_{DEP}} + \boldsymbol{F^i_{Stokes}}.$$

. From the results shown in Figure 3.14, it is clear that the acceleration process of the particle is very short($\sim 10^{-9}$m or $\sim 10^{-5}$s). Thus we can treat all the particle's motion process as a

quasi-steady process in the modeling. It is also possible to neglect gravity effect due to the fact that the density difference against the liquid and particle is very small. That is, we can consider that the gravity is balanced by the buoyancy all the time.

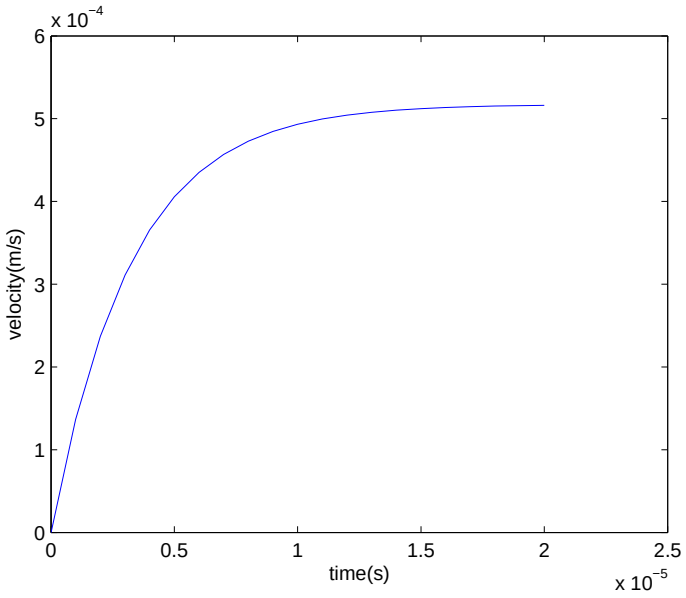

Figure 3.14: Translation velocity changes during acceleration process

To calculate the hydrodynamic force, the modeling approach uses finite element method which allows for incorporating the Maxwell Stress Tensor to calculate the DEP force. Most previous analyses only take into account the dipole approximation to the DEP force [55, 74]. However, the dipole approximation does not adequately described the physical situation at the region of null electric field or if the particle size is comparable to the extent of electric field non-uniformity [111, 115]. There has been work carried out on the particle's trajectory prediction under DEP force using the Maxwell stress tensor [116]. To extend this work, we have implemented the hydrodynamic force solver and Newton-Rhapson method to compute the particle's trajectory in the DEP-based microfluidic system.

3.5.2 Program structure

A programme was written using the Matlab software to take advantage of the connectivity with the Comsol softwere. The flowchart is shown in Figure 3.15. There are three major routines in our modeling. One is the calculation of the hydrodynamic force. The second routine is the calculation of the DEP force. We used the Maxwell Stress Tensor to calculate the DEP force. Both parts were written in Comsol software, which can translate into the finite element domain for analysis. The third part is to find the terminal velocity of particle at each position. Newton-Rhapson method was used in this part. Our code can be used to analyze 3D geometries.

All the simulations performed used the following parameters:

1. The amplitude of applied sine wave voltage is 5V with the frequency of 1MHZ.

2. The particle employed is the polystyrene bead, which has the density of 1060kg/m^3, the surface conductivity of 0.00002S/m, and the relative permittivity of 2.55.

3. The liquid employed is the dextrose solution, which has the density of 1060kg/m^3, the conductivity of 0.00003S/m, and the relative permittivity of 80. The viscosity is 0.001Pa·s

3.5.3 Calculation of DEP force

The governing equation for the electric field is

$$\nabla \cdot ((\sigma + \mathrm{j}\omega\varepsilon_0\varepsilon_r)\nabla V) = 0 \tag{3.15}$$

in which, σ is the conductivity of dielectrics, ω is the anglar velocity, ε is the permittivity, V is the applied velocity, and j is $\sqrt{-1}$.

Boundary Settings:

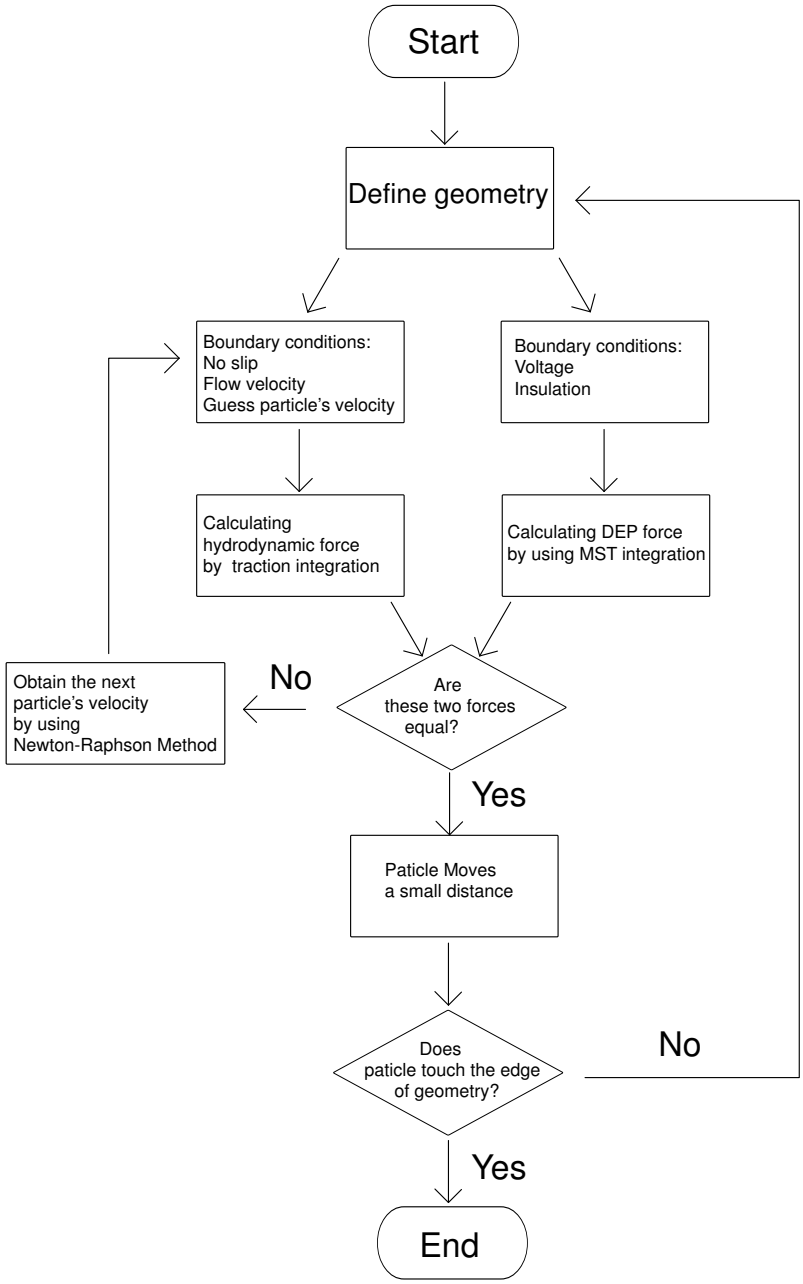

Figure 3.15: Flowchart of trace programme

Boundary	**Boundary condition**	**Expression**
Surface electrodes	Electric potential	$V = V_0$
Perimeter Surfaces	Electrical insulation	$\boldsymbol{n} \cdot \boldsymbol{J} = 0$
Internal non-electrode	Continuity	$\boldsymbol{n} \cdot (\boldsymbol{J}_1 - \boldsymbol{J}_2) = 0$

By applying the boundary conditions shown below one can then evaluate the electric potential everywhere in the system and extract the corresponding electric fields using the relation $\boldsymbol{E} = -\nabla\varphi$

Dielectrophoretic force (time-averaged)

According to Equation 3.13, we can calculate the particle's DEP force.

3.5.4 Calculation of hydrodynamic force

Stokes Flow Governing Equation is

$$\begin{cases} \nabla \cdot (-p\vec{\vec{I}} + \eta(\nabla \boldsymbol{u} + (\nabla \boldsymbol{u})^T)) = 0 \\ \nabla \cdot \boldsymbol{u} = 0. \end{cases} \tag{3.16}$$

Boundary Settings:

Boundary	**Boundary condition**	**Expression**
Inflow surface	Laminar inflow average velocity	$\boldsymbol{u} = \boldsymbol{u}_0$
Outflow Surface	Laminar outflow outlet pressure	$\boldsymbol{p} = 0$
Top and bottom surfaces	No slip	$\boldsymbol{u} = 0$
Particle surface	No slip	$\boldsymbol{u} = \boldsymbol{u}_1$
Side surface	Symmetry	$\boldsymbol{n} \cdot \boldsymbol{u} = 0$, $\boldsymbol{t} \cdot \boldsymbol{T} = 0$

Total stress tensor is

$$\vec{\vec{\tau}} = -p\vec{\vec{I}} + \eta(\nabla \boldsymbol{u} + (\nabla \boldsymbol{u})^T). \tag{3.17}$$

Hydrodynamic force is

$$\boldsymbol{F}_{fluid} = \oint \vec{\vec{\tau}} \cdot \boldsymbol{n} \mathrm{d}A. \tag{3.18}$$

3.5.5 Code validation

After verifying the validity of the code with analytical 2-D and 3-D problems, such as the parallel plate capacitor, a direct comparison with previous work on μm-sized particles was undertaken in order to further ensure the quality of the numerical method used. The values reported by Rosales and Lim [111] were used for comparison. The structure used by Rosales and Lim to calculate the strength of the DEP force consisted of a set of inter electrodes of $50\mu m$ height, $40\mu m$ diameter, and $50\mu m$ (center to center)inter-electrode spacing as shown in Figure 3.16.

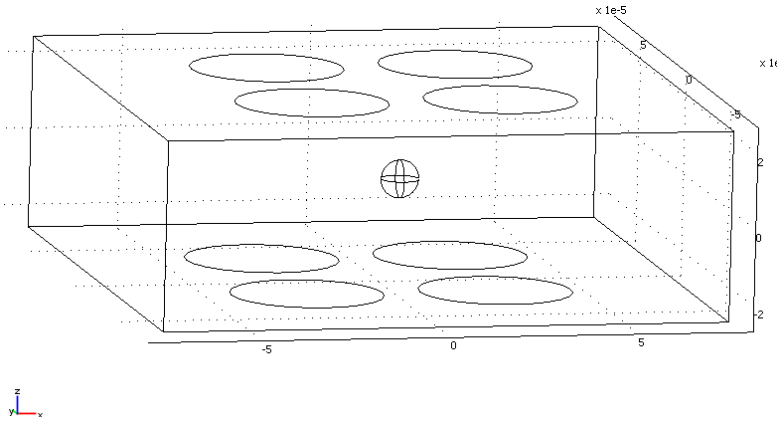

Figure 3.16: Schematic of structure

In this setup, the strongest field gradients are produced along the edges of the electrodes. A calculation of the DEP force on a polystyrene bead situated at different positions of the trap, which compares favorably with [111]. The accuracy of the solution is remarkable considering the fact that the model has no free parameter for adjustment.

3.5.6 Summary

In the numerical modeling, we used surface integration to calculate the DEP force and hydrodynamic force, which can give a more accurate result. However, the simulation is time consuming because of the repeated meshing needed in each step. Besides, we did not optimise the code for hardware usage, such as the memory usage and CPU usage. This slow the overall analysis.

3.6 Conclusion

In this chapter, we discussed the theory background of DEP-based microfluidic system. In addition, we also showed the modeling environment, which can predict the motion trajectory of particles in the device. The use of MST and traction in the force calculation makes it universal to compute the force for arbitrary geometries. In the following chapters, we will carry out some experiments to validate the model presented here. Additionally, we will optimise our design before fabrication, which will be shown in the following chapters.

Chapter 4

Size-Based Particle Sorting

4.1 Introduction

DEP has been increasingly used to sort micro-particles. In the micro-structures, to get high electric fields or gradients does not require high voltage. It is also easy to fabricate the electrodes using micro-fabrication techniques. Besides, the micro-electrodes produce forces in a range well suited for cell manipulation. Separation of cells has been carried out by many researchers based on the differences of their electrical properties. According to the different signs of the CM-factors, one sub-population experiences p-DEP and the other n-DEP [68, 69]. In such a situation, the p-DEP sub-population will be attracted to the electrodes whereas the n-DEP sub-population will be repelled away. The particles can be also separated based upon different DEP force magnitudes due to either differences in particle radius or some electrical property. In this case, the force magnitudes are of the same sign, but of different strength, allowing separation. For this method, researchers have fabricated for many different geometries of the electrodes, such as the planar parallel electrodes [79], trapezoidal electrodes [80],paired electrodes [84], convergent electrodes [117], and 3D electrodes [43, 81–83].

However, they have many drawbacks as discussed previously. The 3D electrodes are difficult to fabricate. The planar structures need a long time or a long distance to increase the resolution, and thus have low efficiency. The separation efficiency, obtained in practice is modest and there is a great need for improvement. High resolution sorting of particles in micrometers as well as in sub-micrometers domains would be of tremendous value in many areas, such as polymer chemistry, life science and material science.

In this section, a concept based on negative dielectrophoretic forces in a micro-fluidic channel for particle sorting is proposed. The size of the grid can affect the resolution. We do not need a long distance or a long time to improve the resolution. This will be shown in the simulation result.

4.2 System design

The DEP force increases in proportion to the field intensity and the gradient. In order to realize separation of micro-particles, it is necessary to form a local high-field region in the electrode system which can be switched on on demand. Figure 4.1 depicts the construction of a three-dimensional grid-like electrode system for this effect. Both sets of electrodes are parallel strips. Figure 4.2 shows the expected results. As shown in Figure 4.3, the flow direction is along the diagonal. The larger particles would move along the first horizontal electrode. The smaller particles would move along the second horizontal electrode, and the smallest particles would move along the third horizontal electrode. The space between the tapered electrodes is like a gate to control the entrance of the different sized particles. The mechanism will be shown in the later part.

The device consists of two glass plates, on which strip electrodes (made of ITO) are fab-

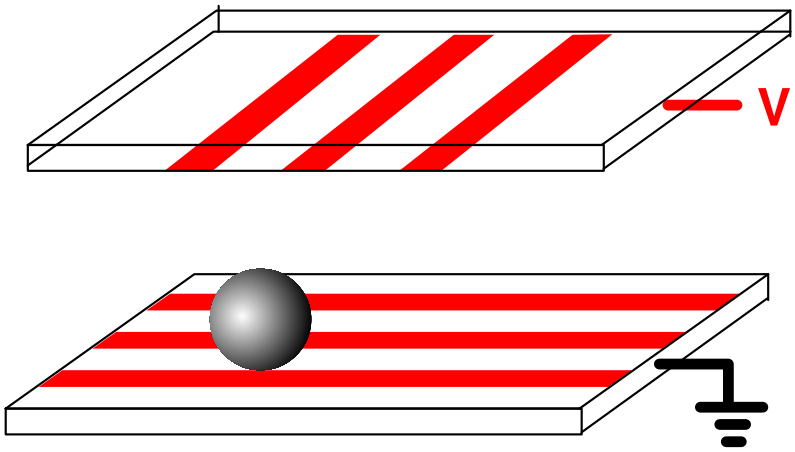

Figure 4.1: Schematic diagram of grid electrode system

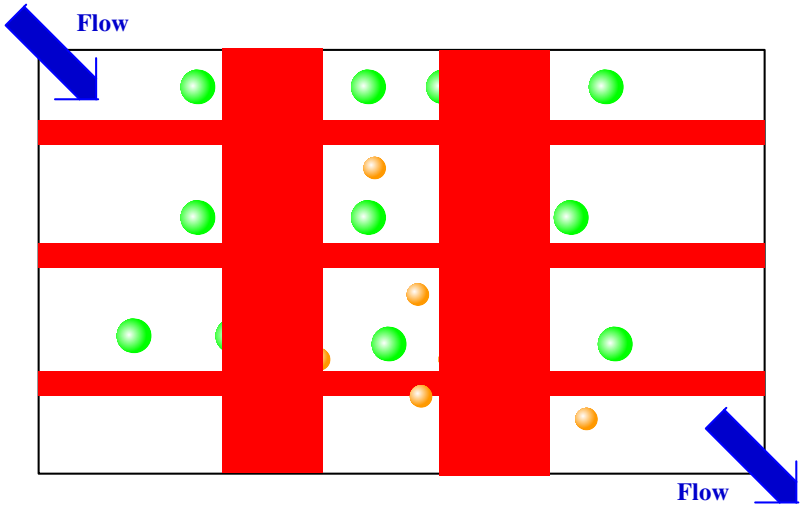

Figure 4.2: Schematic diagram of sorting result

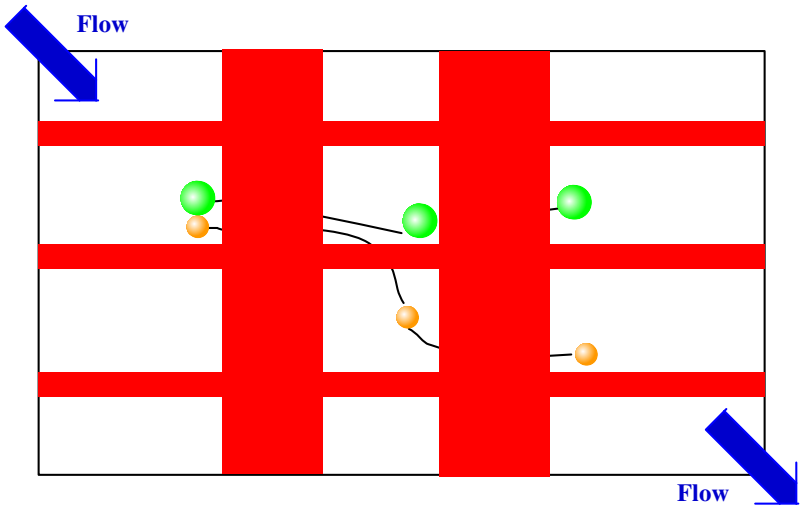

Figure 4.3: Different sized particles trace

ricated. The top and bottom glass plates are placed together with a spacer between them so that their electrodes face each other and cross at right angles to form the grid. The space between the two glass plates serves as a chamber which is filled with particle suspension. The width and horizontal and vertical spacings of the electrodes should be of the same order of size as the particle to be handled. When both the top and bottom electrodes are energized by appropriate AC signals, high-field regions will be developed at their intersections. Such similar electrode structures are widely employed in flat-panel visual display systems, in which the space between the two glass plates is filled with liquid-crystal medium and the strip electrodes are made of materials such as ITO, which possesses both high electrical conductivity and optical transparency. Also, as a DEP electrode system, ITO electrodes have the advantage of allowing visual observation of a particle's behaviour in three dimensions. If a particle's behaviour is observed using a microscope, for example, then the top electrodes are located between the particles and an objective lens and will not disturb the optical path if their optical transparency is good.

4.3 Modeling

Figure 4.4 shows the electric field distribution. We can see that the minimum electric field exists in between the two bottom electrodes. This means that once the particle enters this grid structure, it will be pushed down to the substrate. Hence, we can choose the starting point of the simulation as the middle location between the two bottom electrodes. Figure 4.6 shows 0-DEP force iso-surface in Z direction. It can be found that there are two different areas in Figure 4.6 separeted by the 0-DEP force iso-surface: particle will experience DEP force towards substrate when it is further to the electrode while particle will experience DEP force away from substrate when it is close to the electrode. If the particle's position is in the area where the DEP force is towards substrate, the particle will move along the electrode. If the particle's position is outside this area, the particle will move away from substrate and go across the electrodes.

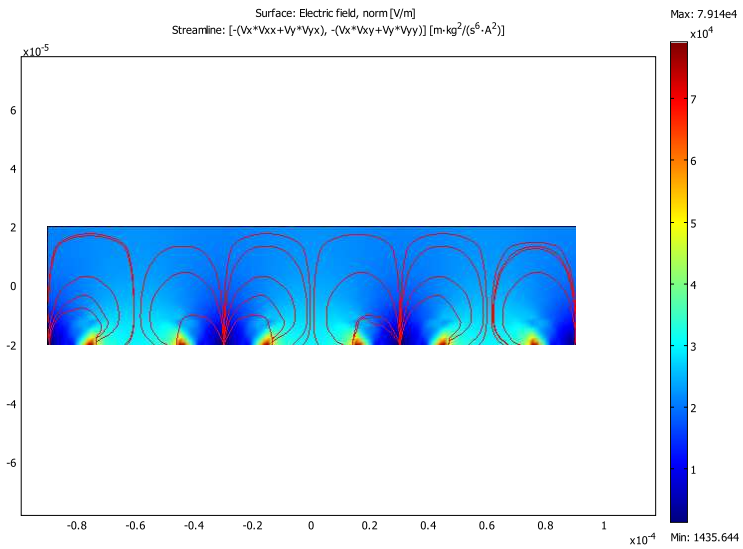

Figure 4.4: Electric field distribution

First we study the direction of fluid flow(θ in Figure 4.5) for this device with all other parameters fixed. We simulated the particle's trajectory for different directions ($\theta = 30°$,$\theta =$

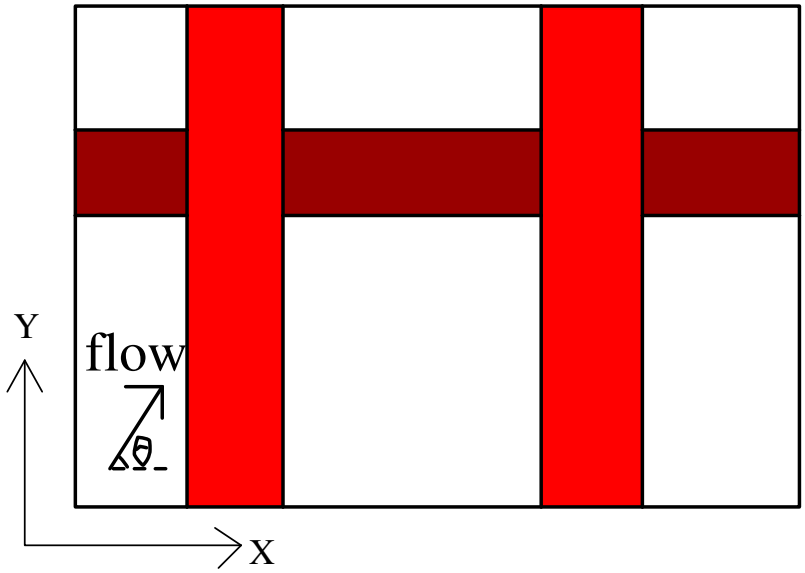

Figure 4.5: Flow direction

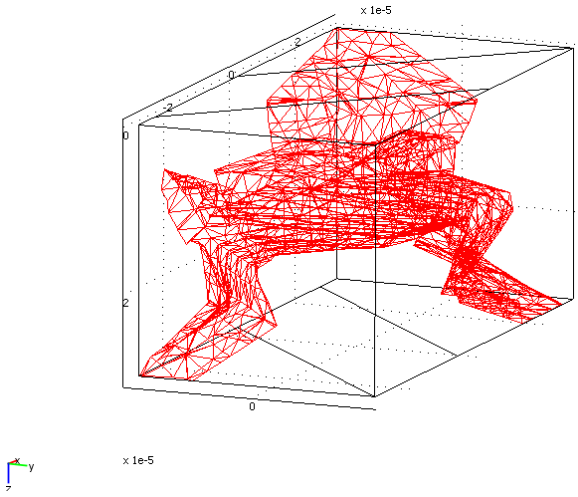

Figure 4.6: iso-surface of 0-DEP force in Z direction

45°,$\theta = 60°$) as shown in Figure 4.7,4.8,4.9. For a given flow rate, we can see that the particle's behaviour is different for the three different flow directions. Particles tend to go along the bottom electrodes and no z-direction movement when $\theta = 30°$ (Figure 4.7). This is because the hydrodynamic force in the y direction is very small compared to that of DEP force. Then there is an 'equilibrium' position in the y direction between the hydrodynamic force and DEP force for this particle. When $\theta = 60°$(Figure 4.9), particles tend to cross and migrate towards the top electrodes. This is because the hydrodynamic force in the y direction is larger than that of DEP force. When the particles move towards the horizontal electrode, the DEP force in the y direction is not able to balance the hydrodynamic force. As a result, particles move to the edge of horizontal electrode. At the meantime, the DEP force in the z direction will increase and push the particles up and towards the top substrate. As the particles move up, the DEP force in the x direction will increase and prevent them from moving in the x direction, and hence only movement is allowed in the y direction. When $\theta = 45°$ (Figure 4.8), the hydrodynamic force in the x direction and y direction are comparable to that of DEP force in this arrangement. Hence, particles tend to move along the flow direction. Here we can see that the particles' behavior is due to the change in the hydrodynamic force in the x-direction and y-direction. To optimize the direction of flow (θ), we should consider the hydrodynamic force in the x-direction ($\propto \cos\theta$) and y-direction ($\propto \sin\theta$) on a particle. The product of these two factors provides a measure of effectiveness of the microarray and varies as $\sin 2\theta$, which is maximum at $\theta = 45°$.

The spacing,L, between the electrodes is another important factor for consideration. We shall compute for $10\mu m$-particle and $5\mu m$-particle. Figure 4.10 shows the calculated results. For a given spacing between two electrodes, there exists a maximum flow rate to keep the particle moving along the bottom electrode without crossing it. Figure 4.10(b) shows the relationship between the maximum flow velocity and the electrodes' spacing for a fixed voltage. We can

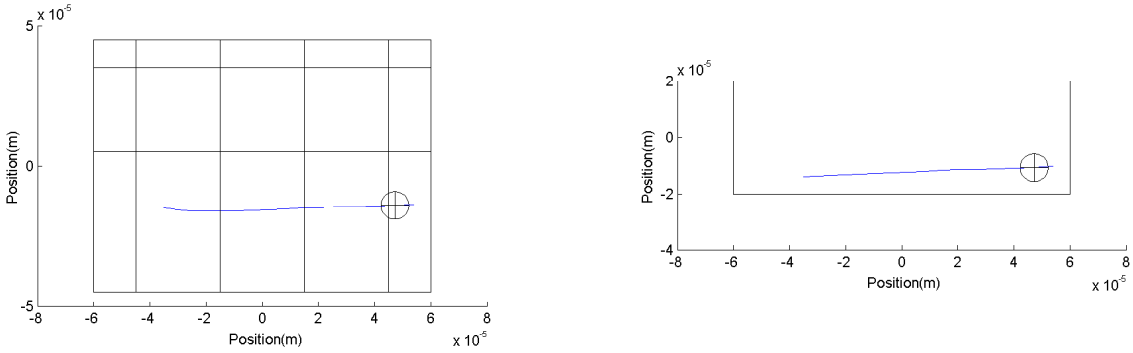

(a) Top view of the trajectory (b) Side view of the trajectory

Figure 4.7: Particle's trajectory ($\theta = 30°$)

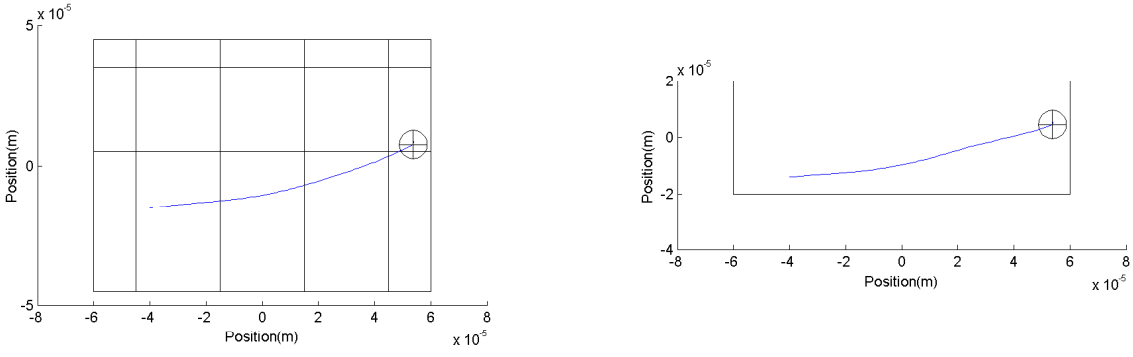

(a) Top view of the trajectory (b) Side view of the trajectory

Figure 4.8: Particle's trajectory ($\theta = 45°$)

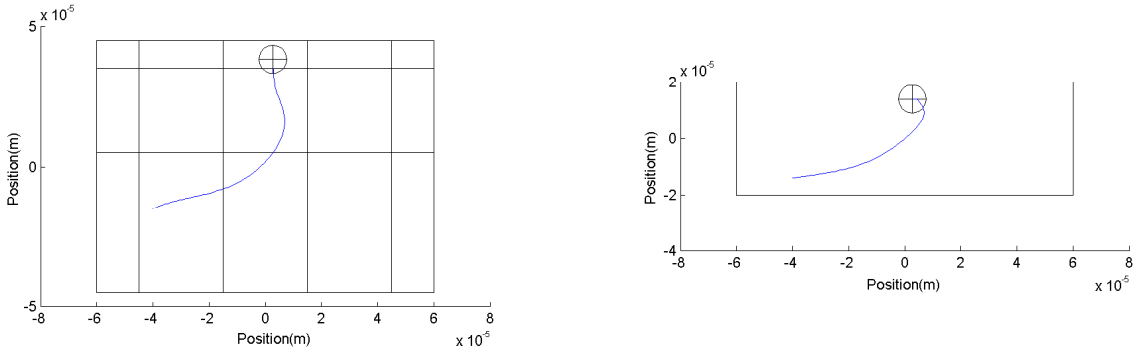

(a) Top view of the trajectory

(b) Side view of the trajectory

Figure 4.9: Particle's trajectory ($\theta = 60°$)

see that the larger the spacing, the lower the flow velocity, to keep the particles following the bottom electrode. This is because as the separation increases, the electric field becomes weaker. Consequently, the particle will find it easier to go across the bottom horizontal electrode, and then will be pushed upwards due to the increasing DEP force in the z direction. When the particles reach a certain height, it will move across the bottom electrode, instead of following the direction of the bottom electrode. As a result, we can improve our design as shown in Figure 4.11. With tapered electrodes, different space can sort different sized particles.

Next we maintain a constant spacing of $50\mu m$. The simulated trajectories for the $10\mu m$ and $5\mu m$-diameter particles are shown in Figure 4.12. From Figure 4.12(a), we can see that the particle tends to go across the horizontal electrodes. Under the same condition, the $10\mu m$-particle moves along the horizontal electrode. After a space of one grid, we can see that the $10\mu m$-particle and $5\mu m$-particle are sorted into two streams.

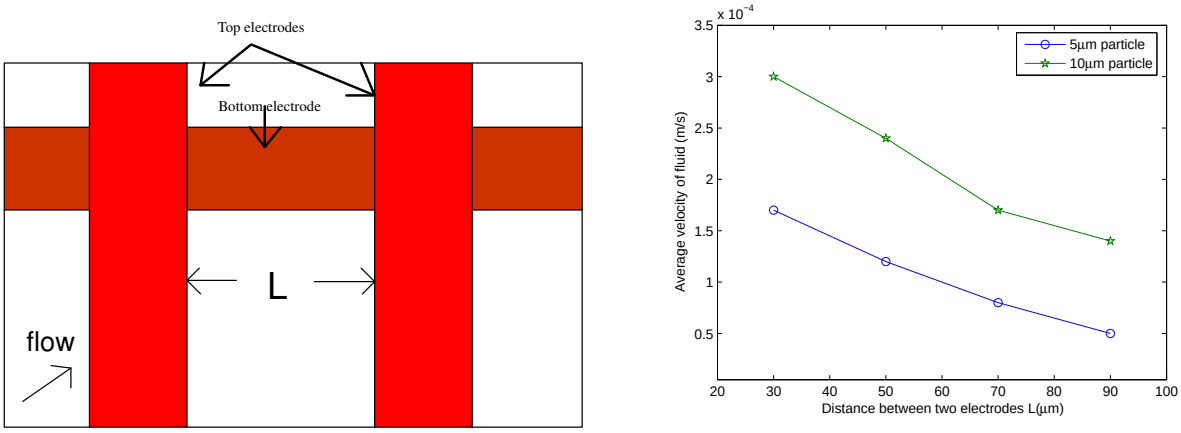

(a) Top view of schematic

(b) Critical flow velocity varies distance between two electrodes

Figure 4.10: Model predictions

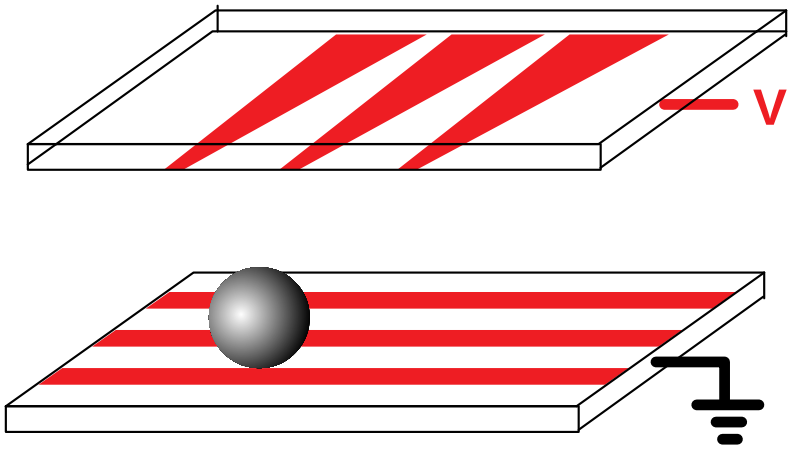

Figure 4.11: Schematic diagram of grid electrode system

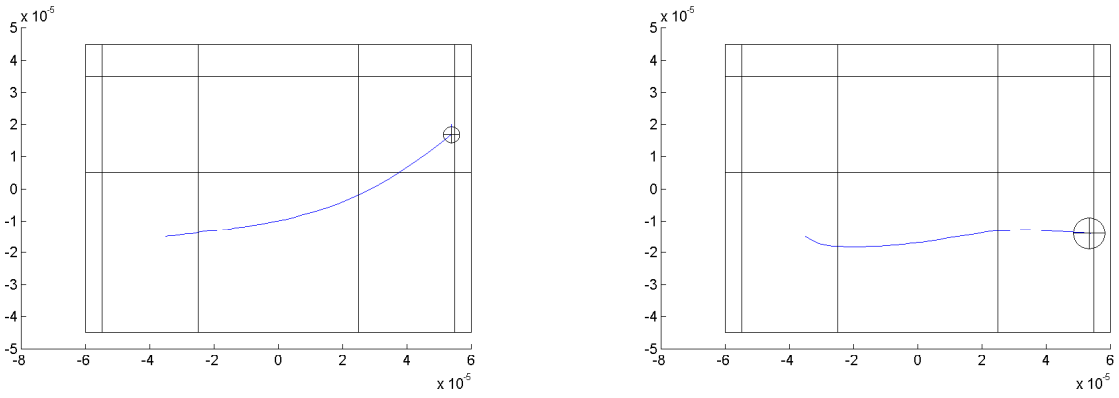

(a) The trajectory of small particles $R = 2.5\mu m$ (b) The trajectory of large particles $R = 5\mu m$

Figure 4.12: The trajectory of different sized particles

4.4 Fabrication

The fabrication process for making such a sorting device essentially involves normal photolithography followed by the etching process. The fabrication process flow for making the grid electrodes is shown in Figure 4.13 and Appendix C.1. Line edge roughness(LER) is very important in this fabrication. The electrodes will be short if LER is worse. This factor is affected by PR thickness, UV dose, etch time and etch solution. To run different split of experiment, we can get the optimization of these parameter as following.

4.4.1 ITO Etching

The strip electrodes were fabricated by etching the ITO coating on the glass substrate. Firstly, a layer of photoresist AZ2001 was spun onto the ITO glass at a speed of 2500rpm, resulting in a 1μm-thick film. Following the coating, soft-bake was done on a hotplate for 2 minutes and followed by exposure to UV light. After exposure, the sample was developed in the AZ400K solvent. Following that, the ITO etcher (mixture of hydrochloric acid, ferric chloride and water in proportion) is chosen to etch the electrode pattern. The ferric chloride is used to increase the

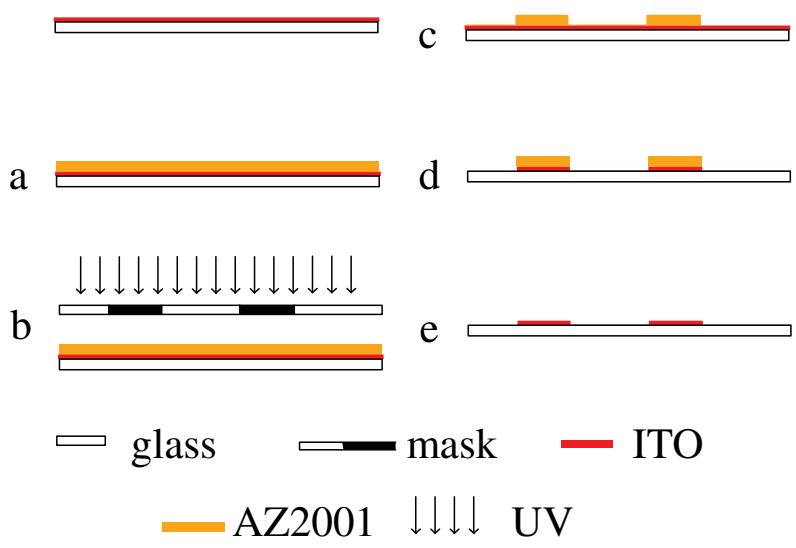

Figure 4.13: Fabrication process of the grid electrodes

etching rate. Finally, the unexposed AZ2001 was removed by acetone, leaving an ITO electrode pattern. The electrical resistance between neighbouring electrodes was higher than 10 M. The ITO strip electrodes were connected to the external lead wires using electrically conductive epoxy resin glue. The finished electrodes DEP chip is shown in Figure 4.14.

4.4.2 Packaging

This is a rectangular flow chamber with $W \times L \times H = 3\text{mm} \times 6\text{mm} \times 40\mu\text{m}$, formed by double sided tape attached on the ITO glass temporarily, as shown in the Figure 4.15. The advantages of using double-sided tape is for the ease of patterning and for the required thickness between the two pieces of ITO glass. But it can only be used for a short period. If the micro-device is to be used for a long period, glue would be used to seal it.

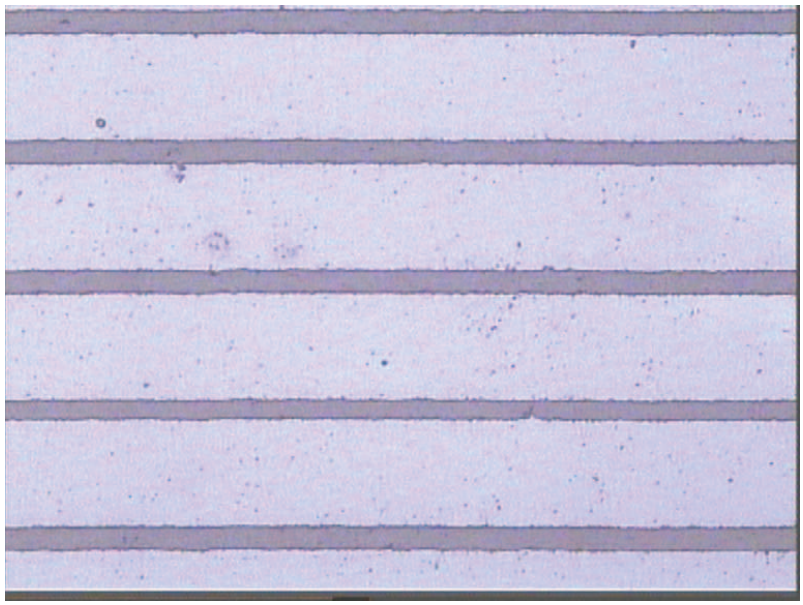

Figure 4.14: Finished electrode geometry

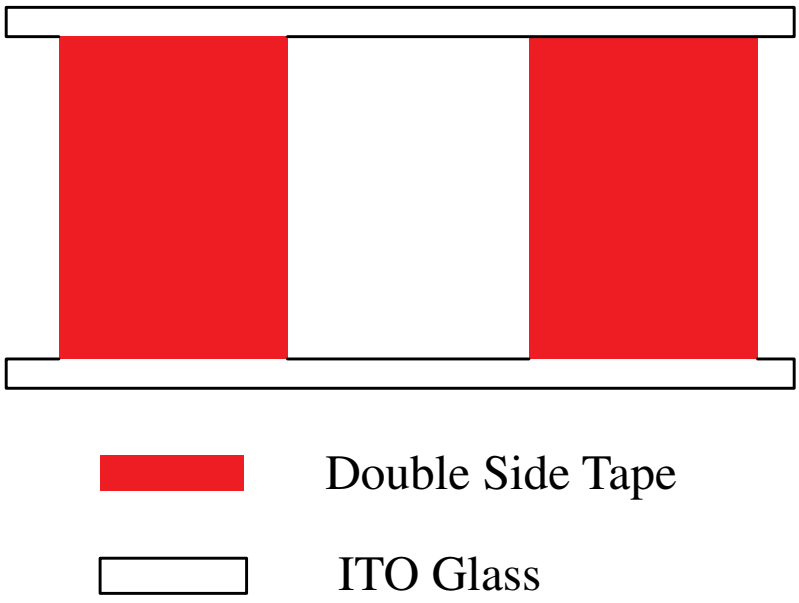

Figure 4.15: Schematic diagram of bonding process

4.5 Methods and Material

Instead of using living cells as test particle, polystyrene beads are used for preliminary studies. The reason for this is that during the verification stage it is important to minimize variations in the test parameters so that the accuracy of the models can be rigorously determined. This is possible using beads, which have accurately determined physical and electrical properties. The materials and methods used in test of the micro-device are described in detail in the following section.

4.5.1 Experimental system

Fluidics

The 1ml syringe filled with beads suspension was placed on a syringe pump, which can be controlled by computer. Fluid inlet and outlet holes of 1.05mm diameter were drilled on the top glass slide. The output was connected to the 1mm-outer-diameter needle via silicon tube. The 0.8mm-inner-diameter tubing connected to the outlet on the flow chamber top was connected to the waste disposal unit.

Optical system

An inverted fluorescence microscope was used in these experiments along with a video camera to capture the particles' motion. The CCD camera was connected to a DVD recorder, which can record analog signal. The optical system is shown in Figure 4.16.

Figure 4.16: The optical system setup

Electrical excitation

Sine wave excitation at 10MHz was generated by a four-channel signal generator. This signal generator can generate four phase related waveforms. One set of electrodes were set to ground whereas the other electrodes were set to 20V(peak to peak voltage). The signal was measured using a digital oscilloscope. The generator is shown in Figure 4.17

4.5.2 Material Preparation

Indium-Tin Oxide(ITO) glass

ITO glass substrates(Unpolished Slides $8 \sim 12\Omega/\square$ 50×75mm) were used. Before fabrication, they are cleaned according to the following steps:

1. The ITO substrates are placed in a beaker and ultrasonically cleaned for 20 minutes with acetone.

2. Subsequently substrates are rinsed with plenty of deionized water and dried, using ionized

Figure 4.17: The electrical excitation setup

nitrogen gas gun.

3. After that the solvent is changed to absolute ethanol and again exposed for 20 minutes in the ultrasonic cleaner.

4. Finally, oxygen and argon plasma are used to clean the substrates for 5 minutes.

Stock solutions

Bead stock solutions are made of 18.2M$\Omega \cdot$ cm deionized water with 0.01wt% Tween 20 and glucose(16%). The glucose is added to bring the solution's gravity to 1.06g/cm^3, which is the same as that of beads, so that gravity effect can be neglected. Tween 20 is used to prevent particle adhering to the substrate. Solvent's conductivity is measured using a conductivity meter before each use.

Beads

Polystyrene beads, with density of 1.062g/cm^3, of five different bead diameters are used. They are 3.0μm (5% std. dev.), 5μm (5% std. dev.), 9.9μm (5% std. dev.), 8μm (5% std. dev.), and 20μm (5% std. dev.). 0.1ml of each bead solution is resuspended in 10ml of stock solution. All solutions with beads are refrigerated and used within one weeks.

Measurement of the chamber height

We measured the flow chamber height with a microscope by focusing on the electrodes on the bottom ITO glass and then focusing on the top ITO glass. The difference between the two focused points therefore determined the chamber height.

4.6 Results

Experimental results using single-sized particle suspensions agreed well with the theoretical model. For a given device, when we keep the voltage as 7V, at the lower flow rates(less than 120μl/h), all the beads(5μm) moved along the electrodes. When the flow rate is increased, the particles move past and across the bottom electrode. This agrees with our earlier simulation results.

Figure 4.18 shows the result of particle sorting of based on three particle sizes. The fluid flows from the left-top corner to the right-bottom corner. In this experiment, the flow rate was 15$\mu ml/h$ and the voltage was 15V. We can see the larger particles(20μm) moving along the upper horizontal electrode while the smaller particles(10μm) move along the lower horizontal electrode. And the smallest particles(5μm) are not blocked by these two electrodes, and hence move to the next electrodes.

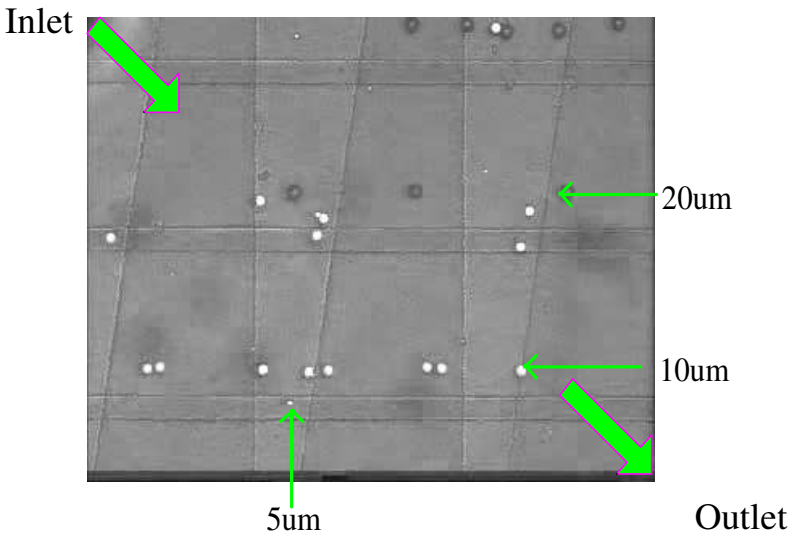

Figure 4.18: Experimental result of sorting particles of three sizes(20μm, 10μm, 5μm)

Figure 4.19 shows the comparison between the experimental result and simulation result. The match between the simulation results and experimental results in Figure 4.19 has validated the model. It appears that the difference is larger when the flow rate is higher with accompanying greater experimental uncertainty. The major cause of this mismatch/discrepancy lies in the difficulty to control very accurately the fluid flow. The larger the flow rate, the higher the uncertainty. Another finding is that almost all the experimental data have the same parallel shift with regard to the simulation results. This may include numerical error, which is analyzed in Appendix B. For example, in calculation, we assumed the temperature of experiment is a constant and no variations between measurement results and actual device. These factors contribute such an "offset" error. This error can be up to 18.4% (for the $10\mu m$ particle). In addition, although the symmetry of the ideal electrode structure precludes any substrate-liquid material interface or charge relaxation effects from affecting the electric fields, the actual physical situation could have asymmetries that cause these effects to appear. In this design, the distance between the two electrodes (L) is very important since it will affect the resolution. A

final source of error could be that heat generation causes inhomogeneities in the electrical properties of the system, which could alter the electric fields. To remove this final source of error and to include the inter-facial effects in the non-symmetrical electrode geometries, it is then necessary to calculate the electric field while taking into account frequency and temperature effects; this is for future work.

As expected, the small particles passed through the electrode easier. In the experiment, we can sort two groups of particles with 20% difference in size. Theoretically, the device can separate any two different particles based on size and material. Separations of particle of $< 1\mu m$ are difficult due to the fact that Brownian motion may play a role and high frequency is also needed because of high surface charge and conductivity.(For larger particles, these effects can be neglected. However, channel height will limit the particle's size.)

4.7 Conclusions

In this section, a three-dimensional grid-like electrode system has demonstrated its potential for sorting particles of different size using negative dielectrophoretic force. This DEP-based micro-fluidic device creates a body force on solid micro-particles to move them across electrical barriers. The design is simple and can be easily fabricated. In this design, we use top-bottom electrodes structure, which increases the electric field as compared with the planar electrodes structure. In addition, we do not need any special alignment during packaging. The modeling tool was further verified experimentally by measuring the flow rate and the applied voltage. Using this sorter, we can achieve sorting with a resolution of 20% difference in size ($8\mu m$ and $10\mu m$) in the experiment. This system could find useful applications in the biomedical and biotechnological sciences. It could be incorporated into laboratory-on-a-chip devices that

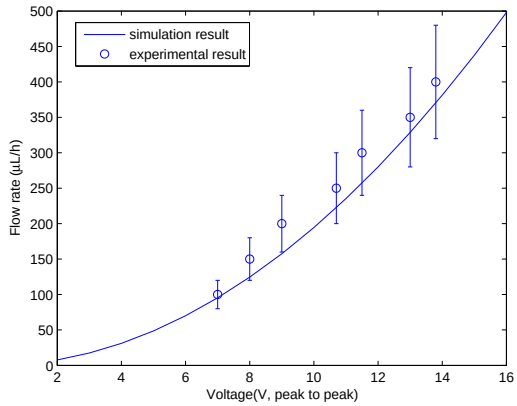

(a) $5\mu m$-particle, $L = 30\mu m$

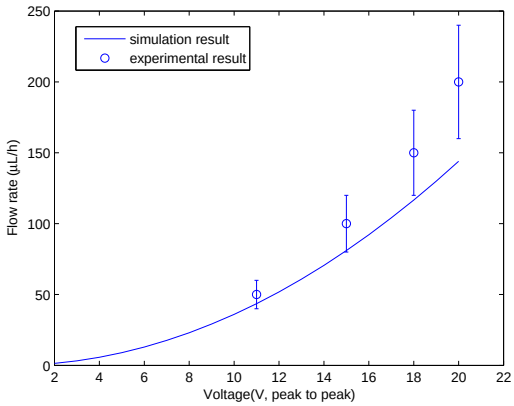

(b) $5\mu m$-particle, $L = 90\mu m$

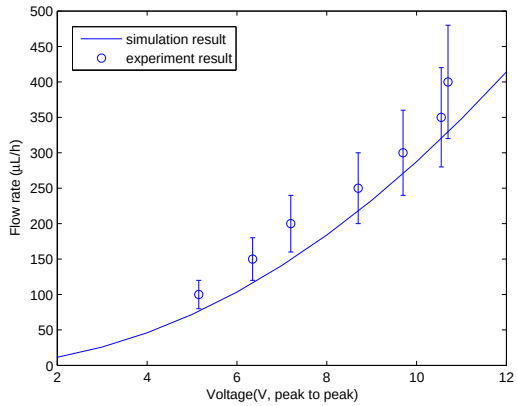

(c) $10\mu m$-particle, $L = 30\mu m$

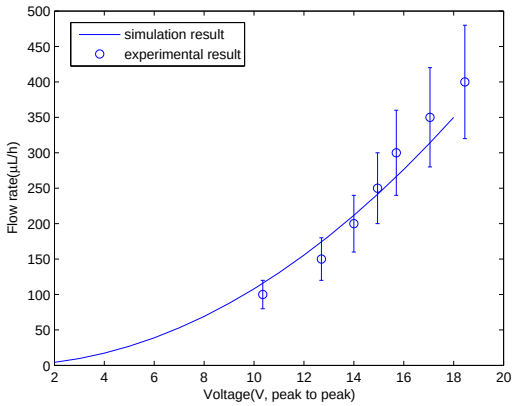

(d) $10\mu m$-particle, $L = 90\mu m$

Figure 4.19: Comparison of experiment and simulation for critical flow rate

employ micro-electrode structures for the electro-kinetic manipulation and characterization of micro-particles.

Chapter 5

Microwell for Single Particle Trap

5.1 Introduction

Micro-patterning of single cells is used to study single-cell physiology in which these cells can interact with other cells or agents introduced into the device. The present microarray can be used for cell patterning directly. Cell patterning are used to manipulate cell-cell interactions [118–125]. Cell patterning can also be used to study cell-matrix interactions [126–128]. Also, cell patterning can be used for image-based cell selection. In addition, cell patterning has the potential to improve device efficiency like the cell-based bio-sensors -using living cells as sensing element for applications like toxin detection [129] and defense monitoring [130].

In this chapter, we introduce a method that utilizes negative dielectrophoresis (nDEP) force generated by inter-digital electrodes to trap polystyrene (PS) beads. Multilayer electrodes DEP chip is used for single-particle trap. The results show the remarkable capability of positioning and registration of particle trapping with single-particle resolution. This design introduces many advantages. The addressable control with multiplexing technique allows large array and small control panel. This provides flexibility. Many biological experiments can be conducted

on this device. Firstly, the surface of particle can be modified in solution to present various functional chemical groups to facilitate binding of bio-molecules via mechanical means like rotational flows to enhance the efficiency of chemical reactions. Secondly, particles made of various materials such as polystyrene, silica, metal or metal oxides can be used for a variety of bio-applications. For example, an assembly of quantum dot encoded particles can facilitate the performance of multiplexed biological assays. Finally, this device has the potential for addressable control. This is a dynamic device. It has a chamber so that external flow can be linked to the device. The number of trapped beads per well depends on the dimensions of the micro-well and the relative strengths between the nDEP force and hydrodynamic force. The SU-8 micro-wells were fabricated by photo-lithography, and the electrodes by wet etching of ITO glass. PS beads with diameters of 10μm and 20μm were used to validate the design. As such, we are able to ascertain the critical relationship between the applied voltage and the flow rate for the beads to be trapped. A high density trapping of single bead in the micro-well array was also realized. Numerical analysis was carried out to study the mechanics and performance of trap. Good correlations between the simulation and the experimental results were obtained.

5.2 System design

Biological detection normally takes a long time, and living cells usually can not tolerate AC power applied for a prolonged period. To eliminate these drawbacks, a particle trap chip with 3D micro-structure array based on negative DEP dragging force is fabricated via photo-lithography. Particles can be held by DEP force and trapped in the concave micro-structures array. Furthermore, due to adhesion between cell and the surface of micro-structure, the AC power can be switched off for long-term biological investigation under continuously supplied

culture medium. The fabrication process and preliminary results are discussed in the following session. The structure of DEP chip consists of ITO top electrode, flow chamber, middle electrode on SU-8 surface and SU-8 layer with micro-cavity array. The multilayer electrodes DEP chip consists of three parts, as shown in Figure 5.1. The middle part consists of a 3D micro-structures array with many cavities and middle electrode for DEP, which are made of thick photoresist (SU-8), and metal layer (Ti), respectively. The opening of the micro-cavity is 30μm. Figure 5.2 shows the expected result. From Chapter 4, we know that the particles will go along the bottom electrodes and be pushed down by the DEP force. In the mentioned figure, particles are trapped in the well. If another particle comes along, it will go straight through without being trapped because the well is already filled. It has been shown in one paper[131] that the well has reached its maximum efficiency with a depth equal to 1.5 times the particle diameter, and increasing it further has no effect on the trapping strength. In this work, we will make the device with the different depths to test our design. To further validate our design, we will also conduct the test with the different channel heights.

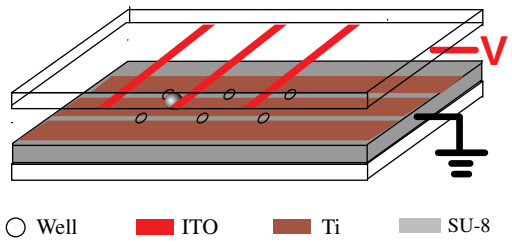

Figure 5.1: Schematic diagram of 3D electrode system

5.3 Modeling

A 3D model of this multi-electrode DEP chip was analyzed with the COMSOL software shown in Figure 5.3: the width of electrode is 50μm; the width of channel is 80μm; the diameter of

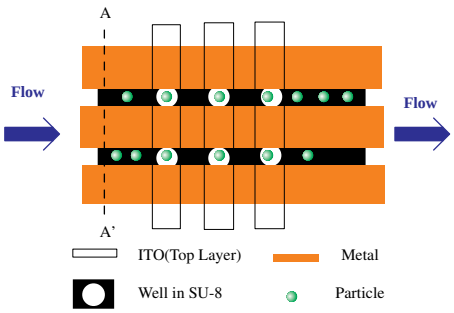

Figure 5.2: Schematic diagram of trapping result

particle is 20μm; and channel's height is 40μm. To study the effect of depth, we vary the depth of the well(H). For the DEP simulation, a 20V(p – p) AC signal is applied on the top and middle electrodes at 1MHz. For the results shown in Figure 5.4, the highest electric field was near the edge of the middle electrode. The SU-8 micro-cavity possessed the lowest electric field. As such, the particle will move away from the edge of middle electrode by the negative DEP force and get trapped into the SU-8 cavity also due to the negative DEP force.

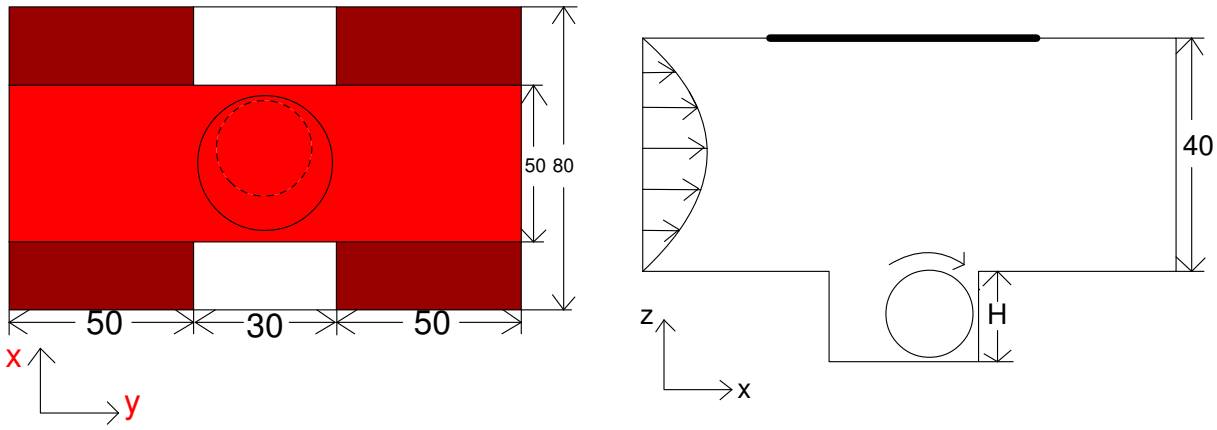

(a) Topview (b) Sideview

Figure 5.3: Configuration of simulation (unit:μm)

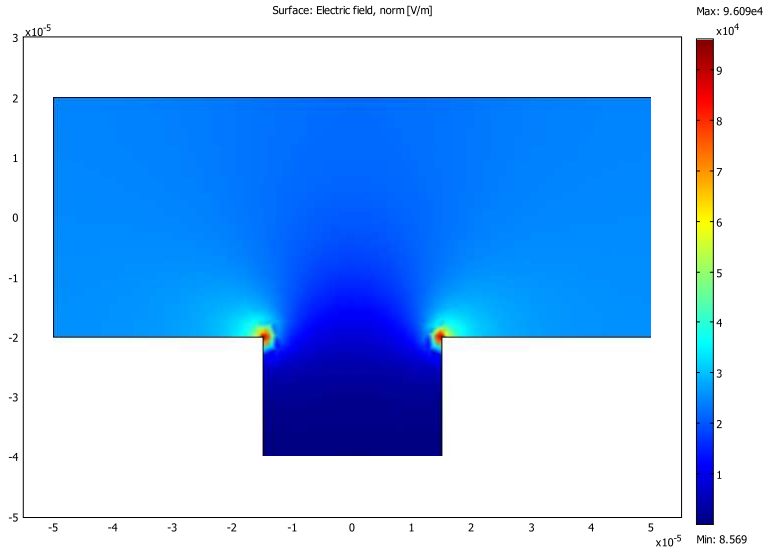

Figure 5.4: Simulation result of electric field in the 3D structure

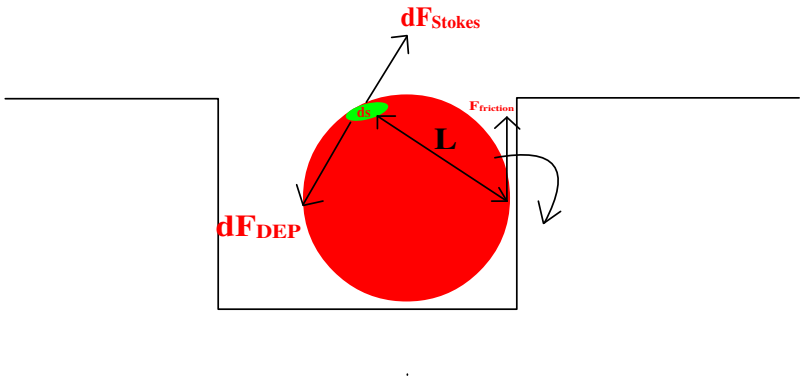

Figure 5.5: Force analysis

5.3.1 Basic equations

To investigate the strength required for holding particles, we need to find the relationship between the release voltage and release flow rate. We assume that there is a frictional force($\boldsymbol{F}_{friction}$) between the particle and the wall of the well as shown in Figure 5.5, since they are in contact. The particle will rotate during the releasing process. This is due to the faster flow field in the region outside the well. We also know that the torque of the frictional force $\boldsymbol{T}_{friction} = 0$, with the contact point as the pivot. Thus, the particle will tend to roll up along the wall when released. Because of the complexity of the structure and the dynamic release process, we shall simplify the calculation; i.e. consider this process as the quasi-static non-slip rolling process. In another word, the resultant force and resultant torque are always equal as shown in the following

$$\begin{cases} \boldsymbol{F}_1 + \boldsymbol{F}_2 + \boldsymbol{F}_{friction} &= 0 \\ \boldsymbol{T}_{DEP} + \boldsymbol{T}_{Stokes} &= 0 \end{cases} \tag{5.1}$$

where $\boldsymbol{F}_1 = \oint_S \boldsymbol{dF_{DEP}}$ is particle's DEP force in y-direction, and $\boldsymbol{F}_2 = \oint_S \boldsymbol{dF_{Stokes}}$ is particle's Stokes force in y direction, $\boldsymbol{T}_{DEP} = \oint_S \boldsymbol{dF_{DEP}} \cdot \boldsymbol{L}$ and $\boldsymbol{T}_{Fluid} = \oint_S \boldsymbol{dF_{Stokes}} \cdot \boldsymbol{L}$ are the torque of particle's DEP force in y-direction and that of particle's Stokes force in y direction, respectively. As shown in Chapter 3, we calculate the torque of unit Stokes force and unit DEP force separately. As is known,

$$\begin{cases} \boldsymbol{T}_{DEP} &= V^2 \boldsymbol{t}_{DEP} \\ \boldsymbol{F}_{DEP} &= V^2 \boldsymbol{f}_{DEP} \\ \boldsymbol{T}_{Stokes} &= Q \boldsymbol{t}_{Stokes} \\ \boldsymbol{F}_{Stokes} &= Q \boldsymbol{f}_{Stokes} \end{cases} \tag{5.2}$$

in which, t and f are the unit value of torque and force (DEP and Stokes force/torque correspond to $1V$ and $1m^3/s$ conditions), V is the voltage and Q is the flow rate. From here, we can get

the relation between V and Q.

5.3.2 Selection of released point

Although quasi-static process is assumed, one may note that the relative magnitude of the DEP torque and hydrodynamic torque will change during the releasing process. Therefore, we should select a reasonable particle's position for the calculation. Figure 5.6(a) shows the normalized hydrodynamic torque and DEP torque at different positions. In this simulation, the well's diameter is 30μm; and channel's height is 40μm. The results suggest that the DEP torque will increase first and then decrease if particle is released. In contrast, the hydrodynamic torque will always increase during the releasing process. Figure 5.6(b) shows the relative change of the DEP torque and hydrodynamic torque. It appears that the hydrodynamic torque increases slower than DEP torque before Position 3(particle at the entrance of well as shown in Figure 5.6). On the contrary, the hydrodynamic torque increases faster than DEP torque after position 3. Now we should select a position, at which particle's DEP torque equals to its hydrodynamic torque; and hydrodynamic torque is larger than DEP torque when the particle is at the other positions. The data (Figure 5.6(b)) clearly shows that we should select position 3 as the releasing point to do the calculation according to Equation 5.1.

5.3.3 Effect of well depth

Previous work has shown that the trapping strength is affected by the well depth [131]. In this study, we will study the releasing process. Intuitively, the depth of the well should be important for such a micro-well structure, as it should be more difficult to release a particle from a deep trap. In this study we fixed the maximum flow velocity at 0.0015m/s, the particle's radius at 10μm, and change the depth of well to see how it affects the hydrodynamic torque.

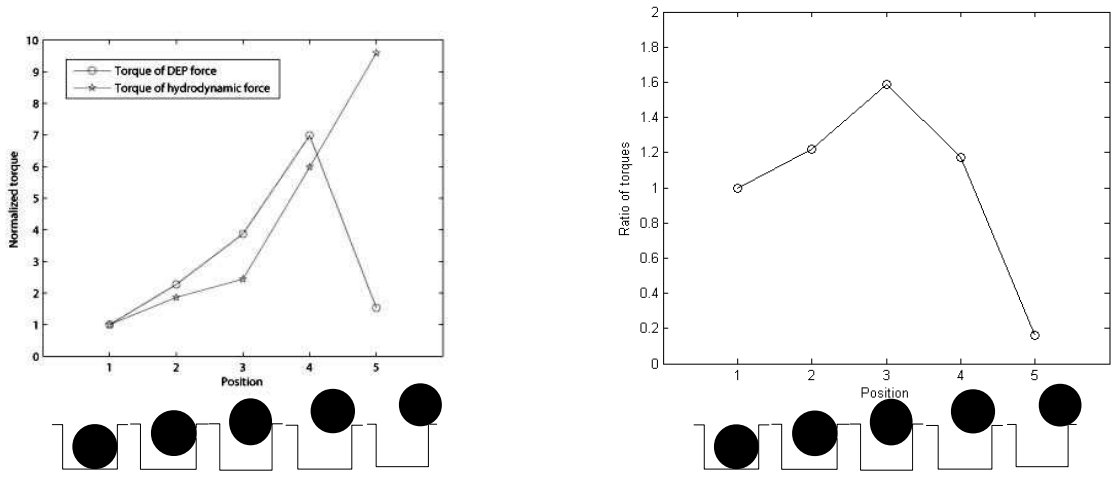

(a) Torques of hydrodynamic force and DEP force

(b) The ratio of DEP torque and hydrodynamic torque

Figure 5.6: Torques at different position

Initially, the particle is located at the bottom. We want to find out how the well depth affects the initial motion of particle. Figure 5.7(a) shows the DEP torque changes with the depth of well while Figure 5.7(b) shows the hydrodynamic torque changes with the depth of well. Clockwise direction is considered positive as shown in 5.3(b). The results suggest that the hydrodynamic torque will decrease to zero and change direction(become negative) when the well become deeper. In contrast, the DEP torque will always decrease without changing the direction as the well becomes deeper. The results indicate that if the depth of well go beyond 2.4 times the particle's radius(Figure 5.7(b)), the DEP torque and the Hydrodynamic torque will both take on the same direction, which means the particle cannot roll up along the side wall. This implies that the particle cannot be released by fluid flushing even when we shut down the voltage.

Now we know that the releasing point locates at the entrance of the well (Position 3 in Figure 5.7). Figure 5.8 shows the critical maximum flow velocity for the releasing process based on Equation 5.1. In this calculation, we fixed the peak to peak voltage at 10V. We find

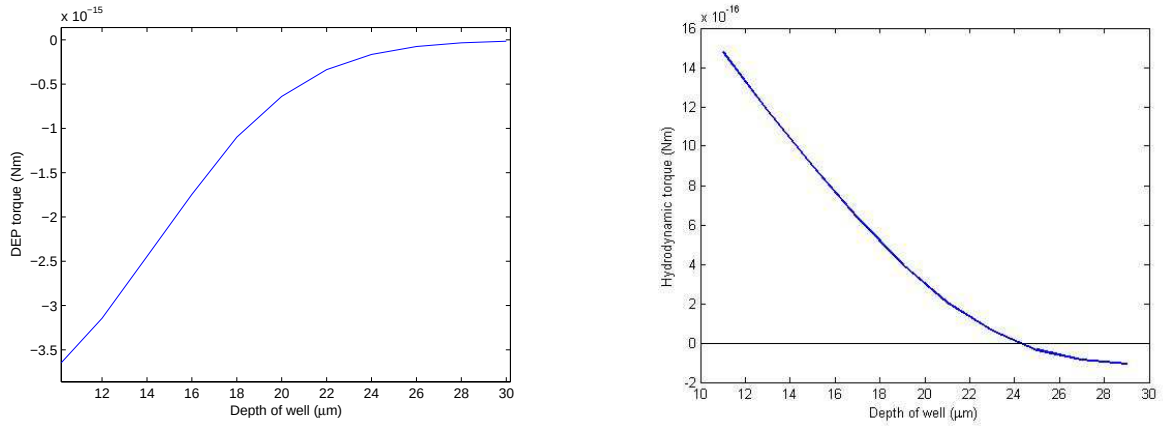

(a) DEP torque (b) Hydrodynamic torque

Figure 5.7: Torque VS depth of well

that the curve has a turning point when the well depth is around $15\mu m$. This turning point is worth noting. If the depth of well is deeper than about 1.5 times the particle's radius, the releasing flow rate will become a constant, indicating that the depth of the well becomes less effective.

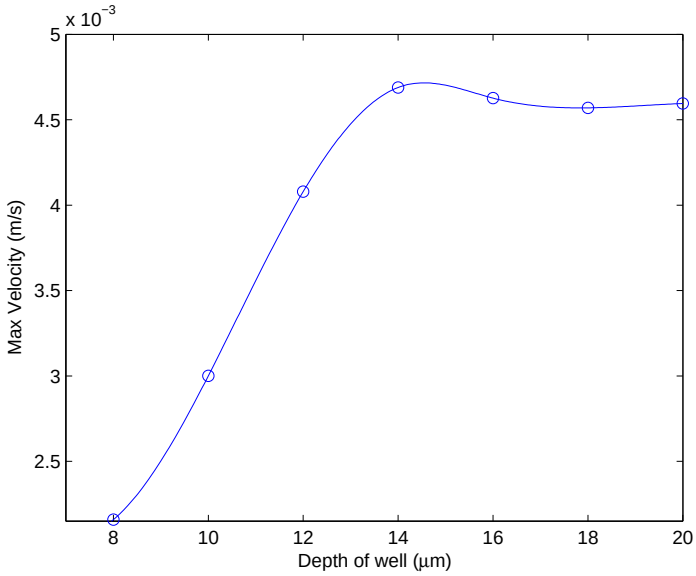

Figure 5.8: Effect of depth on critical flow velocity

5.4 Fabrication

The fabrication process for making such a device essentially involves forming the well in the SU-8 followed by the lift-off process. The fabrication process flow for making such 3D structure is shown in Figure 5.9 and Appendix C.2.

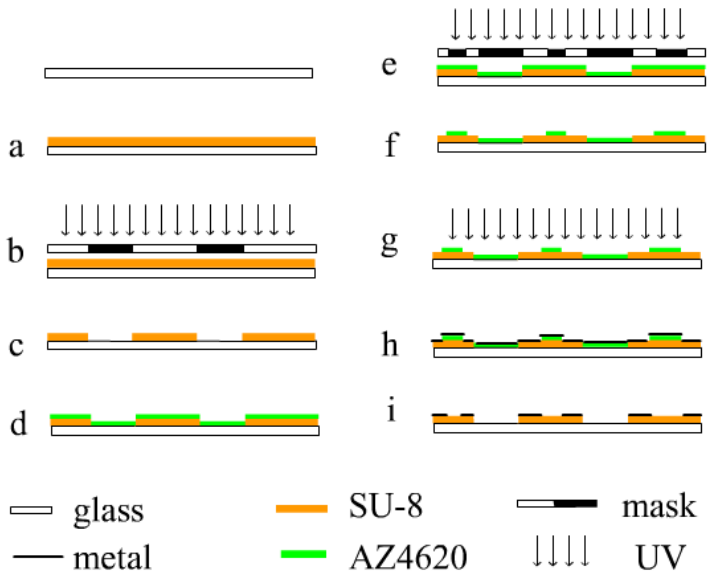

Figure 5.9: Fabrication process of 3-layer structure

ITO etching follows the procedure described in Section 4.4.1 and Appendix C.1.

5.4.1 Well Formation

This substrate preparation leaves the wafer sufficiently clean (see also section 4.5.2). Following the preparation, SU-8 25 was spun onto the wafer. SU-8 was first deposited onto a stationary wafer, followed by a 5-second slow spread and a 30-second faster spin, resulting in a nominally $20\mu m$ thick layer. Following the coating, the wafer was pre-baked at 65 degree and 95 degree for 3 minutes and 5 minutes, respectively. After the pre-bake, contact lithography was used to define the holes in the SU-8. The key to performing this lithography step was to obtain good

contact between the mask and the SU-8 by minimizing any air-gap. One ensure that there is minimum exposure that would harden the photoresist without overexposing to the wells. After exposure a post-bake on a hotplate was performed. The final step was to develop the SU-8 in developer. This developer would remove the unexposed regions of the photoresist. Four minutes was sufficient to open up the holes. Use of ultrasonic could help for this step. In the ultrasonic cleaner, the developer is subjected to the vibration transducers. This creates small cavitation bubbles in the liquid. The cavitation bubbles implode and removed the unexposed photoresist. The developing time required becomes much shorter in the presence of the ultrasonic.

5.4.2 Middle layer Formation

This step is to fabricate the electrode of the middle layer. Lift-off process was used in this step. Lift-off process consists of three steps. Firstly, reversed pattern was deposited on the wafer. Then a layer of metal was sputtered onto the wafer. Finally the reversed pattern was removed and the required electrode pattern was the residue. AZ4620 was chosen as the mask material for its easily controllable characteristic. The process was the normal lithography process which is similar to those described in Section 4. As a result, the mask layer would be around $5\mu m$, which is much thicker than the metal layer in the subsequent sputtering. It is easy to facilitate the removal of AZ4620 after the sputtering. As for the other parameters, such as the time of baking, development, and so on, they are increased accordingly. Following the patterning, a layer of titanium is sputtered onto the sample. The thickness of the metal is nearly 1/10 of that of the mask. The use of titanium is to ensure good adhesion to the SU-8 and low residual stress. Finally, the AZ4620 remaining was removed using acetone in the ultrasonic cleaner.

However, using acetone to strip the photoresist is not conducive because acetone is very aggressive and the SU-8 would be dissolved during the process of removing the AZ4620. We

propose a new lift-off process. A slight modification was made in step g as shown in Figure 5.9. After opening up the holes on SU-8, a hard-bake step was introduced on the hotplate for 20 minutes at 250 degree to increase the strength of the cross-linked SU-8. After patterning AZ4620 (step f), the device was exposed again under UV light (step g). Then the solvent, AZ400K can be used to remove the AZ4620 pattern instead of acetone. AZ400K is less corrosive than the acetone, and SU-8 can remain in AZ400K for a long time without deterioration. As such, the SU-8 well is intact.

5.4.3 Packaging

The final product is a rectangular flow chamber with $W \times L \times H = 3mm \times 10mm \times 30\mu m$, formed by double sided tape attached on the ITO glass, shown in Figure 4.15 and Appendix C.3. The advantages of using double sided tape are for ease of patterning and also reasonably good quality bonding between the two pieces of ITO glass. The finished multilayer electrodes DEP chip is shown in Figure 5.10.

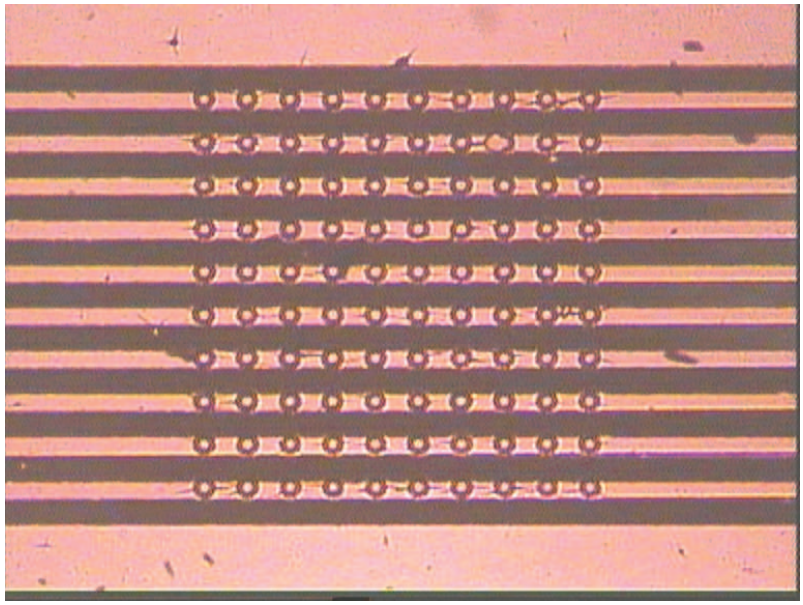

Figure 5.10: Finished 3D trap structure

5.5 Methods and Material

The material and methods were shown earlier in Section 4.5.

5.6 Results

The 10 by 10 microwell array was fabricated and 20μm fluorescent particles were used to test the device. Figure 5.11 shows the trapped particles in the well. It is apparent that this design works well for the trapping of single particles.

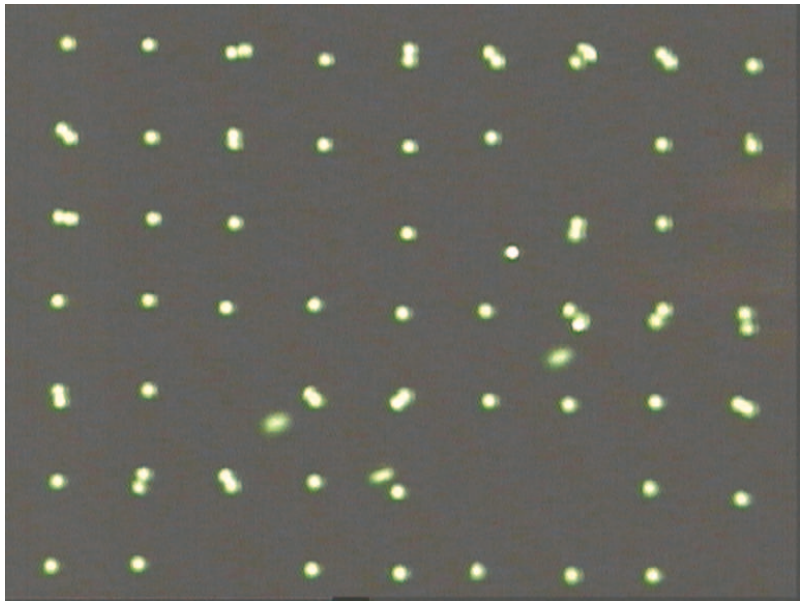

Figure 5.11: Experimental result for trapping of the particles

Figure 5.12, Figure 5.13 and Figure 5.14 show the comparison between the experimental result and simulation result. Figure 5.12 indicates the critical maximum release flow velocity for different depth wells. A 10V peak to peak voltage was applied. Figure 5.13 is the critical releasing flow velocity versus voltage at different well depth (8μm and 18μm) where the channel height is maintained at 40μm. Figure 5.14 is the critical releasing flow velocity versus voltage with the channel height kept at 70μm at the well depth of 8μm and 18μm. We have fabricated

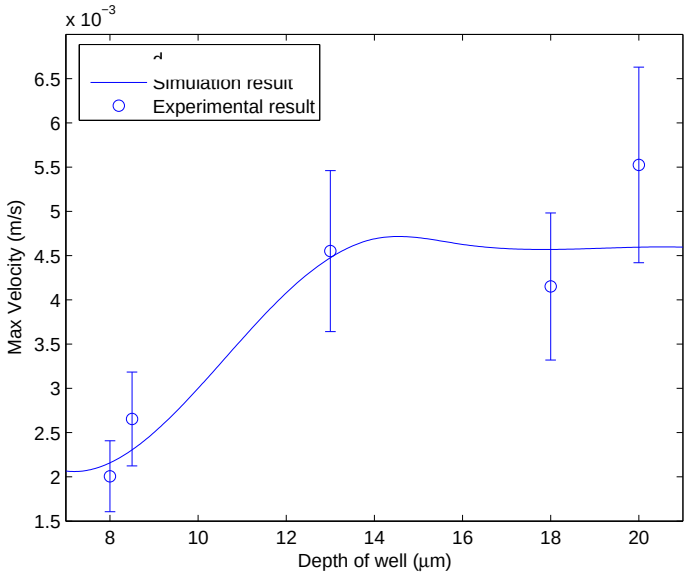

Figure 5.12: Comparison of experimental results and simulation results on changing the depth of the well

several devices to validate our prediction.

We can see from all the three graphs that the experimental results have the same trend as the simulation results, although there are differences in terms of magnitude. For the case of the well depth of 8μm (Figure 5.13(a) and Figure 5.14(a)), the experimental results agree well with the numerical prediction. However, the experimental results at 18μm deep well were not so well predicted(Figure 5.13(b) and Figure 5.14(b)).

A major cause of this mismatch comes from the model, which is based on a non-slip friction assumption. In our experiment, we cannot guarantee that it is non-slip friction between the particle and the wall of well during the releasing process. Other causes of error may include numerical uncertainty, and the adhesion between the particle and wall of well in the experiments. In addition, the actual physical device could have some small differences vis-a-vis our original design due to some uncertain fabrication factors, such as the environmental temperature,the baking time, the etching time and so on. A final source of error could be that heat generation

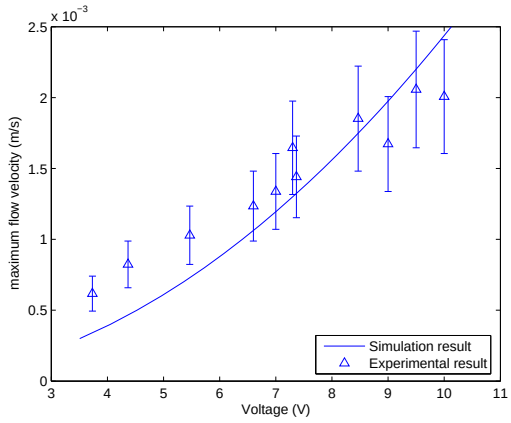

(a) The depth of the well is $8\mu m$

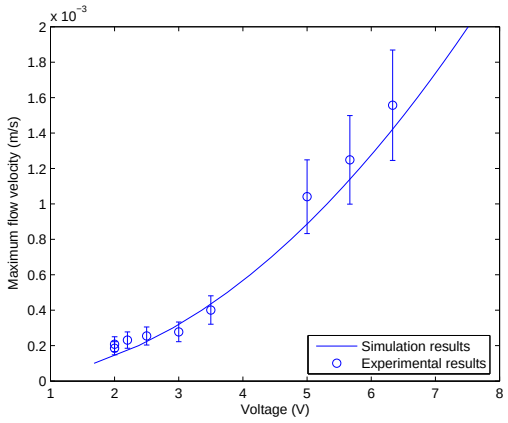

(b) The depth of the well is $18\mu m$

Figure 5.13: Critical releasing flow velocity and voltage when the channel height is $40\mu m$

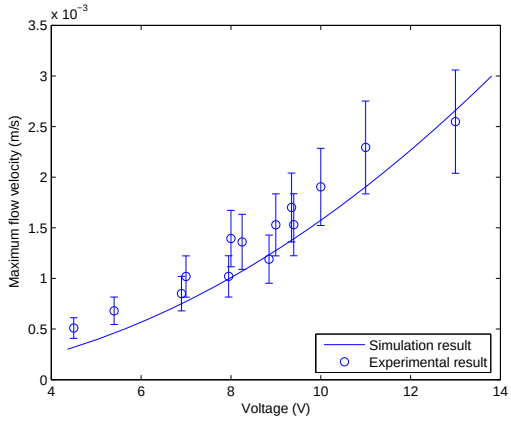

(a) The depth of the well is $8\mu m$

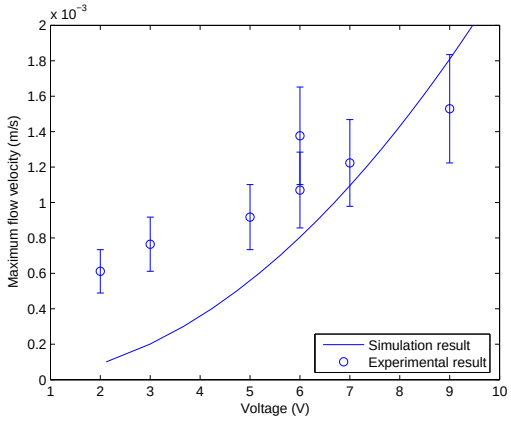

(b) The depth of the well is $18\mu m$

Figure 5.14: Critical releasing flow velocity and voltage when the channel height is $70\mu m$

causes inhomogeneities in the electrical properties of the system, which could alter the electric fields. To remove this final source of error and to include the inter-facial effects properly in non-symmetrical electrode geometries, it is necessary to calculate the electric field while taking into account frequency and temperature effects; this is for future work.

5.7 Conclusions

In this study, the simulation and experimental working of a 3D micro-structure array were demonstrated. Calculation of the DEP force, and trapping efficiency can be achieved with Comsol Multiphysics 3.3 simulation. The particle trapping can be achieved with the 3D micro-structures. By tracking the movements of beads subjected to the DEP force using a video camera, we can verify the simulation and the experimental results. It is found that the particle could experience the largest difference between DEP torque and hydrodynamic torque. As such, we use the entrance of well as the particle position to carry out our simulation. It is found that beyond a certain value the depth of the well does not influence the release. Furthermore, we also found that the particle cannot be released even after we have shut down the electric field when the depth of the well was deeper than a certain value ($1.5 times of particle's diameter$). This system not only can provide the platform for the study on DEP trapping, but also has the potential to sort the particles of different sizes. Besides, a new lift-off process for two-layer photoresist was proposed.

Chapter 6

Microarray with addressable control

6.1 Introduction

In previous chapters(Chapter 4 and Chapter 5),we have demonstrated two microdevices. However, the grid-like device cannot trap particles, and the micro-well array is more difficult to fabricate. Their usage may thus be limited. As we know, DEP chip has the advantage of free labeling, low cost, and ease of control. Here, another microarray is proposed. The results show that this third device can trap single particle, and sort different particles as well. This design introduces many advantages. Firstly, the design is very simple,and the fabrication can be carried out easily. Secondly, this microarray can be scaled up to a large number of traps, which is necessary in large-scale practical use. Finally, the addressable control allows the sorting of desired particles during experiment(addressable control). This provides flexibility. Many biological experiments can be conducted on this device.

6.2 System design

6.2.1 Design

The main part of the design is very simple as shown in Figure 6.1(a) and Figure 6.1(b). The top electrodes and bottom ones have jagged-like structures. The shape of the 'jag' can be triangle, square, sector and so on. This is to create non-uniform electric field. The gap between the top and bottom should be in the same order of the size of particles. When the sample particles are introduced into this microdevice, some particles can be trapped in the jagged area when passing through this array of electrodes.

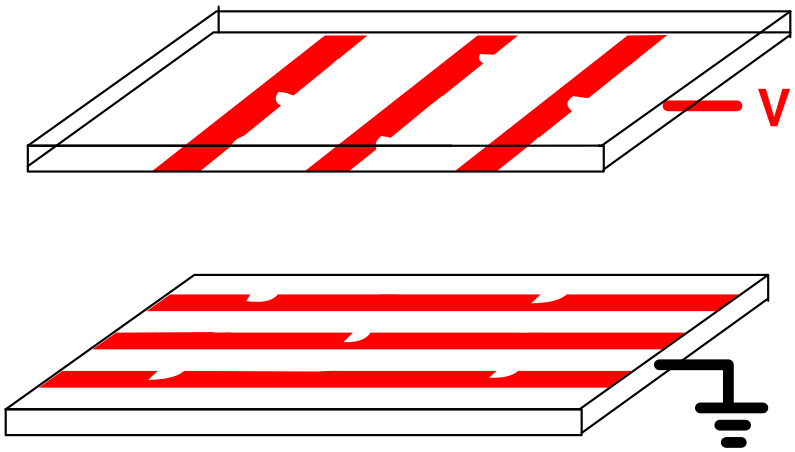

(a) 3D view of the main part of the design

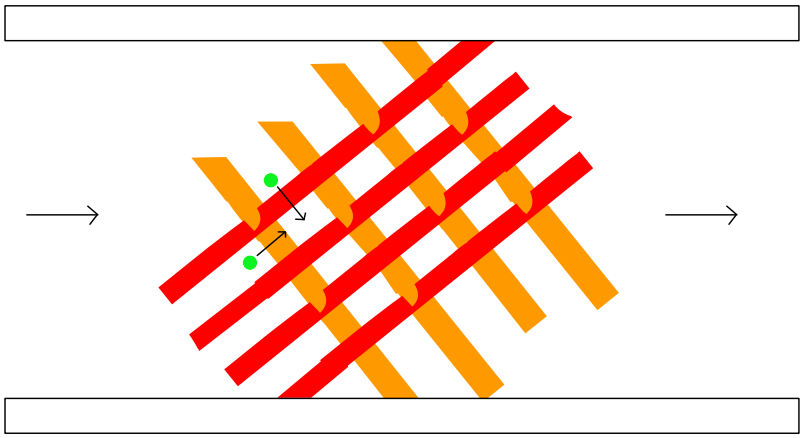

(b) Top view of the main part of the design

Figure 6.1: Jagged-like structure design

6.2.2 Capture mode

With the electrodes being energized by different potential, a non-uniform electric field will be generated due to the potential difference between the top electrodes and bottom electrodes. The electric field between the jagged area and top electrode can form a 3D cage which can trap particles. Particles can be captured in this trap when the equilibrium point between the fluid force (Stokes force) and the nDEP force is located in the vicinity of the jagged area. If particles have different properties then this device acts as a sorter.

6.2.3 Release modes

After the particles are trapped, two different ways can be employed to release particles from the traps. One is to decrease the voltage (shown in Figure 6.2). The trapped particles will then move across the electric cage along with the fluid. This is because the fluid force (Stokes force) is now larger than the nDEP force. The second way to release particles is to increase the voltage (shown in Figure 6.3). The trapped particles will be pushed back out of the trap's entrance and then they will move downstream along the electrode. This is because the nDEP force is larger than the Stokes force. If the adjustment of the voltage is controlled carefully, only one particle will be released at one time for either method. Pulsed waveform can be used for improving the separation thereby particle is released one at a time (shown in Figure 6.4 and Figure 6.5, respectively). Pulsed waveform can reduce the electrostatic interaction between particles.

Still, if the voltage is unchanged, increasing or decreasing the flow rate are other ways to release particles. However, this is not a satisfactory method due to its slow response and imprecise control.

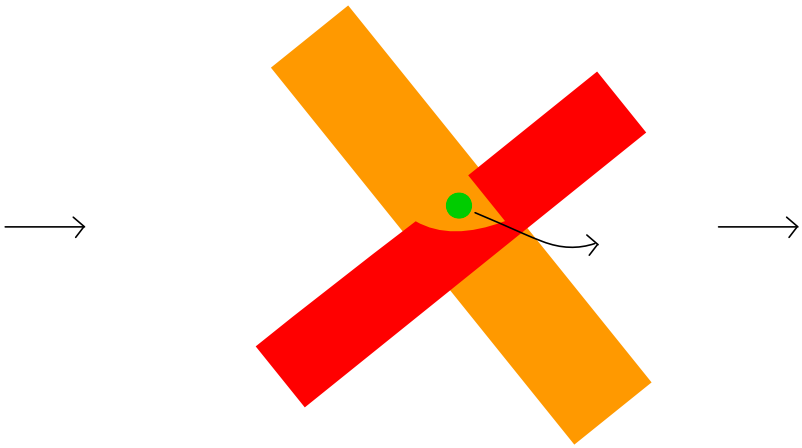

Figure 6.2: Release particles by decreasing the voltage

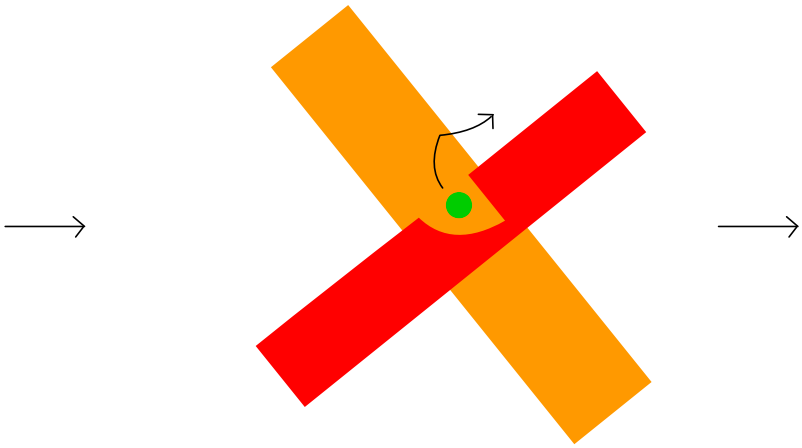

Figure 6.3: Release particles by increasing the voltage

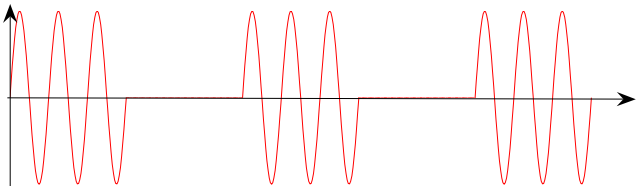

Figure 6.4: An improved waveform to release particles by decreasing the voltage between the top and bottom electrodes

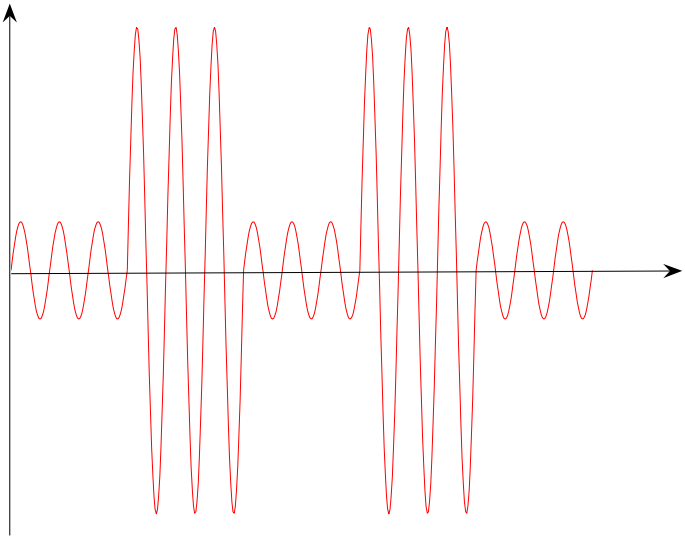

Figure 6.5: An improved waveform to release particles by increasing the voltage between the top and bottom electrodes

6.2.4 Sorting modes

Particle Selection in one trap

Sometimes more than one particle can be found in one trap due to variation of particle properties,e.g.the shape, the size, the elasticity, the conductivity, the permittivity, etc. These particles can form a line in the trap because of the jagged shape of the electric cage. The two release modes mentioned above provide us the means to select a particular particle for release as shown in Figure 6.6. Here the flow rate is assumed to be unchanged. Suppose No.2 particle is the one we want to keep. No.3 particle can be released by decreasing the voltage followed by increasing the voltage to release No.1 particle. This release order will prevent other particles from being trapped again.

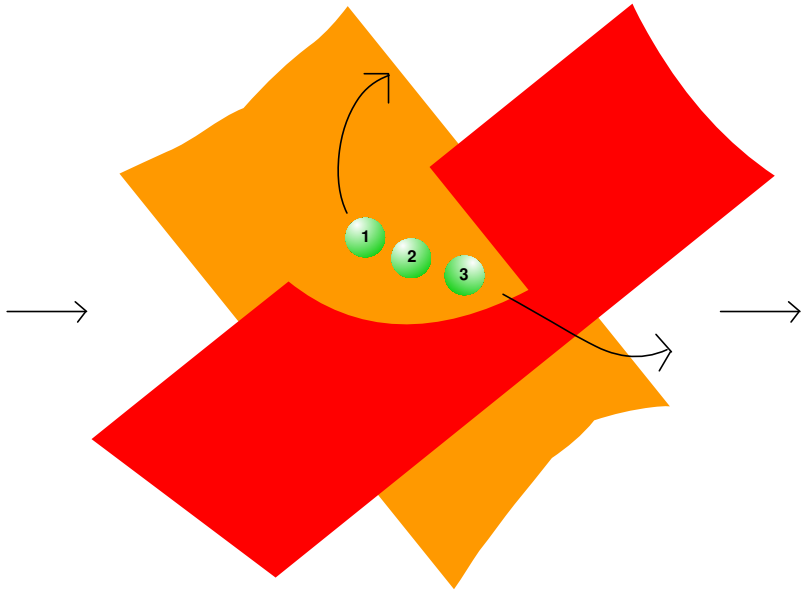

Figure 6.6: Particle selection process in one trap

Arbitrary Particle Selection (Addressable control)

An experiment is carried out to check this function. Suppose the trapped particles are the same in electrical property. As mentioned above, we can release the particles that we do not need, and keep the ones interested, by using addressable control.

To explain further, some simplifying assumptions are set out below (and shown in Figure 6.7):

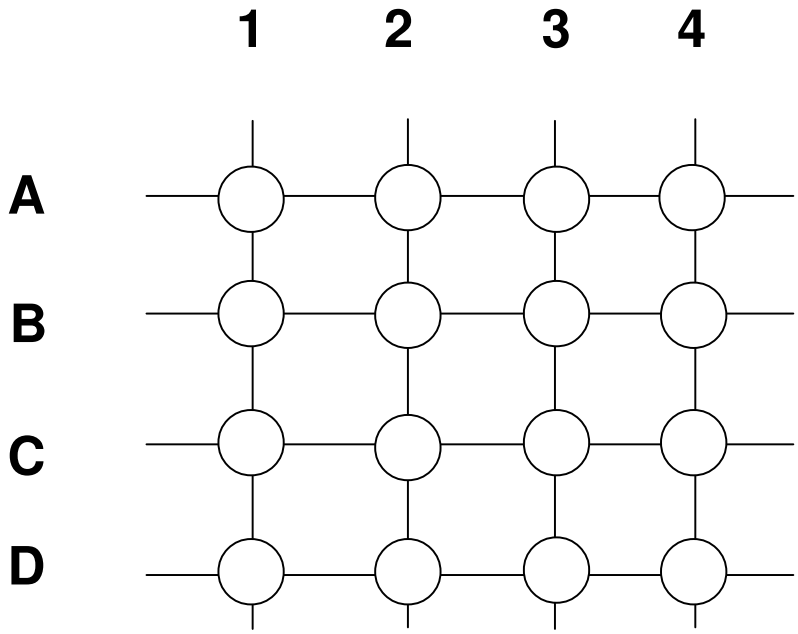

Figure 6.7: Schematic of top view of the 4×4 microarray

1. A 4×4 microarray is fabricated.

2. A, B, C, D are the top electrodes and 1, 2, 3, 4 are the bottom electrodes.

3. Only one single particle to be captured in each trap.

4. Particles at Position B2 and Position C3 are about to be released.

5. The trapping voltage is set to be between 10V and 15V.

6. The flow rate is kept unchanged.

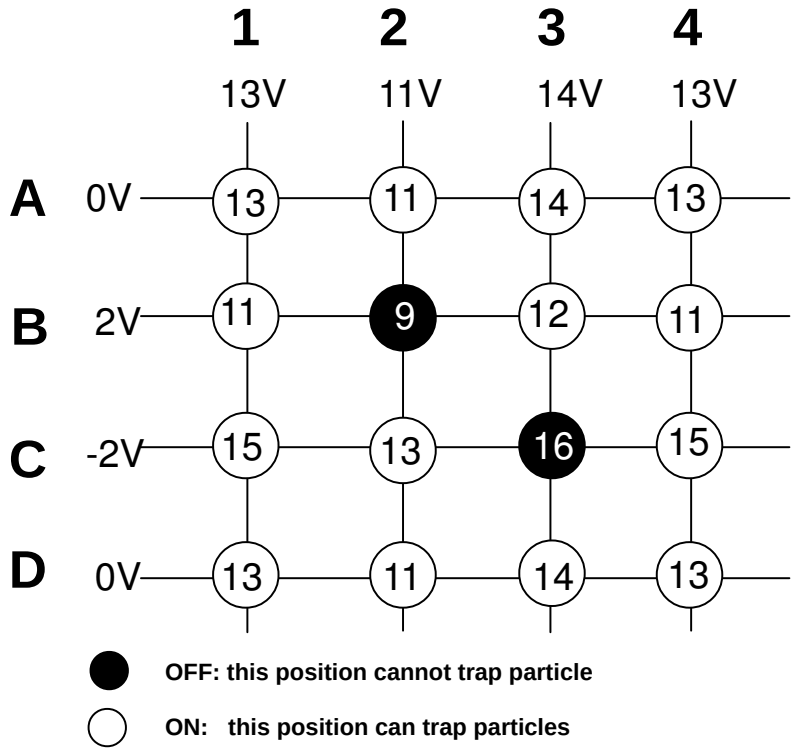

Figure 6.8: Schematic of addressable control

Based on these conditions, the voltage can be applied as shown in Figure 6.8. The potential difference at B2 is 9V which is less than 10V. That means the nDEP force cannot balance the hydrodynamic force (Stokes force). As such the particle at B2 cannot be entrapped. Additionally, the potential difference at position C3 is 16V which is more than 15V. It implies that the nDEP force is larger than the fluid force (Stokes force) in the jagged cavity. Consequently, the particle will be pushed out of the entrance instead of staying in the cage. Except for B2 and C3, the potential difference at all other positions is between 10V and 15V, which means an equilibrium point between nDEP force and Stokes force exists in the jagged cavity. As a result, particles can be captured at all the positions other than B2 and C3.

6.3 Modeling

A 3D model of this DEP chip shown in Figure 6.9 was analyzed with the COMSOL software. The width of electrode is 50μm; the width of channel is 80μm; and channel's height is 40μm. To study the capacity of the trap, we changed the diameter of particle and fixed the size of jagged cavity with $R = 35\mu m$ as shown in Figure 6.9(c). We also change the relevant flow rate and applied voltage to study the performance of the trap. For the DEP simulation, an AC signal is applied on the top and bottom electrodes with 10V (peak to peak) at 1M Hz. With the

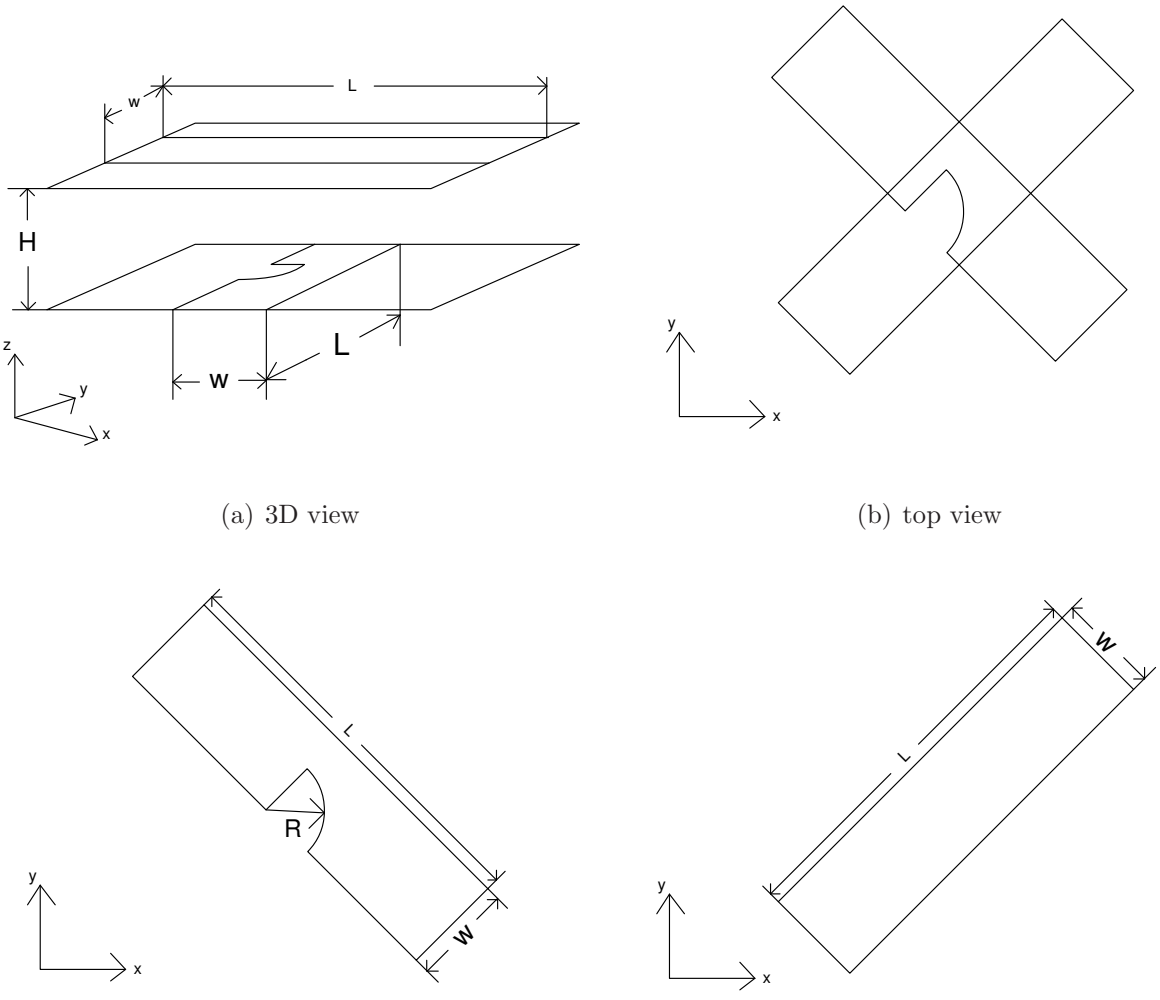

(a) 3D view

(b) top view

(c) Jagged electrode

(d) Strip electrode

Figure 6.9: Configuration of unit microarray:$R = 35\mu m$,$w = 50\mu m$,$L = 150\mu m$,$H = 40\mu m$

electrodes being energized by different potential, a non-uniform electric field will be generated

due to the potential difference between the top electrodes and bottom electrodes. We selected a surface level at $5\mu m$ from the bottom to examine the DEP force distribution using the dipole approximation. From the results shown in Figure 6.10, the highest DEP force is found near the edge of the electrode. The DEP force form a virtual 3D cage which can trap particles. Suppose the flow direction is in the x direction. We can see that the virtual wall will block the particle in the suspension as shown in the figure.

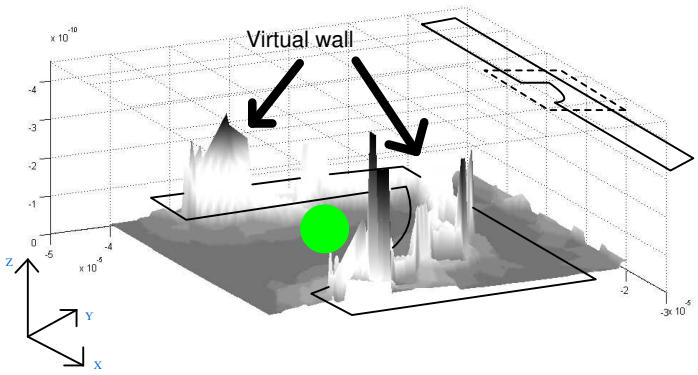

Figure 6.10: Distribution of DEP force in the highlight area

6.3.1 Trapping different number of particles

The size of the virtual cage depends on the flow rate and the relative voltage between the top and bottom electrodes. By adjusting these two parameters, we can make a virtual cage suitable for a single particle with a certain size. After obtaining the distributions of electric field, the region where particles can be trapped can be found. The region is highlighted by the force contour in Figure 6.11. By adjusting the applied voltage and the flow rate, it is possible to trap different number of particles as desired. From Figure 6.11(a)-6.11(d), we increased the voltage while leaving the flow rate fixed, it is clear that the trap region becomes smaller and smaller.

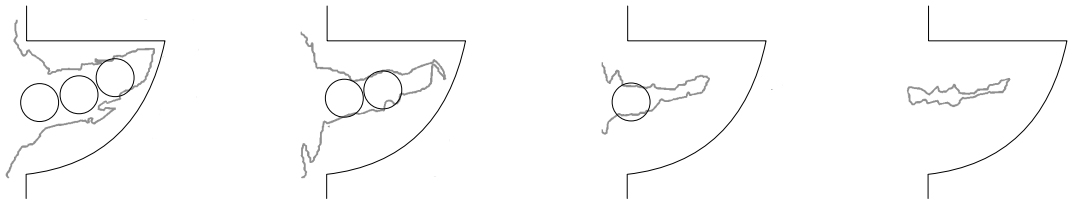

(a) Simulation voltage:1V (b) Simulation voltage:2V (c) Simulation voltage:5V (d) Simulation voltage:8V

Figure 6.11: Capacity of the trap

6.3.2 Different Releasing methods

Previous description in Chapter 3 showed that the model works well for the trajectory for particles under the influence of DEP force and Stokes force. In this study, we will use the same method to study the trapping and releasing process. The only difference of this model is that the jagged-edge was introduced. Figure 6.12 shows the critical maximum flow velocity for the releasing process and trapping process. For each particle, the trapping flow rate and releasing flow rate are different. These two curves bound a region which we shall call the 'trap area' as shown in Figure 6.12. Outside this area, the particle cannot be trap. Once a particle is trapped, we can get the particle out of the trap by increasing voltage or decreasing voltage as mentioned before (increasing flow rate or decreasing flow rate). Another important observation is that the trap areas for $10\mu m$-particle and $5\mu m$-particle do not overlap. This means we can sort different sized particles using this device. When $5\mu m$-particle is trapped, the DEP force of $10\mu m$-particle will be prevented from entering the trap as shown in Figure 6.3. If $10\mu m$-particle is trapped, the hydrodynamic force of $5\mu m$-particle will overcome the DEP force as shown in Figure 6.2. The experimental results will be presented below.

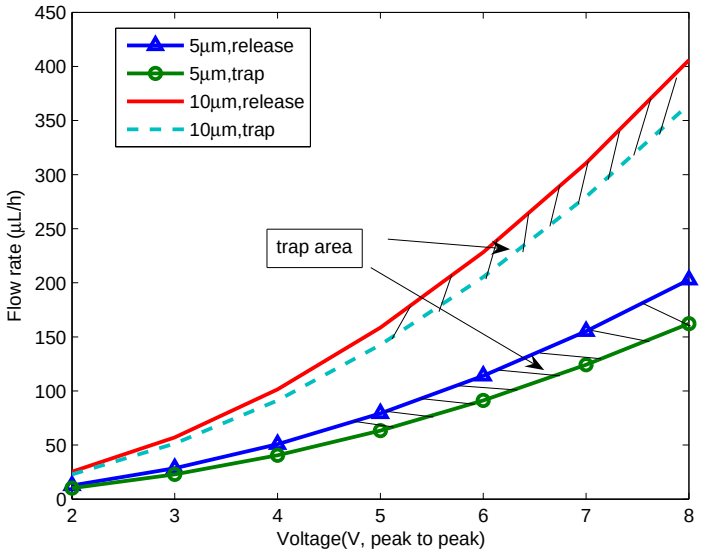

Figure 6.12: Simulation results for trap and release flow rate

6.4 Fabrication

Basic micro-fabrication technologies, such as photolithography, sputtering and so on, can be used for the fabrication, which is similar to the LCD fabrication process.The fabrication process for making such electrodes is shown in Figure 4.13 and not repeated here.

6.4.1 ITO Etching

ITO etching follows the procedure described previously in Section 4.4.1 and Appendix C.1.

6.4.2 Packaging

This is a rectangular flow chamber with $W \times L \times H = 3mm \times 10mm \times 30\mu m$, formed by double sided tape attached to the ITO glass, shown in Figure 4.15. The packaging process follows the procedure described previously in Section 5.4.3 and Appendix C.3. The finished multilayer electrodes DEP chip is shown in Figure 5.10.

6.5 Materials and Methods

The materials and methods were shown in section 4.5.

Figure 6.13 shows the control circuit.

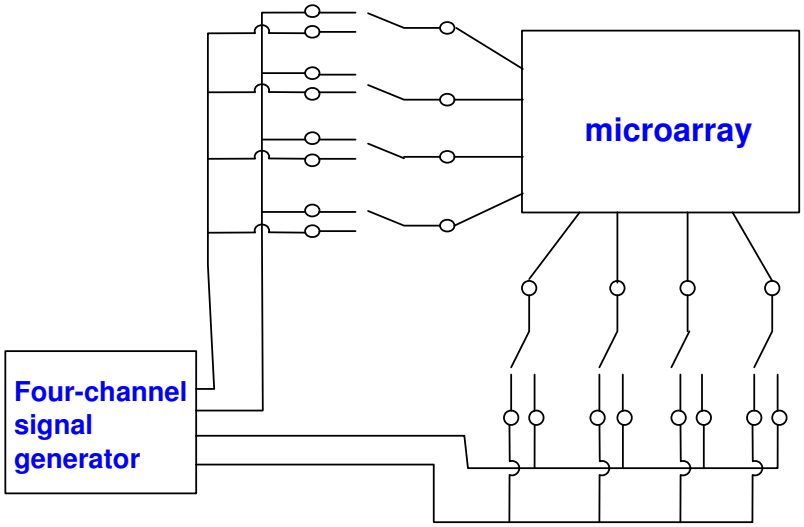

Figure 6.13: Control circuit

6.6 Experimental Results

By using the setup as shown in Figure 6.1 and Figure 6.13, we can perform experiment to verify our analysis.

6.6.1 Capture Mode

As shown in Figure 6.14, particles can be captured in the jagged trap due to the fact that the equilibrium point balance between the Stokes force and the nDEP force is located in the jagged area. The first image (Figure 6.14(a)) was taken 20 seconds after the flow was applied. Three particles were trapped already, while one trap was vacant. In Figure 6.14(b), all the traps have trapped particles. In trap 1 and trap 4 there were two particles, while there was one

particle in the other traps. And by Figure 6.14(c), 46 seconds after the start of the flow, more than one particle have been loaded into each trap. Figure 6.14(c) and Figure 6.14(d) show a similar situation with two or three particles being loaded into traps. We can see that three is the maximum number of particles that can be trapped in one trap due to the trap size (shown in Figure 6.14(c) and 6.14(d)). By comparing trap 1 in Figure 6.14(c) with trap 1 in Figure 6.14(d), it may be suggested that the particle at the entrance cannot be held tightly when this trap is full.

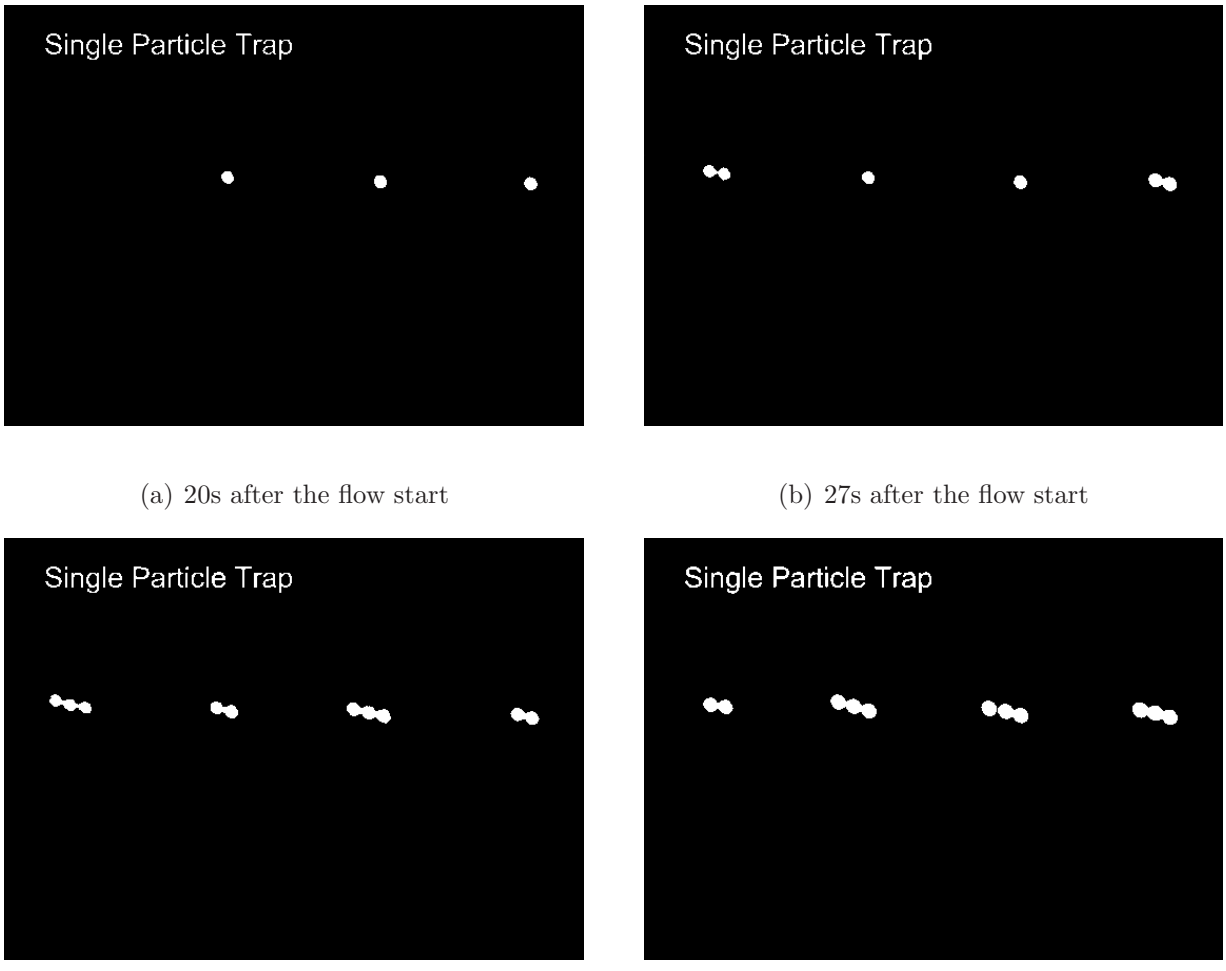

(a) 20s after the flow start

(b) 27s after the flow start

(c) 46s after the flow start

(d) 96s after the flow start

Figure 6.14: Capture mode

One of the requirements is that the traps must be capable of holding only one particle per site. Figure 6.14 shows after loading it is possible that some traps will hold more than one

particle. We can employ the techniques discussed to release excessive particles in those traps that hold more particles. The following sections will discuss this mode in details.

6.6.2 Release mode

In this experiment, the flow rate of fluid was kept unchanged because voltage can be more easily controlled. Two different ways can be employed to release particles in the traps. One is to decrease the voltage (shown in Figure 6.2). The trapped particles went right across the electric cage along with the fluid. This is because the Stokes force of the fluid is larger than the nDEP force and there is no equilibrium point in the jagged cavity after the voltage was decreased. The other way to release particles is to increase the voltage (shown in Figure 6.3). The trapped particles were pushed back to the entrance of the trap and they went along the electrode to the downstream. This is because the nDEP force is larger than the Stokes force of the fluid in the jagged cavity and the equilibrium point is located outside the cavity after the increase in voltage. During the experiment, it was found that single particle can be entrapped in the trap. This result demonstrates that the number of trapped particles can be controlled as shown in Figure 6.15. That is, after the configuration shown in Figure 6.14(d), we increased the voltage to release particles so that only two particles in each trap were left(Figure 6.15(a)). In succession, we increased voltage continually. We can see that only single particles were trapped in each trap as shown in Figure 6.15(b). Conversely, if the voltage is unchanged, it is possible to increase or decrease the flow rate to release the particles. However, this mode of control is less precise.

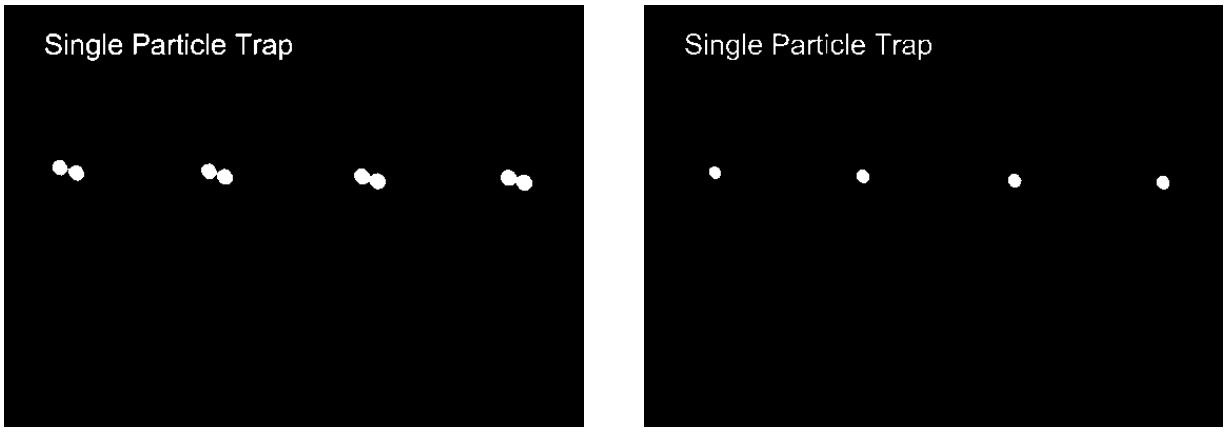

(a) 120s after the flow start (b) 125s after the flow start

Figure 6.15: Single particle trap

6.6.3 Addressable control

Figure 6.16 shows the picture of the trapped particles taken from experiment. The flow rate was fixed in the experiment.

Based on the above conditions, the voltage can be applied as shown in Figure 6.17. The potential difference at position B2 was 9V which is less than 10V. In other words, the nDEP force was smaller than the Stokes force of the fluid in the jagged cavity. We can therefore see one of the particles was released as shown in Figure 6.16(b). Subsequently, at 10 seconds later, another particle was released as shown in Figure 6.16(c) when the voltage was decreased(Figure 6.18). As a result, trap $(2, 1)$(Row 2, Column 1) was cleared up as shown in figure 6.16(d). This is due to the fact that no equilibrium point between the nDEP force and Stokes force is located in the jagged cavity.

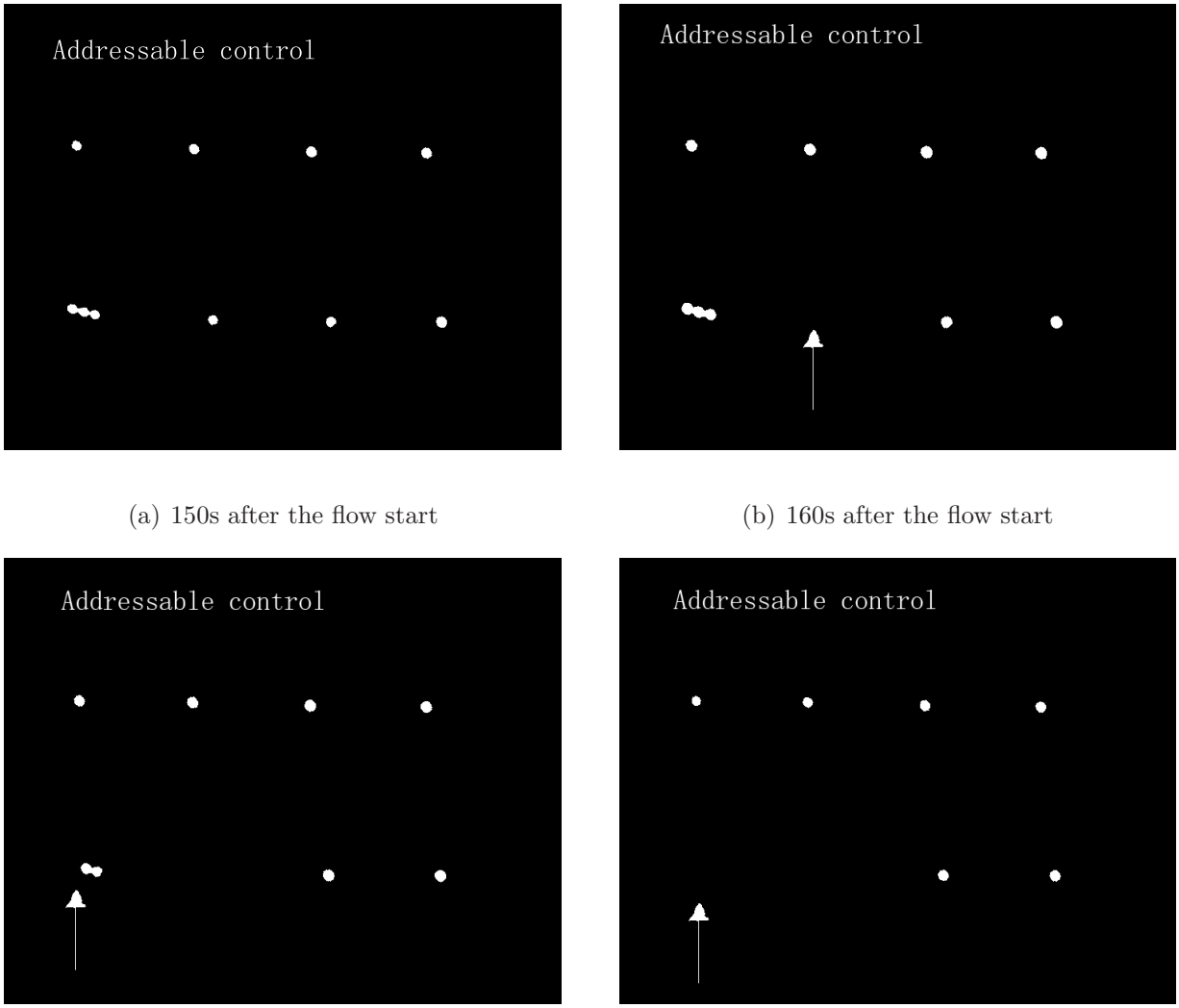

(a) 150s after the flow start

(b) 160s after the flow start

(c) 170s after the flow start

(d) 180s after the flow start

Figure 6.16: Addressable control

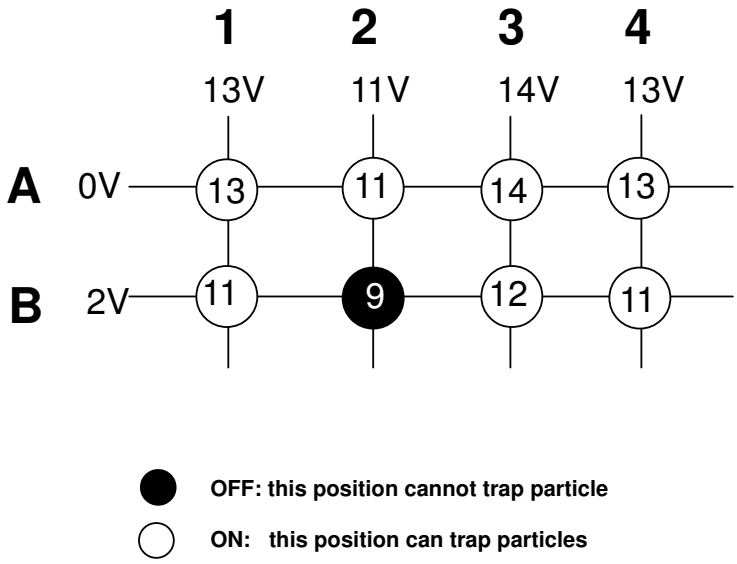

Figure 6.17: Schematic of addressable control

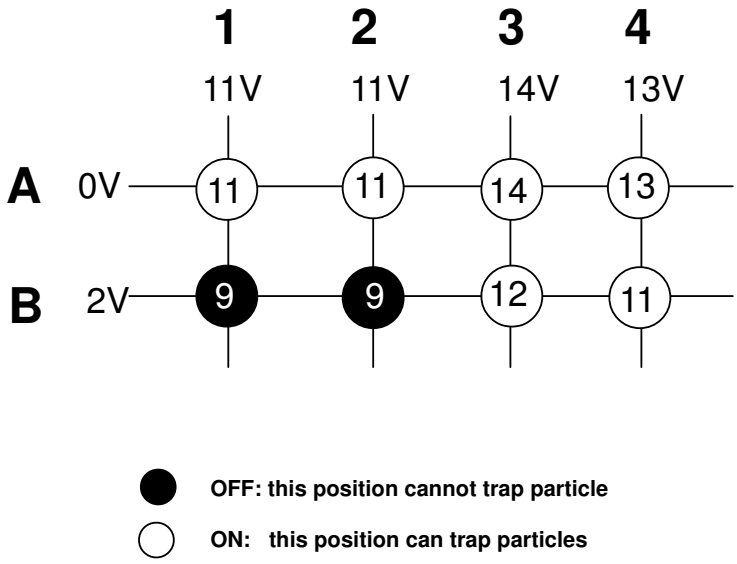

Figure 6.18: Schematic of addressable control

6.6.4 Comparison between experimental results and simulation result

The simulation results are shown above in Figure 6.12. Figure 6.19 shows the comparison between the experimental and simulation results. The first feature to note is that for all bead sizes considered the experimental data lies within the predictions or calculations from the simulation as shown in Figure 6.19. In another word, the concurrence between the simulation and experimental results is reasonably good. For the $10\mu m$ particles, the experimental results agree with the prediction results (Figure 6.19(c) and Figure 6.19(d)). There is, however, larger variation between the experiment and simulation for the $5\mu m$ particles. Ideally the concurrence should be independent of the particle size employed, $5\mu m$ or $10\mu m$ particle. A major cause of this variation can be traced to the inherent assumptions in the simulation. We assume that there is no interaction force between particle and substrate and the particle's motion is quasi-static process. Other causes of the variation may include Brownian motion of the different size particle in the lower force confining regions, and even effects of electrohydrodynamic (EHD) flows. In addition, although the perfect symmetry of the ideal electrode structure precludes any substrate-liquid material interface or charge relaxation effects from affecting the electric fields, the actual physical setup could have asymmetries that cause these effects to appear. A final source of error could be that heat generation causes inhomogeneities in the electrical properties of the system, which could alter the electric fields. To remove this final source of error and to include the inter-facial effects fully in non-symmetrical electrode geometries, it is necessary to calculate the electric field while taking into account the frequency and temperature effects. This is deferred to future work.

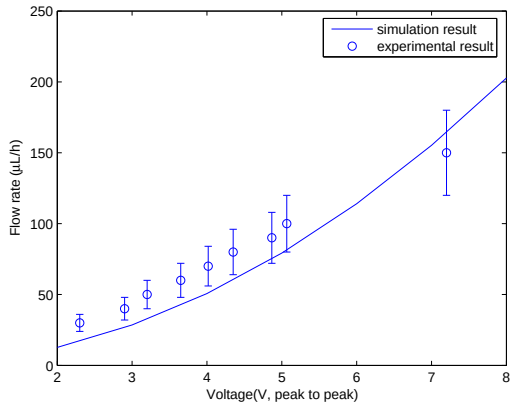

(a) Release flow rate for $5\mu m$-particle

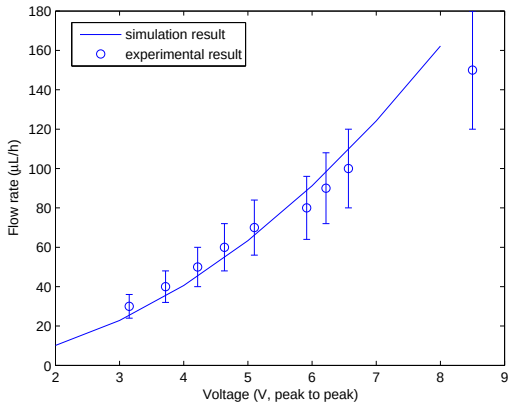

(b) Trap flow rate for $5\mu m$-particle

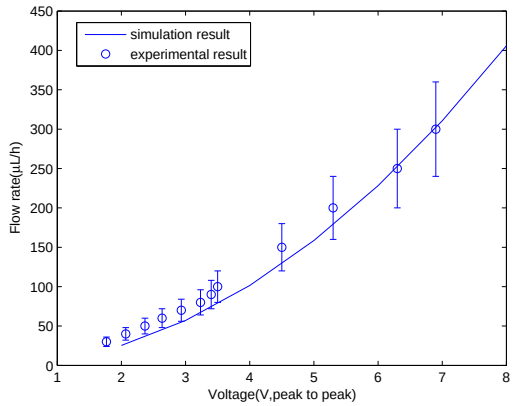

(c) Release flow rate for $10\mu m$-particle

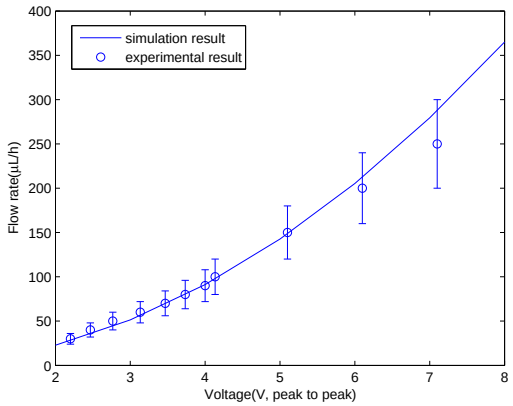

(d) Trap flow rate for $10\mu m$-particle

Figure 6.19: Comparison of experiment and simulation

6.6.5 Measurement of the sorting efficiency

In the above sections, we study the performance for one single trap. It is necessary to study the efficiency for the whole microarray if this design is to be adopted for routine use. The traditional way to investigate the efficiency is to measure the percentage of particles at inlet and outlet and find the difference. However, there are many issues to be resolved for this design if we use the traditional method. The major issue comes from the fabrication. We cannot yet control the quality if large array was fabricated. If we made a small array, the number of traps is much smaller than the number of lost particles due to the adhesion. For example, we have a 100-trap chip. Suppose 10^6 particles come in from inlet and $9 * 10^5$ particles go out through outlet. The number of lost particles is much larger than that of traps ($10^5 >> 100$).In addition, although the symmetry of the ideal electrode structure precludes any substrate-liquid material interface or charge relaxation effects from affecting the electric fields, the actual physical setup could have asymmetries that cause these effects to appear. Therefore, to investigate the performance of this microarray, a new method should be introduced. Figure 6.20 shows the scheme of the method. Two sets of parallel electrodes were used before and after the microarray. The energized electrodes will form a virtual wall to block particles. The first set of electrodes is switched on to collect the particles coming from the inlet. After some time, the second set of electrodes is switched on while the first set of electrodes is switched off. Then the second set of electrodes can collect the rest of particles after the sorting. The whole process is recorded by the camera. By comparing the number of particles before and after the microarray, we can calculate the efficiency. With this method, we can thus make a smaller microarray and still get a reasonable result.

In this experiment, we premixed $10\mu m$ particles and $5\mu m$ particles in the ratio of $1 : 5$. The

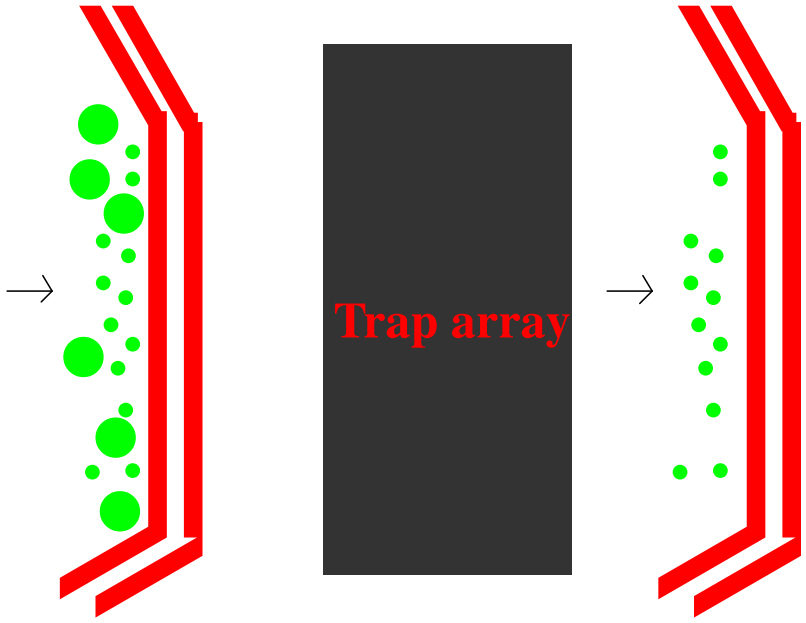

Figure 6.20: Schematic of measurement of efficiency

sorting experiment is repeated 5 times (results shown in Table 6.1). Then we calculated the average result. The result shows that the sorting efficiency of this microarray is around 80%. The major problem comes primarily from the fabrication as mentioned above. There is plenty of room to improve the efficiency if the fabrication quality is improved.

No. of particles before sorting		No. of particles after sorting	
$10\mu m$	$5\mu m$	$10\mu m$	$5\mu m$
71	478	31	476
10	131	1	130
12	307	2	300
78	396	21	390
13	251	1	248

Table 6.1: Five experiments of sorting

6.7 Cell operation

6.7.1 Cell preparation

Human chronic myelogenous leukaemia (K562) cells were incubated at 37°C under 5% CO_2. They were grown in RPMI (Roswell Park Memorial Institute) Glutamax medium supplemented with 10% FCS(Fetal Calf Serum). Prior to the experiment, cells were washed and resuspended in isotonic medium consisting of 8.5% (w/v) sucrose plus 0.3% (w/v) dextrose buffer[71]. The final conductivity of the medium was adjusted to 5mS/m using PBS (Phosphate Buffered Saline) and the final conductivity which was verified with a conductivity meter.

6.7.2 DEP experiments with cells

Signals between 0V and 5V(peak to peak) and frequency of 100KHz were used. The experimental set up and electrode arrangement were used as described in section 4.5. Cells were used immediately after resuspension to minimise the experimentation time. The experiment was observed by microscope and recorded on video camera.

6.7.3 Results and discussions

As shown in Figure 6.21(a), live cells can be captured in the jagged trap. The first image (Figure 6.21(a)) was taken 3min46s after the flow was applied. Eight cells were trapped already, while one trap was left vacant (right-top corner). The voltage can be applied by similar method as shown in Figure 6.8. In Figure 6.21, cells were released one by one in sequence. In Figure 6.21(g), another cell came from upstream and was trapped again at position $(3, 1)$ during the releasing process. In succession, this cell was released again as shown in Figure 6.21(h) 7 seconds later. Finally, trap $(3, 2)$ was cleared up when the voltage was decreased as shown in

Figure 6.21(j). As shown in Figure 6.21, we can control release at any arbitrary position in this microarray. This open a door for sorting different cells with similar electrical properties using DEP.

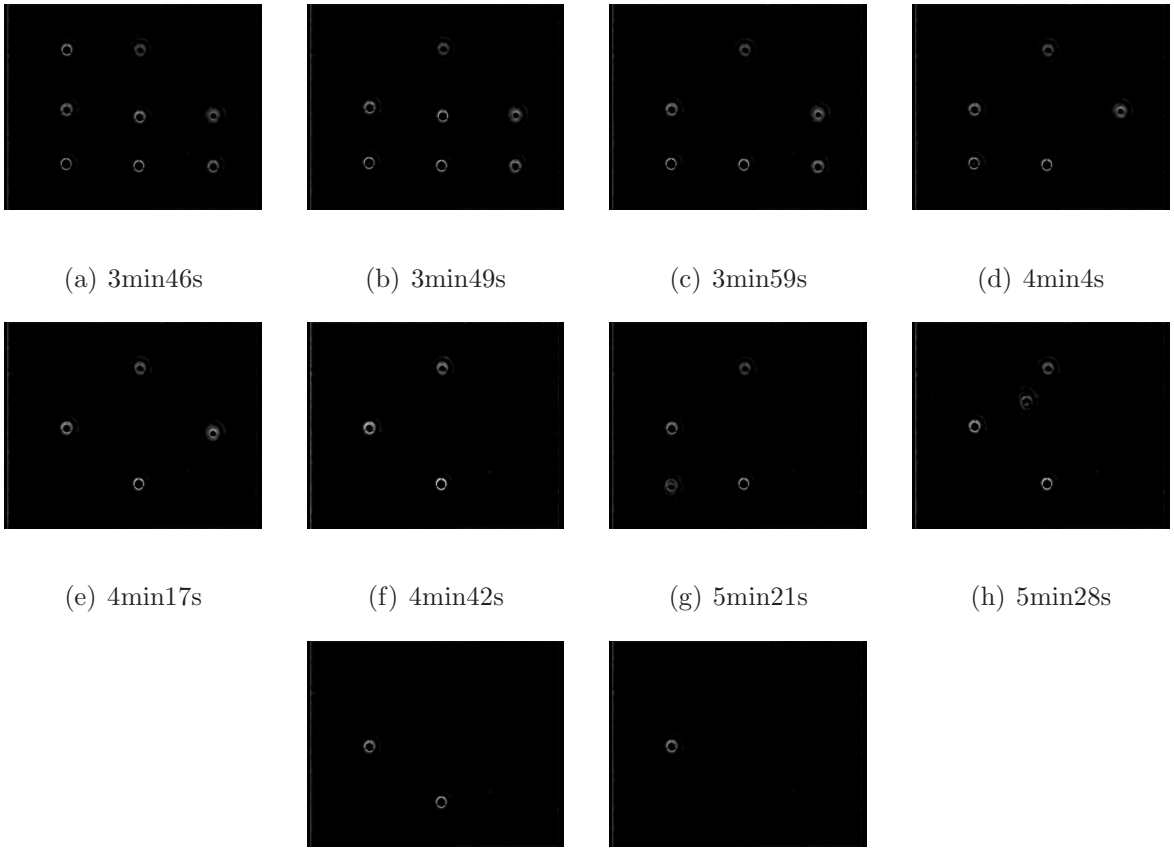

(a) 3min46s (b) 3min49s (c) 3min59s (d) 4min4s

(e) 4min17s (f) 4min42s (g) 5min21s (h) 5min28s

(i) 5min42s (j) 6min14s

Figure 6.21: Addressable control. Cells(K562) were released one by one in sequence. (a)Eight cells were trapped. (b)Trap $(1, 1)$ was emptied. (c)Trap $(2, 2)$ was emptied. (d)Trap $(3, 3)$ was emptied. (e)Trap $(3, 1)$ was emptied. (f)Trap $(2, 3)$ was emptied. (g)Another cell was trapped again at $(3, 1)$. (h)Trap $(3, 1)$ was emptied again. (i)Trap $(1, 2)$ was emptied. (j)Trap $(3, 2)$ was emptied.

The change from polystyrene beads to live cells has been shown repeatedly in previous work. However, many other issues should be considered when using DEP on living cells. Cells can be damaged from joule heating, non-isotonic balancing, trans-membrane loading and

electrochemical effects.

When a conductive medium is exposed to a electric field, heating of the medium occurs, which can and will damage cells. The definition of the unit power generation is shown in the following[132]:

$$W = \sigma \boldsymbol{E}^2 \tag{6.1}$$

where σ is the conductivity of medium. To mitigate this effect, we can minimize the electric fields by lowering the applied voltages.

We should consider the ion concentration when we change the media conductivity. The Na^+-K^+ pump have a direct and crucial role in regulating cell volume. It controls the solute concentration inside the cell, thereby regulating the tonicity that can make a cell swell or shrink. If we put the cells in a hypotonic solution(that is, a solution having a low solute concentration and therefore a high water concentration), there is a net movement of water into the cells, causing them to swell and burst. That is why we use sugar additives to keep the solution as a isotonic medium.

The electroporation will occur when the induced cell membrane voltage exceeds certain critical values[133, 134]. The membrane is like a capacitor or an electrical high-pass filter. To minimize transmembrane loading, we can increase the signal frequency and limit the applied signal voltage.

The production of harmful products in the media under electric field can damage live cells. When sugar-containing media was exposed to electric field, hydrogen peroxide was produced to inhibit cell growth [135]. It is demonstrated that this inhibition was exacerbated with higher conductivity medium, lower signal frequencies, and higher signal voltages. To minimize this effect, we can lower the signal voltage and increase the signal frequency.

6.8 Conclusions

A microarray for single particle trap with addressable control was demonstrated in this section. The fabrication process is a fairly quick and simple process. Therefore, this design can be scaled up to a large array easily. It has the potential to pattern hundreds of thousands of cells on a single microscope slide. We had not only tested polystyrene beads, but also live cells. Both of them worked as expected. Single particle can be captured as well as single cell. Besides, by electronic control, particles in each trap can be controled individually. We can control the number of particles or cells in one trap and we also can release the particles or cells selectively. Sorting particles of different sizes is also presented in this section. Other protocols may also be implemented on the chip. We are developing applications and protocols in which the user may choose to bring specific biological particles into contact with cells to fuse these cells with a liposome carrying drugs or DNA, and study the transfection process or infection process.

Chapter 7

Conclusions

7.1 Review of findings

Three new micro-fluidic devices were designed in this work. All of the devices are based on top-bottom electrodes structure, with which we can obtain high electric field. One device is a grid-like structure. This can sort particles with different sizes. The resolution of size discrimination can be lower than 20%. The main contribution of this device is the simple design of this device, which only needs simple fabrication, though it is a 3D structure. Alignment is not critical. It is easy for commercialization.

The second device is the micro-well structure, which can trap single particles. The size of the well entrance will sort out the suitable particles. It still has the potential to carry out the addressable control due to the LCD-like design.

The third device is the jagged electrodes. The test results showed that the device can sort micro-particles based on different sizes. To investigate the sorting efficiency, we developed a methodology for the test. Two groups of parallel electrodes are set up before and after the trap array. By comparing the ratio of two groups of particles blocked by the two groups of parallel

electrodes, we can evaluate the efficiency of this design, which was as high as 80%. Besides sorting, this third device can also be used to trap and release single particles at each site selectively via multiplexing technique. The test results show that it can trap not only single particles, but also certain number of particles. By adjusting the flow rate and the voltage carefully, we can control the number of trapped particles. One key contribution is that this new design has integrated the sorting and trapping functions into one simple structure. This device can perform the sorting and trapping simultaneously, which could improve the overall efficiency. To sort out the desired particles after trapping, multiplexing technique is used in the control panel. Another advantage is that the number of the particles in each site can be controlled. Additionally, the new design can be duplicated on a large microarray due to its simplicity of fabrication and use of multiplexing technique. Given these multi-functions and simple fabrication, commercialization of the design is possible. We also tested the device with live cells. The results show that the device works well with live cells. We can sort out the desired cells.

All the three devices tend to push the cells to the top or bottom substrate. This attachment can be conducive for cells' integrity at times.

In the modeling part of the study, we study the particle's motion under hydrodynamic force and DEP force. In this model, the rotation of particles was considered, which had not been reported before. Although the results showed that rotation does not affect the Stokes force in the horizontal direction, it has important implications in the overall consideration of the particle's motion under the coupled DEP force and hydrodynamic force, especially in the modeling of micro-well. Besides this, interaction between two particles was investigated. When designing the single particle trap or particle sorter, we must solve the problem on how to separate two particles. This is because the interaction between two particles cannot be

avoided in the experiment. Results showed that CM factor can affect the ratio of electrostatic interaction force between two particles and their own DEP force. At the crossover frequency, the interaction force is small compared to the DEP force. Therefore, we can neglect the interaction effect in the experiment. This finding is of crucial importance in terms of the trapping of single particle, since it provides the basis for the neglect of the interaction force between two particles in the calculation. We also calculated the particle's trajectories in the simulation. We treated the particle's motion in the device as a quasi-steady process. DEP force was calculated via the Maxwell stress tensor while the hydrodynamic force was the integration of the traction. Both used finite element method in conjunction with the Comsol software.

In the fabrication part, a new lift-off process for the two-layer photoresist was proposed in Chapter 5 when we tried to pattern a layer of metal on SU-8. AZ photoresist was used as a sacrificial layer on SU-8 layer. SU-8 layer was hardened first, followed by the coating of the AZ layer. AZ400k was used to remove the AZ mask layer. Results suggest that this lift-off process is a reliable solution for the problem on how to remove the positive photoresist on the negative photoresist. This fabrication process provides a novel solution for doing the lift-off process on SU-8 using the AZ as a sacrificial layer. It is useful for other researchers who want to conduct the similar fabrication process.

7.2 Recommendations

The system application described in this thesis has been realized as in a proof-of-concept. Nonetheless, several significant challenges exist in achieving a truly useful device from the samples depicted in previous Chapters. These can be divided into issues related to design, fabrication, modeling, and testing.

7.2.1 On Design

In this study, we only demonstrated a concept and have proved it. For routine use, we need to sort out many other issues. For example, we should scale up the microarray to a large number and design a smart control panel. Additionally, we also need to investigate the interaction between adjacent traps. To increase the efficiency of the chip, we must increase the density of traps. Consequently, the trap will be affected by the adjacent traps during operation. This problem can be solved by careful modelling and experiment.

7.2.2 On Fabrication

There is room for improvement on fabrication. Packaging is always a problem in the fabrication of MEMS. There is no standard solutions even in the industry. In this study, double side tape was used to bond the two pieces of glass. We chose this due to the simple operation and the certain thickness of the double sided tape. However, in precised manufacturing, double side tape cannot be used and preserved for a long time in the liquid such as water. This bonding problem could be overcome using the standard packaging technique in the LCD fabrication process.

7.2.3 On Modelling

Investigating the heating in micro-systems is crucial because the biological cells will require that the temperature rise,if any, should be small. Previous work [111] strongly suggest that heating could be a major factor in these systems and presents an upper limit to the voltages that one can apply at the micro-scale. The heating effect was not included in our simulation. Fortunately, it should not be too difficult to calculate the temperature distributions. Such in-

vestigations should also include an experimental component to measure the actual temperature distributions. Besides, there is also room for optimization of our code in Matlab. The communication between Matlab and Comsol entails much memory and CPU. It will dramatically speed up the analysis by optimising the memory usage and CPU usage.

7.2.4 On Testing

In testing, PS particles were used to test the device. However, cells are different from PS particles. We have only tested K562 in our experiments. Other cells should be tested in the future. Several issues, such as the sorting efficiency, trapping efficiency and responsibility of the cells within the electric field, need to be addressed. In addition, more experiments needs to be undertaken to determine the effects of the traps on cells within the electric fields. The DEP force on cells cannot be very large due to the small voltage. Consequently, the flow rate cannot be very high if we want to trap cells. Some improvement of design needs to be done to increase the throughput of the device.

Reference

[1] GH Wu, RH Datar, KM Hansen, T Thundat, RJ Cote, and A Majumdar. Bioassay of prostate-specific antigen (PSA) using microcantilevers. *NATURE BIOTECHNOLOGY*, 19(9):856–860, SEP 2001.

[2] Y Arntz, JD Seelig, HP Lang, J Zhang, P Hunziker, JP Ramseyer, E Meyer, M Hegner, and C Gerber. Label-free protein assay based on a nanomechanical cantilever array. *NANOTECHNOLOGY*, 14(1):86–90, JAN 2003.

[3] A Subramanian, PI Oden, SJ Kennel, KB Jacobson, RJ Warmack, T Thundat, and MJ Doktycz. Glucose biosensing using an enzyme-coated microcantilever. *APPLIED PHYSICS LETTERS*, 81(2):385–387, JUL 8 2002.

[4] A Daridon, M Sequeira, G Pennarun-Thomas, H Dirac, JP Krog, P Gravesen, J Lichtenberg, D Diamond, E Verpoorte, and NF de Rooij. Chemical sensing using an integrated microfluidic system based on the Berthelot reaction. *SENSORS AND ACTUATORS B-CHEMICAL*, 76(1-3):235–243, JUN 1 2001. 8th International Meeting on Chemical Sensors (IMCS-8), BASEL, SWITZERLAND, JUL 02-05, 2000.

[5] EMJ Verpoorte, BH Vanderschoot, S Jeanneret, A Manz, HM Widmer, and NF Derooij.

3-Dimensional micro-flow manifolds for miniaturized chemical-analysis systems. *JOURNAL OF MICROMECHANICS AND MICROENGINEERING*, 4(4):246–256, DEC 1994.

[6] SR Liu, YN Shi, WW Ja, and RA Mathies. Optimization of high-speed DNA sequencing on microfabricated capillary electrophoresis channels. *ANALYTICAL CHEMISTRY*, 71(3):566–573, FEB 1 1999.

[7] PC Simpson, D Roach, AT Woolley, T Thorsen, R Johnston, GF Sensabaugh, and RA Mathies. High-throughput genetic analysis using microfabricated 96-sample capillary array electrophoresis microplates. *PROCEEDINGS OF THE NATIONAL ACADEMY OF SCIENCES OF THE UNITED STATES OF AMERICA*, 95(5):2256–2261, MAR 3 1998.

[8] YN Shi, PC Simpson, JR Scherer, D Wexler, C Skibola, MT Smith, and RA Mathies. Radial capillary array electrophoresis microplate and scanner for high-performance nucleic acid analysis. *ANALYTICAL CHEMISTRY*, 71(23):5354–5361, DEC 1 1999.

[9] P Belgrader, D Hansford, GTA Kovacs, K Venkateswaran, R Mariella, F Milanovich, S Nasarabadi, M Okuzumi, F Pourahmadi, and MA Northrup. A minisonicator to rapidly disrupt bacterial spores for DNA analysis. *ANALYTICAL CHEMISTRY*, 71(19):4232–4236, OCT 1 1999.

[10] SW Lee and YC Tai. A micro cell lysis device. *SENSORS AND ACTUATORS A-PHYSICAL*, 73(1-2):74–79, MAR 9 1999.

[11] PCH Li and DJ Harrison. Transport, manipulation, and reaction of biological cells on-chip using electrokinetic effects. *ANALYTICAL CHEMISTRY*, 69(8):1564–1568, APR 15 1997.

[12] EA Schilling, AE Kamholz, and P Yager. Cell lysis and protein extraction in a microfluidic device with detection by a fluorogenic enzyme assay. *ANALYTICAL CHEMISTRY*, 74(8):1798–1804, APR 15 2002.

[13] MT Taylor, P Belgrader, BJ Furman, F Pourahmadi, GTA Kovacs, and MA Northrup. Lysing bacterial spores by sonication through a flexible interface in a microfluidic system. *ANALYTICAL CHEMISTRY*, 73(3):492–496, FEB 1 2001.

[14] LC Waters, SC Jacobson, N Kroutchinina, J Khandurina, RS Foote, and JM Ramsey. Microchip device for cell lysis, multiplex PCR amplification, and electrophoretic sizing. *ANALYTICAL CHEMISTRY*, 70(1):158–162, JAN 1 1998.

[15] K Chun, G Hashiguchi, H Toshiyoshi, and H Fujita. Fabrication of array of hollow microcapillaries used for injection of genetic materials into animal/plant cells. *JAPANESE JOURNAL OF APPLIED PHYSICS PART 2-LETTERS*, 38(3A):L279–L281, MAR 1 1999.

[16] Y Huang and B Rubinsky. Microfabricated electroporation chip for single cell membrane permeabilization. *SENSORS AND ACTUATORS A-PHYSICAL*, 89(3):242–249, APR 15 2001.

[17] YC Lin, CM Jen, MY Huang, CY Wu, and XZ Lin. Electroporation microchips for continuous gene transfection. *SENSORS AND ACTUATORS B-CHEMICAL*, 79(2-3):137–143, OCT 15 2001.

[18] DT Chiu. A microfluidics platform for cell fusion - Commentary. *CURRENT OPINION IN CHEMICAL BIOLOGY*, 5(5):609–612, OCT 2001.

[19] A Stromberg, A Karlsson, F Ryttsen, M Davidson, DT Chiu, and O Orwar. Microfluidic device for combinatorial fusion of liposomes and cells. *ANALYTICAL CHEMISTRY*, 73(1):126–130, JAN 1 2001.

[20] S Takayama, E Ostuni, XP Qian, JC McDonald, XY Jiang, P LeDuc, MH Wu, DE Ingber, and GM Whitesides. Topographical micropatterning of poly(dimethylsiloxane) using laminar flows of liquids in capillaries. *ADVANCED MATERIALS*, 13(8):570+, APR 18 2001.

[21] E Tamaki, K Sato, M Tokeshi, K Sato, M Aihara, and T Kitamori. Single-cell analysis by a scanning thermal lens microscope with a microchip: Direct monitoring of cytochrome c distribution during apoptosis process. *ANALYTICAL CHEMISTRY*, 74(7):1560–1564, APR 1 2002.

[22] AMP Turner, N Dowell, SWP Turner, L Kam, M Isaacson, JN Turner, HG Craighead, and W Shain. Attachment of astroglial cells to microfabricated pillar arrays of different geometries. *JOURNAL OF BIOMEDICAL MATERIALS RESEARCH*, 51(3):430–441, SEP 5 2000.

[23] GM Walker, MS Ozers, and DJ Beebe. Insect cell culture in microfluidic channels. *BIOMEDICAL MICRODEVICES*, 4(3):161–166, JUL 2002.

[24] MS Yang, CW Li, and J Yang. Cell docking and on-chip monitoring of cellular reactions with a controlled concentration gradient on a microfluidic device. *ANALYTICAL CHEMISTRY*, 74(16):3991–4001, AUG 15 2002.

[25] T Lehnert, MAM Gijs, R Netzer, and U Bischoff. Realization of hollow SiO2 micronozzles

for electrical measurements on living cells. *APPLIED PHYSICS LETTERS*, 81(26):5063–5065, DEC 23 2002.

[26] C Schmidt, M Mayer, and H Vogel. A chip-based biosensor for the functional analysis of single ion channels. *ANGEWANDTE CHEMIE-INTERNATIONAL EDITION*, 39(17):3137–3140, 2000.

[27] J Xu, XB Wang, B Ensign, M Li, L Wu, A Guia, and JQ Xu. Ion-channel assay technologies: quo vadis? *DRUG DISCOVERY TODAY*, 6(24):1278–1287, DEC 15 2001.

[28] JL Zabzdyr and SJ Lillard. Measurement of single-cell gene expression using capillary electrophoresis. *ANALYTICAL CHEMISTRY*, 73(23):5771–5775, DEC 1 2001.

[29] R McBeath, DM Pirone, CM Nelson, K Bhadriraju, and CS Chen. Cell shape, cytoskeletal tension, and RhoA regulate stem cell lineage commitment. *DEVELOPMENTAL CELL*, 6(4):483–495, APR 2004.

[30] DJ Bakewell and H Morgan. Dielectrophoresis of DNA: Time- and frequency-dependent collections on microelectrodes. *IEEE TRANSACTIONS ON NANOBIOSCIENCE*, 5(1):1–8, MAR 2006.

[31] CF Chou, JO Tegenfeldt, O Bakajin, SS Chan, EC Cox, N Darnton, T Duke, and RH Austin. Electrodeless dielectrophoresis of single- and double-stranded DNA. *BIOPHYSICAL JOURNAL*, 83(4):2170–2179, OCT 2002.

[32] RH Carlson, CV Gabel, SS Chan, RH Austin, JP Brody, and JW Winkelman. Self-sorting of white blood cells in a lattice. *PHYSICAL REVIEW LETTERS*, 79(11):2149–2152, SEP 15 1997.

[33] P Wilding, LJ Kricka, J Cheng, G Hvichia, MA Shoffner, and P Fortina. Integrated cell isolation and polymerase chain reaction analysis using silicon microfilter chambers. *ANALYTICAL BIOCHEMISTRY*, 257(2):95–100, MAR 15 1998.

[34] JR Wu. Acoustical tweezers. *JOURNAL OF THE ACOUSTICAL SOCIETY OF AMERICA*, 89(5):2140–2143, MAY 1991.

[35] A Ashkin, JM Dziedzic, JE Bjorkholm, and S Chu. Observation of a single-beam gradient force optical trap for dielectric particles. *OPTICS LETTERS*, 11(5):288–290, MAY 1986.

[36] N Pamme and C Wilhelm. Continuous sorting of magnetic cells via on-chip free-flow magnetophoresis. *LAB ON A CHIP*, 6(8):974–980, 2006.

[37] PY Chiou, AT Ohta, and MC Wu. Massively parallel manipulation of single cells and microparticles using optical images. *NATURE*, 436(7049):370–372, JUL 21 2005.

[38] W Choi, SH Kim, J Jang, and JK Park. Lab-on-a-display: a new microparticle manipulation platform using a liquid crystal display (LCD). *MICROFLUIDICS AND NANOFLUIDICS*, 3(2):217–225, APR 2007.

[39] DR Albrecht, VL Tsang, RL Sah, and SN Bhatia. Photo- and electropatterning of hydrogel-encapsulated living cell arrays. *LAB ON A CHIP*, 5(1):111–118, 2005.

[40] F Arai, C Ng, H Maruyama, A Ichikawa, H El-Shimy, and T Fukuda. On chip single-cell separation and immobilization using optical tweezers and thermosensitive hydrogel. *LAB ON A CHIP*, 5(12):1399–1403, 2005.

[41] FF Becker, XB Wang, Y Huang, R Pethig, J Vykoukal, and PRC Gascoyne. Separation of human breast-cancer cells from blood by differential dielectric affinity. *PROCEED-*

INGS OF THE NATIONAL ACADEMY OF SCIENCES OF THE UNITED STATES OF AMERICA, 92(3):860–864, JAN 31 1995.

[42] J Cheng, EL Sheldon, L Wu, A Uribe, LO Gerrue, J Carrino, MJ Heller, and JP O'Connell. Preparation and hybridization analysis of DNA/RNA from E-coli on microfabricated bioelectronic chips. *NATURE BIOTECHNOLOGY*, 16(6):541–546, JUN 1998.

[43] S Fiedler, SG Shirley, T Schnelle, and G Fuhr. Dielectrophoretic sorting of particles and cells in a microsystem. *ANALYTICAL CHEMISTRY*, 70(9):1909–1915, MAY 1 1998.

[44] Y Huang, KL Ewalt, M Tirado, TR Haigis, A Forster, D Ackley, MJ Heller, JP O'Connell, and M Krihak. Electric manipulation of bioparticles and macromolecules on microfabricated electrodes. *ANALYTICAL CHEMISTRY*, 73(7):1549–1559, APR 1 2001.

[45] Y Huang, S Joo, M Duhon, M Heller, B Wallace, and X Xu. Dielectrophoretic cell separation and gene expression profiling on microelectronic chip arrays. *ANALYTICAL CHEMISTRY*, 74(14):3362–3371, JUL 15 2002.

[46] GH Markx, Y Huang, XF Zhou, and R Pethig. Dielectrophoretic characterization and separation of microorganisms. *MICROBIOLOGY-UK*, 140(Part 3):585–591, MAR 1994.

[47] J Voldman, ML Gray, M Toner, and MA Schmidt. A microfabrication-based dynamic array cytometer. *ANALYTICAL CHEMISTRY*, 74(16):3984–3990, AUG 15 2002.

[48] XB Wang, J Yang, Y Huang, J Vykoukal, FF Becker, and PRC Gascoyne. Cell separation by dielectrophoretic field-flow-fractionation. *ANALYTICAL CHEMISTRY*, 72(4):832–839, FEB 15 2000.

[49] BM Taff and J Voldman. A scalable addressable positive-dielectrophoretic cell-sorting array. *ANALYTICAL CHEMISTRY*, 77(24):7976–7983, DEC 15 2005.

[50] DS Gray, JL Tan, J Voldman, and CS Chen. Dielectrophoretic registration of living cells to a microelectrode array (vol 19, pg 1765, 2004). *BIOSENSORS & BIOELECTRONICS*, 19(12):1765–1774, JUL 15 2004.

[51] J Voldman, M Toner, ML Gray, and MA Schmidt. Design and analysis of extruded quadrupolar dielectrophoretic traps. *JOURNAL OF ELECTROSTATICS*, 57(1):69–90, JAN 2003.

[52] C Reichle, T Muller, T Schnelle, and G Fuhr. Electro-rotation in octopole micro cages. *JOURNAL OF PHYSICS D-APPLIED PHYSICS*, 32(16):2128–2135, AUG 21 1999.

[53] T Schnelle, R Hagedorn, G Fuhr, S Fiedler, and T Muller. 3-Dimensional electric-field traps for manipulation of cells-calculation and experimental-verification. *BIOCHIMICA ET BIOPHYSICA ACTA*, 1157(2):127–140, JUN 11 1993.

[54] T Schnelle, T Muller, and G Fuhr. Trapping in AC octode field cages. *JOURNAL OF ELECTROSTATICS*, 50(1):17–29, SEP 2000.

[55] J Suehiro and R Pethig. The dielectrophoretic movement and positioning of a biological cell using a three-dimensional grid electrode system. *JOURNAL OF PHYSICS D-APPLIED PHYSICS*, 31(22):3298–3305, NOV 21 1998.

[56] N Manaresi, A Romani, G Medoro, L Altomare, A Leonardi, M Tartagni, and R Guerrieri. A CMOS chip for individual cell manipulation and detection. *IEEE JOURNAL OF SOLID-STATE CIRCUITS*, 38(12):2297–2305, DEC 2003. IEEE International Solid-State Circuits Conference, SAN FRANCISCO, CALIFORNIA, FEB 09-13, 2003.

[57] B He, L Tan, and F Regnier. Microfabricated filters for microfluidic analytical systems. *ANALYTICAL CHEMISTRY*, 71(7):1464–1468, APR 1 1999.

[58] AY Fu, C Spence, A Scherer, FH Arnold, and SR Quake. A microfabricated fluorescence-activated cell sorter. *NATURE BIOTECHNOLOGY*, 17(11):1109–1111, NOV 1999.

[59] N Pamme and A Manz. On-chip free-flow magnetophoresis: Continuous flow separation of magnetic particles and agglomerates. *ANALYTICAL CHEMISTRY*, 76(24):7250–7256, DEC 15 2004.

[60] K Cheung, S Gawad, and P Renaud. Impedance spectroscopy flow cytometry: On-chip label-free cell differentiation. *CYTOMETRY PART A*, 65A(2):124–132, JUN 2005.

[61] S Gawad, L Schild, and P Renaud. Micromachined impedance spectroscopy flow cytometer for cell analysis and particle sizing. *LAB ON A CHIP*, 1(1):76–82, 2001.

[62] M Groschl. Ultrasonic separation of suspended particles - Part I: Fundamentals. *ACUSTICA*, 84(3):432–447, MAY-JUN 1998.

[63] NR Harris, M Hill, S Beeby, Y Shen, NM White, JJ Hawkes, and WT Coakley. A silicon microfluidic ultrasonic separator. *SENSORS AND ACTUATORS B-CHEMICAL*, 95(1-3):425–434, OCT 15 2003. 16th EUROSENSORS Conference, PRAGUE, CZECH REPUBLIC, SEP 15-18, 2002.

[64] MP MacDonald, GC Spalding, and K Dholakia. Microfluidic sorting in an optical lattice. *NATURE*, 426(6965):421–424, NOV 27 2003.

[65] JC Giddings. Field-flow fractionation of macromolecules. *JOURNAL OF CHROMATOGRAPHY*, 470(2):327–335, MAY 26 1989.

[66] JC Giddings. Field-flow fractionation-analysis of macromolecular, colloidal, and particulate materials. *SCIENCE*, 260(5113):1456–1465, JUN 4 1993.

[67] T Muller, T Schnelle, G Gradl, SG Shirley, and G Fuhr. Microdevice for cell and particle separation using dielectrophoretic field-flow fractionation. *JOURNAL OF LIQUID CHROMATOGRAPHY & RELATED TECHNOLOGIES*, 23(1):47–59, 2000.

[68] I Doh and YH Cho. A continuous cell separation chip using hydrodynamic dielectrophoresis (DEP) process. *SENSORS AND ACTUATORS A-PHYSICAL*, 121(1):59–65, MAY 31 2005.

[69] H Morgan, MP Hughes, and NG Green. Separation of submicron bioparticles by dielectrophoresis. *BIOPHYSICAL JOURNAL*, 77(1):516–525, JUL 1999.

[70] J Cheng, EL Sheldon, L Wu, MJ Heller, and JP O'Connell. Isolation of cultured cervical carcinoma cells mixed with peripheral blood cells on a bioelectronic chip. *ANALYTICAL CHEMISTRY*, 70(11):2321–2326, JUN 1 1998.

[71] PRC Gascoyne, XB Wang, Y Huang, and FF Becker. Dielectrophoretic separation of cancer cells from blood. *IEEE TRANSACTIONS ON INDUSTRY APPLICATIONS*, 33(3):670–678, MAY-JUN 1997. Annual Meeting of the Industry-Applications-Society, LAKE BUENA VISTA, FL, OCT 08-12, 1995.

[72] GH Markx, MS Talary, and R Pethig. Separation of viable and nonviable yeast using dielectrophoresis. *JOURNAL OF BIOTECHNOLOGY*, 32(1):29–37, JAN 15 1994.

[73] MS Talary, JPH Burt, JA Tame, and R Pethig. Electromanipulation and separation of cells using travelling electric fields. *JOURNAL OF PHYSICS D-APPLIED PHYSICS*, 29(8):2198–2203, AUG 14 1996.

[74] XB Wang, Y Huang, JPH Burt, GH Markx, and R Pethig. Selective dielectrophoretic confinement of bioparticles in potential-energy wells. *JOURNAL OF PHYSICS D-APPLIED PHYSICS*, 26(8):1278–1285, AUG 14 1993.

[75] MS Talary, KI Mills, T Hoy, AK Burnett, and R Pethig. Dielectrophoretic separation and enrichment OF CD34+ cell subpopulation from bone-marrow and peripheral-blood stem-cells. *MEDICAL & BIOLOGICAL ENGINEERING & COMPUTING*, 33(2):235–237, MAR 1995.

[76] KF Hoettges, MB McDonnell, and MP Hughes. Use of combined dielectrophoretic/electrohydrodynamic forces for biosensor enhancement. *JOURNAL OF PHYSICS D-APPLIED PHYSICS*, 36(20):L101–L104, OCT 21 2003.

[77] YL Li and KVIS Kaler. Dielectrophoretic fluidic cell fractionation system. *ANALYTICA CHIMICA ACTA*, 507(1):151–161, APR 1 2004.

[78] MD Vahey and J Voldman. An equilibrium method for continuous-flow cell sorting using dielectrophoresis. *ANALYTICAL CHEMISTRY*, 80(9):3135–3143, MAY 1 2008.

[79] Jason G. Kralj, Michael T. W. Lis, Martin A. Schmidt, and Klavs F. Jensen. Continuous dielectrophoretic size-based particle sorting. *ANALYTICAL CHEMISTRY*, 78(14):5019–5025, JUL 15 2006.

[80] S Choi and JK Park. Microfluidic system for dielectrophoretic separation based on a trapezoidal electrode array. *LAB ON A CHIP*, 5(10):1161–1167, 2005.

[81] HO Fatoyinbo, D Kamchis, R Whattingham, SL Ogin, and MP Hughes. A high-throughput 3-D composite dielectrophoretic separator. *IEEE TRANSACTIONS ON BIOMEDICAL ENGINEERING*, 52(7):1347–1349, JUL 2005.

[82] BY Park and MJ Madou. 3-D electrode designs for flow-through dielectrophoretic systems. *ELECTROPHORESIS*, 26(19):3745–3757, OCT 2005.

[83] J Park, B Kim, SK Choi, S Hong, SH Lee, and KI Lee. An efficient cell separation system using 3D-asymmetric microelectrodes. *LAB ON A CHIP*, 5(11):1264–1270, 2005.

[84] T Schnelle, T Muller, G Gradl, SG Shirley, and G Fuhr. Paired microelectrode system: dielectrophoretic particle sorting and force calibration. *JOURNAL OF ELECTROSTATICS*, 47(3):121–132, SEP 1999.

[85] EG Cen, C Dalton, YL Li, S Adamia, LM Pilarski, and KVIS Kaler. A combined dielectrophoresis, traveling wave dielectrophoresis and electrorotation microchip for the manipulation and characterization of human malignant cells. *JOURNAL OF MICROBIOLOGICAL METHODS*, 58(3):387–401, SEP 2004.

[86] H Morgan, NG Green, MP Hughes, W Monaghan, and TC Tan. Large-area travelling-wave dielectrophoresis particle separator. *JOURNAL OF MICROMECHANICS AND MICROENGINEERING*, 7(2):65–70, JUN 1997.

[87] C Rusu, R van't Oever, MJ de Boer, HV Jansen, JW Berenschot, ML Bennink, JS Kanger, BG de Grooth, M Elwenspoek, J Greve, J Brugger, and A van den Berg. Direct integration of micromachined pipettes in a flow channel for single DNA molecule study by optical tweezers. *JOURNAL OF MICROELECTROMECHANICAL SYSTEMS*, 10(2):238–246, JUN 2001.

[88] Dino Di Carlo, Liz Y. Wu, and Luke P. Lee. Dynamic single cell culture array. *LAB ON A CHIP*, 6(11):1445–1449, 2006.

[89] K Sato, Y Kawamura, S Tanaka, K Uchida, and H Kohida. Individual and mass operation of biological cells using micromechanical silicon devices. *SENSORS AND ACTUATORS A-PHYSICAL*, 23(1-3):948–953, APR 1990. 5TH INTERNATIONAL CONF ON SOLID-STATE SENSORS AND ACTUATORS AND EUROSENSORS 3, MONTREUX, SWITZERLAND, JUN 25-30, 1989.

[90] DR Jung, R Kapur, T Adams, KA Giuliano, M Mrksich, HG Craighead, and DL Taylor. Topographical and physicochemical modification of material surface to enable patterning of living cells. *CRITICAL REVIEWS IN BIOTECHNOLOGY*, 21(2):111–154, 2001.

[91] VP Zharov, TV Malinsky, and RC Kurten. Photoacoustic tweezers with a pulsed laser: theory and experiments. *JOURNAL OF PHYSICS D-APPLIED PHYSICS*, 38(15):2662–2674, AUG 7 2005.

[92] G Fuhr, WM Arnold, R Hagedorn, T Muller, W Benecke, B Wagner, and U Zimmermann. Levitation, holding, and rotation of cells within traps made high-frequency fields. *BIOCHIMICA ET BIOPHYSICA ACTA*, 1108(2):215–223, JUL 27 1992.

[93] G Fuhr, H Glasser, T Muller, and T Schnelle. Cell manipulation and cultivation under AC electric-field influence in highly conductive culture media. *BIOCHIMICA ET BIOPHYSICA ACTA-GENERAL SUBJECTS*, 1201(3):353–360, DEC 15 1994.

[94] J Voldman, RA Braff, M Toner, ML Gray, and MA Schmidt. Holding forces of single-particle dielectrophoretic traps. *BIOPHYSICAL JOURNAL*, 80(1):531–541, JAN 2001.

[95] CH Yu, J Vykoukal, DM Vykoukal, JA Schwartz, L Shi, and PRC Gascoyne. A three-dimensional dielectrophoretic particle focusing channel for microcytometry appli-

cations. *JOURNAL OF MICROELECTROMECHANICAL SYSTEMS*, 14(3):480–487, JUN 2005.

[96] BH Lapizco-Encinas, BA Simmons, EB Cummings, and Y Fintschenko. Dielectrophoretic concentration and separation of live and dead bacteria in an array of insulators. *ANALYTICAL CHEMISTRY*, 76(6):1571–1579, MAR 15 2004.

[97] MP Hughes, R Pethig, and XB Wang. Dielectrophoretic forces on particles in travelling electric fields. *JOURNAL OF PHYSICS D-APPLIED PHYSICS*, 29(2):474–482, FEB 14 1996.

[98] TB Jones. Basic theory of dielectrophoresis and electrorotation. *IEEE ENGINEERING IN MEDICINE AND BIOLOGY MAGAZINE*, 22(6):33–42, NOV-DEC 2003.

[99] Herbert Ackland Pohl. Some Effects of Nonuniform Fields on Dielectrics. *Journal of Applied Physics*, 29:1182, 1958.

[100] R Holzel. Electrorotation of single yeast cells at frequencies between 100 Hz and 1.6 GHz. *BIOPHYSICAL JOURNAL*, 73(2):1103–1109, AUG 1997.

[101] T. P. Hunt and R. M. Westervelt. Dielectrophoresis tweezers for single cell manipulation. *BIOMEDICAL MICRODEVICES*, 8(3):227–230, SEP 2006.

[102] H. Zou, S. Mellon, R. R. A. Syms, and K. E. Tanner. 2-dimensional MEMS dielectrophoresis device for osteoblast cell stimulation. *BIOMEDICAL MICRODEVICES*, 8(4):353–359, DEC 2006.

[103] Hsien-Chang Chang, Chao-Hung Chen, I-Fang Cheng, and Chi-Ching Lin. Manipulation of bioparticles on electrodeless dielectrophoretic chip based on AC Electrokinetic control.

In *2007 2nd IEEE International Conference on Nano/Micro Engineered and Molecular Systems, Vols 1-3*, pages 950–953, 345 E 47TH ST, NEW YORK, NY 10017 USA, 2007. IEEE, IEEE. IEEE International Conference of Nano/Micro Engineered and Molecular Systems, Bangkok, THAILAND, JAN 16-19, 2007.

[104] BH Lapizco-Encinas, RV Davalos, BA Simmons, EB Cummings, and Y Fintschenko. An insulator-based (electrodeless) dielectrophoretic concentrator for microbes in water. *JOURNAL OF MICROBIOLOGICAL METHODS*, 62(3, Sp. Iss. SI):317–326, SEP 2005. 5th International Symposium on the Interface between Analytical Chemistry and Microbiology, Washington, DC, APR 19-21, 2004.

[105] S Nedelcu and JHP Watson. Size separation of DNA molecules by pulsed electric field dielectrophoresis. *JOURNAL OF PHYSICS D-APPLIED PHYSICS*, 37(15):2197–2204, AUG 7 2004.

[106] Sampo Tuukkanen, J. Jussi Toppari, Anton Kuzyk, Lasse Hirviniemi, Vesa P. Hytoenen, Teemu Ihalainen, and Paeivi Toermae. Carbon nanotubes as electrodes for dielectrophoresis of DNA. *NANO LETTERS*, 6(7):1339–1343, JUL 12 2006.

[107] Ralph Holzel, Nils Calander, Zackary Chiragwandi, Magnus Willander, and Frank F. Bier. Trapping single molecules by dielectrophoresis. *Physics Review Letters*, 95:128102, 2005.

[108] VP Pastushenko, PI Kuzjmin, and YA Chizmadzhev. Dielectrophoresis and electrorotation-a unified theory of spherically symmetrical cells. *STUDIA BIOPHYSICA*, 110(1-3):51–57, 1985.

[109] ER Mognaschi and A Savini. The action of a non-uniform electric-field upon lossy di-

electric systems ponderomotive force on a dielectric sphere in the field of a point-charge. *JOURNAL OF PHYSICS D-APPLIED PHYSICS*, 16(8):1533–1541, 1983.

[110] R PAUL and KVIS KALER. Effects of particle-shape on electromagnetic torques-a comparison of the effective-dipole-moment method with the maxwell-stress-tensor method. *PHYSICAL REVIEW E*, 48(2):1491–1496, AUG 1993.

[111] Carlos Rosales and Kian Meng Lim. Numerical comparison between Maxwell stress method and equivalent multipole approach for calculation of the dielectrophoretic force in single-cell traps. *ELECTROPHORESIS*, 26(11):2057–2065, JUN 2005.

[112] S. Gawad, L. Schild, and Ph. Renaud. Micromachined impedance spectroscopy flow cytometer for cell analysis and particle sizing. *Lab on a chip*, 1:76–82, 2001.

[113] J Kadaksham, P Singh, and N Aubry. Dielectrophoresis induced clustering regimes of viable yeast cells. *ELECTROPHORESIS*, 26(19):3738–3744, OCT 2005.

[114] N Aubry and P Singh. Control of electrostatic particle-particle interactions in dielectrophoresis. *Europhysics Letters*, 74(4):623–629, MAY 2006.

[115] M WASHIZU, TB JONES, and KVIS KALER. HIGHER-ORDER DIELECTROPHORETIC EFFECTS - LEVITATION AT A FIELD NULL. *BIOCHIMICA ET BIOPHYSICA ACTA*, 1158(1):40–46, AUG 20 1993.

[116] A. Al-Jarro, J. Paul, D. W. P. Thomas, J. Crowe, N. Sawyer, F. R. A. Rose, and K. M. Shakesheff. Direct calculation of Maxwell stress tensor for accurate trajectory prediction during DEP for 2D and 3D structures. *JOURNAL OF PHYSICS D-APPLIED PHYSICS*, 40(1):71–77, JAN 7 2007. Conference of the Institute-of-Physic-Dielectrics-Group, Leicester, ENGLAND, APR 10-12, 2006.

[117] TS Leu, HY Chen, and FB Hsiao. Studies of particle holding, separating, and focusing using convergent electrodes in microsorters. *MICROFLUIDICS AND NANOFLUIDICS*, 1(4):328–335, OCT 2005.

[118] M Navab, SS Imes, SY Hama, GP Hough, LA Ross, RW Bork, AJ Valente, JA Berliner, DC Drinkwater, H Laks, and AM Fogelman. Monocyte transmigration induced by modification of low-density-liporotein in cocultures of human aortic-wall cells is due to induction of monocyte chemotactic protein-1 synthesis and is abolished by high-density-lipoprotein. *JOURNAL OF CLINICAL INVESTIGATION*, 88(6):2039–2046, DEC 1991.

[119] O Quehenberger. Molecular mechanisms regulating monocyte recruitment in atherosclerosis. *JOURNAL OF LIPID RESEARCH*, 46(8):1582–1590, AUG 2005.

[120] RYL Tsai and RDG McKay. Cell contact regulates fate choice by cortical stem cells. *JOURNAL OF NEUROSCIENCE*, 20(10):3725–3735, MAY 15 2000.

[121] KA Purpura, JE Aubin, and PW Zandstra. Sustained in vitro expansion of bone progenitors is cell density dependent. *STEM CELLS*, 22(1):39–50, 2004.

[122] EH Javazon, DC Colter, EJ Schwarz, and DJ Prockop. Rat marrow stromal cells are more sensitive to plating density and expand more rapidly from single-cell-derived colonies than human marrow stromal cells. *STEM CELLS*, 19(3):219–225, 2001.

[123] PW Zandstra, HV Le, GQ Daley, LG Griffith, and DA Lauffenburger. Leukemia inhibitory factor (LIF) concentration modulates embryonic stem cell self-renewal and differentiation independently of proliferation. *BIOTECHNOLOGY AND BIOENGINEERING*, 69(6):607–617, SEP 20 2000.

[124] SN Bhatia, UJ Balis, ML Yarmush, and M Toner. Microfabrication of hepatocyte/fibroblast co-cultures: Role of homotypic cell interactions. *BIOTECHNOLOGY PROGRESS*, 14(3):378–387, MAY-JUN 1998.

[125] DR Albrecht, GH Underhill, TB Wassermann, RL Sah, and SN Bhatia. Probing the role of multicellular organization in three-dimensional microenvironments. *NATURE METHODS*, 3(5):369–375, MAY 2006.

[126] CS Chen, M Mrksich, S Huang, GM Whitesides, and DE Ingber. Micropatterned surfaces for control of cell shape, position, and function. *BIOTECHNOLOGY PROGRESS*, 14(3):356–363, MAY-JUN 1998.

[127] CS Chen, M Mrksich, S Huang, GM Whitesides, and DE Ingber. Geometric control of cell life and death. *SCIENCE*, 276(5317):1425–1428, MAY 30 1997.

[128] A Folch and M Toner. Cellular micropatterns on biocompatible materials. *BIOTECHNOLOGY PROGRESS*, 14(3):388–392, MAY-JUN 1998.

[129] LA Tempelman, KD King, GP Anderson, and FS Ligler. Quantitating staphylococcal enterotoxin B in diverse media using a portable fiber-optic biosensor. *ANALYTICAL BIOCHEMISTRY*, 233(1):50–57, JAN 1 1996.

[130] BM Paddle. Biosensors for chemical and biological agents of defence interest. *BIOSENSORS & BIOELECTRONICS*, 11(11):1079–1113, 1996.

[131] Duc Vinh Le, Carlos Rosales, Boo Cheong Khoo, and Jaime Peraire. Numerical design of electrical-mechanical traps. *LAB ON A CHIP*, 8(5):755–763, 2008.

[132] A Ramos, H Morgan, NG Green, and A Castellanos. Ac electrokinetics: a review of

forces in microelectrode structures. *JOURNAL OF PHYSICS D-APPLIED PHYSICS*, 31(18):2338–2353, SEP 21 1998.

[133] S Archer, TT Li, AT Evans, ST Britland, and H Morgan. Cell reactions to dielectrophoretic manipulation. *BIOCHEMICAL AND BIOPHYSICAL RESEARCH COMMUNICATIONS*, 257(3):687–698, APR 21 1999.

[134] H Glasser and G Fuhr. Cultivation of cells under strong ac-electric field - differentiation between heating and trans-membrane potential effects. *BIOELECTROCHEMISTRY AND BIOENERGETICS*, 47(2):301–310, DEC 1998. International Scientific Meeting on Electromagnetics in Medicine and Biology, CHICAGO, ILLINOIS, NOV 03-05, 1997.

[135] XJ Wang, J Yang, and PRC Gascoyne. Role of peroxide in AC electrical field exposure effects on Friend murine erythroleukemia cells during dielectrophoretic manipulations. *BIOCHIMICA ET BIOPHYSICA ACTA-GENERAL SUBJECTS*, 1426(1):53–68, JAN 4 1999.

Appendix A

Programming in Comsol

A.1 Introduction

Comsol is actually implemented in Matlab as a toolbox. Therefore, Comsol is able to output exactly what it programmed in Matlab to carry out a series of commands in an m file. Each major action performed in Comsol maps to a statement written in the m file, in the order they are performed. For example, if one activates the "Refine Mesh" button, it corresponds to a line in the m file. One is caution to avoid extraneous actions to prevent the m file from becoming too complicated to work with. The following is the procedure on the generation of codes.

1. Open Comsol to set up a model.
2. Set subdomain settings.
3. Boundary settings.
4. Mesh
5. Solve the problem

6. Save as a m-file.

7. Open Comsol with Matlab

8. In Matlab, Open the m-file saved just now

9. Do some modification about the code

A.2 Script details

In Chapter 3, we used this code to calculate the trajectory of the particle. Here, we only discuss two relevant issues which are very important in our code. One is on the change of the position of particle, the other is on the change of boundary index.

A.2.1 Changing the position of particle

We used comsol to design a model and get the DEP force and hydrodynamic force, followed by calculating the displacement and the next position of the particle. The solution requires one to vary the position of particle with the same boundary. With the geometry information we can use the function 'move' to change the position of particle.

A.2.2 Change of the boundary index

The boundary index in Comsol is assigned automatically. Sometimes, when the particle moved over a boundary, the index of the bounday would be changed. This will affect the result of the boundary integration. That means we must know the information of the boundary at each time step. We can use the function 'geomanalyze' to track the index change. By studying the workings on how Comsol numbers the subdomains and the boundaries in conjunction with

the information of the changed geometry the system was solved successfully for any randomly misplaced case.

Appendix B

Error analysis

Here we will study the error in our calculation and experiment. This will help us in analysing the simulation and experimental results. Table B.1 is the uncertainty analysis of different physical variables.The size uncertainty of polystyrene beads is from the supplier. And the uncertainly error of channel width, channel height, and flow viscosity is from the measurement carried out.

No.	**Variable**	**description**	**Value**	**Error**E
1	R	Radius of particle	5μm	5%
2	R	Radius of particle	9.9μm	5%
3	R	Radius of particle	15μm	5%
4	R	Radius of particle	20μm	5%
5	W	Width of channel	5mm	0.02mm
6	H	Height of channel	40μm	2μm
7	η	Viscosity of fluid	0.001Pa $\cdot$ s	3%(1°C)

Table B.1: Uncertainty analysis of individual variable

From volume flow rate $Q = \bar{v}HW$, where $\bar{v}$ is the average velocity of fluid, we can obtain

the error of volume flow rate as

$$E(Q) = E(\bar{v}) + E(W) + E(H). \tag{B.1}$$

As we know, $\boldsymbol{F}_{DEP} \propto R^3$, and $\boldsymbol{F}_{Stokes} \propto R\eta$, thus we can calculate the percentage error of average fluid velocity as $E(\bar{v}) = 2E(R) + E(\eta)$. Therefore, total uncertainty of the volume flow rate is

$$E(Q) = 2E(R) + E(\eta) + E(W) + E(H) \leq 20\%. \tag{B.2}$$

Appendix C

Fabrication Flow Process

C.1 ITO etching process

Step	Description	Machine	Parameters
		etch ITO-glass	
1	clean ITO-glass	benchhood	Acetone Ultrasonic time=20min
2	coat glass	spin coater	AZ2001, speed=2500rpm, thickness=1μm
3	softbake	hotplate	100 deg. C, time=2min
4	expose photoresist	Karl SUSS Mask aligner	dose=60mJ
5	develop photoresist	benchhood	AZ400K:DI water=1:5, time=20s
6	hardbake	hotplate	100 deg. C, time=2min
7	etch ITO	acid-hood	$HCl : FeCl_3 : H_2O$ = 250ml(37%) : 35g : 250ml, 20 deg. C, time=100s
8	strip photoresist	acid-hood	Acetone

C.2 Lift-off process

Step	Description	Machine	Parameters
		Define well in SU-8	
1	clean patterned ITO-glass	benchhood	ethanol, Ultrasonic, time=20min
2	coat wafer	spin coater	SU-8 2015, speed=3000rpm, thickness=20μm
3	softbake	hotplate	95 deg. C, time=7min
4	expose photoresist	Karl SUSS Mask aligner	dose=200mJ
5	postbake	hotplate	95 deg. C, time=5min
6	develop photoresist	benchhood	SU-8 developer, time=2.5min
7	hardbake	hotplate	200 deg. C, time=20min
		Define electrodes in the middle layer	
8	coat photoresist on SU-8	spin coater	AZ4620, speed=2000rpm, thickness=5μm
9	softbake	hotplate	100 deg. C, time=2min
10	expose photoresist	Karl SUSS Mask aligner	dose=180mJ
11	develop photoresist	benchhood	AZ400K:DI water=1:3, time=20s
12	expose photoresist	Karl SUSS Mask aligner	dose=180mJ
13	sputter	RF/DC Denton (2) Sputtering system	Ti, 200w, time=300s, thickness=75nm
14	strip photoresist	acid-hood	AZ400K, Ultrasonic, time=60s
15	strip photoresist	acid-hood	Acetone, Ultrasonic, time=60s

C.3 Packaging process

Step	Description	Machine	Parameters
		Package	
1	Drill holes on the glass	sand blaster/diamond bit	
2	Form channel	hand	$25\mu m$-thick double side tape, super glue
3	alignment	microscope	
4	Tube adapter	hand	Acrylic glass, needle, super glue